Barker, P.F., Camerlenghi, A., Acton, G.D., et al., 1999
*Proceedings of the Ocean Drilling Program, Initial Reports* Volume 178

# 9. Shelf Transect (Sites 1100, 1102, and 1103)[1]

Shipboard Scientific Party[2]

## BACKGROUND AND SCIENTIFIC OBJECTIVES

Sites 1100, 1102, and 1103 (Fig. F1) are part of a transect of the continental shelf, off Anvers Island. They are positioned along multichannel seismic (MCS) reflection profiles on the depositional axis of Lobe 1, one of the four shallow progradational lobes of the continental shelf on the Pacific margin of the Antarctic Peninsula (Larter et al., 1994, 1997). With Site 1097 drilled some 180 nmi (330 km) to the southwest in the trough between Lobes 3 and 4, the continental shelf transect was planned to sample, understand, and date the major changes in geometry of the glacial prograding wedge. These changes are assumed to mark major stages in the development of the ice sheet.

Glacial deposition on the continental shelf and slope is largely confined to the lobes and is described by the internal configuration and geometry of seismic Sequence Groups S1 and S2 (Fig. F2; "Continental Shelf," p. 9, in Barker and Camerlenghi [Chap. 2, this volume]; "Appendix," p. 24, and Fig. AF1, p. 59, both in the "Leg 178 Summary" chapter). These sequence groups are considered to have been produced by ice-stream sediment transport during periodic ice-sheet sediment grounding to the shelf edge over the past 5 m.y. or so (Larter and Barker, 1989, 1991b). Sequence Group S1 is aggradational and moderately progradational. Sequence Group S2 is mainly progradational, with a marked upper boundary where topsets have been eroded and foresets truncated. The two seismic sequence groups are not always continuous between lobes, so strict correlation along the continental shelf cannot be made. However, sequence group geometries are virtually identical in the four lobes of the Antarctic Peninsula continental shelf, and westward to at least 105°W in the Amundsen Sea.

F1. Bathymetric map and main morphologic elements of the continental shelf off Anvers Island, p. 28.

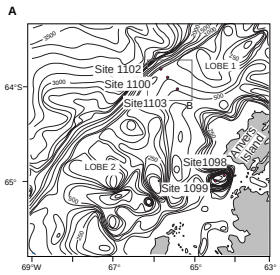


F2. Location of Sites 1100, 1102, and 1103 on MCS profile I95-152 across the continental shelf, p. 30.

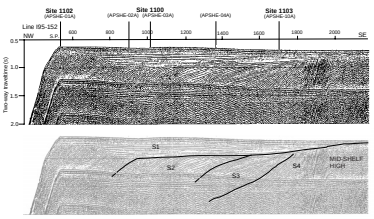


[1]Examples of how to reference the whole or part of this volume.
[2]Shipboard Scientific Party addresses.

Ms 178IR-110

The continental shelf transect as originally planned was composed of five sites (APSHE-01A, -02A, -03A, -04A, and -10A [Fig. F2]). Four of these (APSHE-01A through -04A) were considered primary sites, and APSHE-10A was the alternate for site APSHE-05A (Site 1097), considered less valuable because of later interaction with ridge-crest subduction (Larter and Barker, 1991a). The strategy on the transect was to drill (1) APSHE-01A at the shelf edge to identify and date glacial–interglacial transitions in the youngest S1 foresets, (2) APSHE-03A and APSHE-02A to identify and date the main change in wedge geometry during progradation of the glacial wedge (the onset and completion of S2 topset erosion, respectively), and (3) APSHE-04A to examine the "preglacial"/glacial transition (the conformable boundary between the oldest part of Sequence Group S2 and the youngest Sequence Group S3).

All four sites were to be compared, if possible, to the continental rise sequences.

Operations at Site 1097 revealed that drilling progress in continental shelf glacial sediments would be slower than estimated from previous Ocean Drilling Program experience in similar environments (Leg 119 in Prydz Bay, Antarctica, and Leg 152 on the East Greenland margin). In addition, time spent waiting on ice (icebergs approaching the vessel while drilling) and weather (a 2-m limit on vessel heave when drilling in water depths shallower than 650 m) suggested that the original drilling objectives for the continental shelf transect could not be achieved within the allocated time. We decided to begin the transect by drilling proposed site APSHE-03A (Site 1100) to gain information on the sharp, most easily identifiable erosional truncation at the S1/S2 boundary, estimated to lie at ~400 mbsf. Site 1100 was chosen in 458.6 m of water on the seaward termination of a till body 40 m thick. The till body was presumably deposited during the latest advance of the ice sheet, which apparently did not reach the continental shelf edge at this location (Vanneste and Larter, 1995; Fig. F3). The ship was positioned with a 300-m southeast offset from site APSHE-03A along seismic profile I95-152 (to shotpoint 1010). No penetration was obtained with the 3.5-kHz shipboard sub-bottom profiler. The seafloor topography close to the site is rough because of iceberg grounding.

Drilling progress at Site 1100 was extremely slow because of excessive vessel heave (see "Operations," p. 3). When it was clear that no significant progress was being made at this site (100.9 m of penetration and more than 84 hr spent on site, mainly waiting on weather, excluding the digression to drill Site 1101 on the continental rise), we decided to drill site APSHE-01A (Site 1102). We hoped that softer, less consolidated, recent foreset sediment would allow safer drilling with critical vessel heave. Site 1102 was located according to the original plan at a water depth of 430.5 m, less than 1 km from the sharp edge between the continental shelf and the steep (over 17°) continental slope. The modified objective of the site was to obtain recovery of recent foreset sediments, presumably debris flow deposits, for comparison with older, buried foreset deposits to be drilled at other sites of the continental shelf transect. However, a combination of excessive heave and the presence at the surface of an unstable carapace of loose gravel and boulders (imaged with a camera survey conducted while waiting for heave to subside; see Movie M1, a QuickTime video, and "Seabed Observations, Site 1102," p. 9) prevented the creation of a stable hole. The drill collar penetrated no more than 14 mbsf.

We then decided to drill alternate site APSHE-10A (Site 1103), hoping that, vessel heave permitting, drilling in older formations would result

F3. Location of Site 1100 on deep-tow boomer profile showing the seaward frontal slope of a young till body, p. 31.

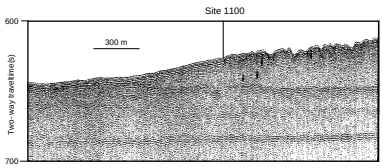


M1. QuickTime video (shelf seabed camera survey, Site 1102).

in better recovery because of the expected higher degree of lithification of the sediments. At this site, seismic Sequence Group S1 unconformably overlies Sequence Group S3 at relatively shallow depth (~210 m), and the S3–S4 transition was expected at ~430 m.

Site 1103 was located in 493.5 m of water, on a rough seafloor with no 3.5-kHz profiler penetration. The unexpected improvement in sea conditions allowed us, finally, to drill as planned. Operations at Site 1103 ended before completion of the drilling program because the Leg 178 drilling time expired at 1130 hr on 26 March.

## OPERATIONS

Operations for the continental shelf transect (Sites 1100, 1102, and 1103) were interrupted by a brief detour to the nearby continental rise (Site 1101), which was cored while waiting for environmental conditions to improve on the shelf (see "Operations," p. 2, in the "Site 1101" chapter). The chronological order of events included drilling Holes 1100A through 1100D, proceeding to and completing operations at Site 1101, returning to Hole 1100D, drilling at Site 1102, and finally drilling and logging at Site 1103. For a summary of drilling at Sites 1100, 1102, and 1103, see Table T1, p. 54, in the "Leg 178 Summary" chapter.

### Site 1100

The 77-nmi distance between Site 1099 in Palmer Deep (Sites 1098 and 1099) and Site 1100 on the outer continental shelf was traversed in 9.6 hr. The average speed was slower than normal because of a combination of 20-ft swell and 8-ft seas, both nearly at right angles to the ship's course.

The beacon was dropped at Site 1100 at 1445 hr on 14 March, and a rotary core barrel bottom-hole assembly (RCB BHA) with a new C-4 coring bit was deployed. Because of the restriction of 2 m maximum heave in 300–650 m water depth, the vessel stood by from 1730 to 2000 hr to allow a large swell to ease.

Hole 1100A was spudded at 2030 hr, and coring proceeded to 33.8 mbsf with no recovery, before operations had to be stopped because of vessel heave. From 0115 to 0745 hr on 15 March, the vessel stood by while a large mixed swell from the west and north-northwest generated heave exceeding 3 m.

At 0930 hr on 15 March, Hole 1100B was spudded with the RCB and drilled ahead with a wash barrel to 34 mbsf. Once the wash barrel was retrieved, rotary coring began. It advanced only 2 m, however, before operations had to be stopped again because of heave. The BHA was tripped to the drill floor, and the throat of the bit was found to contain cobbles and gravel. The bit was cleaned and the BHA reassembled with the core barrel in place.

After the heave had subsided to acceptable levels, Hole 1100C was spudded. Coring advanced only 5 m, however, before heave again exceeded the threshold. When attempts to retrieve the core barrel with the wireline failed, the drill string was tripped to the surface for the second time. The BHA was partially disassembled in an attempt to discover why the core barrel could not be recovered with the wireline. The core barrel was found to contain more than 4 m of olive gray diamict (81% recovery [Table T1]). Investigation of the BHA revealed that a seal-bore

T1. Coring summary for Sites 1100, 1102, and 1103, p. 79.

drill collar, which is a standard fixture for the advanced hydraulic piston core/extended core barrel BHA, had been mistakenly added to the RCB BHA. This collar has a narrower inner diameter (3.8 in) than the standard controlled-length drill collar (4.3 in) normally used with the RCB BHA. The RCB core barrel could not pass through the narrower collar, either down (in Holes 1100A and 1100B) or up (in Hole 1100C), hence the difficulty in recovering core from the first three holes.

Hole 1100D was spudded at 1030 hr on 16 March. RCB coring advanced with poor recovery to 62.5 mbsf and was then stopped while a free-fall funnel (FFF) was deployed. Coring resumed to 76.8 mbsf when operations had to be stopped for a fourth time because of excessive heave. The FFF was reentered at 0330 hr on 17 March. After washing and reaming to bottom, coring resumed and advanced to 100.9 mbsf (Table **T1**). At 1000 hr on 17 March, and for the fifth time on site, coring was interrupted by heave exceeding 2 m (Fig. **F4**). The bit was pulled above the seafloor at 1030 hr.

F4. 3.5-kHz PDR record, Site 1100, 17 March 1998, **p. 32.**

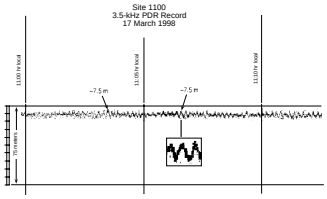


After deliberating whether to remain on site in difficult heave conditions, we decided to move to a new site in deep water (i.e., beyond the heave restriction) 120 nmi southwest. We hoped that after coring at the new site was concluded, the swell would have abated and would allow another attempt at deepening Hole 1100D. Of the 77.8 hr spent on site, only 20.5 were spent coring; 24.8 were inactive, waiting for the swell to abate, and the remaining time was occupied by reentry, tripping pipe, and other activities caused by the primary disruption. At 2030 hr the drill string was recovered and the beacon commanded into standby. The vessel was under way to Site 1101 at 2030 hr on 17 March.

After completing operations at Site 1101, we traveled 127 nmi back to Hole 1100D in 11.2 hr at 11.3 kt. The FFF was reentered at 1700 hr on 20 March. We reached the bottom of the hole and cored from 100.9 to 110.5 mbsf (Core 12R) with 0.54 m of recovery before being forced to stop by the 2-m heave limitation. After waiting about 6 hr, and because hole conditions were not promising, we decided to move to a new site.

## Site 1102

After the hydrophones were retracted, the vessel moved 6 nmi to Site 1102 (prospectus site APSHE-01A) using the thrusters. At 0645 hr on 21 March a beacon was deployed, and Hole 1102A was spudded at 1015 hr on 21 March. Coring advanced only 7.9 m (Core 1R) when excessive heave forced a halt. At 1425 hr on 21 March, Hole 1102B was spudded; however, it advanced only 7.5 m when coring was again suspended for excessive heave. While waiting for the swell to abate, a camera survey of the seabed within a 50-m radius of the site was conducted for 2 hr, allowing the choice of a boulder-free alternative hole position (see Movie **M1,** a QuickTime video, and **"Seabed Observations, Site 1102,"** p. 9). The heave subsided at 0130 hr on 22 March, but only long enough for Hole 1102C to be cored to 6.5 mbsf. Finally, Hole 1102D was spudded at 0945 hr. Unfortunately, hole conditions were poor. After coring to 14 mbsf in 3.25 hr, half the advance was lost when the driller picked up to 7 mbsf to retrieve the core. For the next 1.5 hr, the hole was washed and reamed with high, erratic torque. A total of 3 m was drilled but was again lost when the driller pulled back. It was clear that boulders, rocks, and gravel comprised a much greater portion of the sediment than was visible at the seabed, and the site was virtually undrillable. Of the 34.8 hr spent at Site 1102, 15.3 were passed waiting on weather related to excessive heave and only 8.5 in actual coring. The

remaining time was used for tripping, washing and reaming, and the camera survey.

## Site 1103

At 1730 hr, the vessel began the 16-nmi transit to Site 1103 (prospectus site APSHE-10A), arriving at 2000 hr on 22 March. Hole 1103A was spudded at 0130 hr on 23 March, with low expectations stemming from our recent experience with excessive ship heave. This time, however, fortune smiled, and ship heave was not a problem for the remainder of the leg.

RCB coring advanced quickly to 180.3 mbsf with very low recovery (2.6% or 4.7 m), which was attributed to hard rocks becoming jammed in the core catcher and subsequently preventing the soft till matrix from entering the core barrel. At 1900 hr on 23 March, the third FFF of the leg was deployed as insurance in case the weather deteriorated or an iceberg appeared. Coring resumed at 2015 hr and continued with improving recovery and slowing rates of penetration. Coring ended at 363.7 mbsf at 0730 hr on 25 March to allow time for logging. The average recovery for the hole improved to 12.3% with an average rate of penetration of 15 m/hr (Table T1).

The hole was washed and reamed to prepare for logging. The bit was difficult to release because of gravel inside the pipe, but following release, the bottom of the drill pipe was pulled back to logging depth (74 mbsf). On the first logging run, the triple combination (TC) tool string was unable to pass a tight spot at 242 mbsf. The hole was logged from this depth up to the seafloor with no repeat run. It took 2 hr to work the tool back into the drill pipe, and the bow-spring of the porosity tool was missing, presumably left in the hole. The second log (geological high-sensitivity magnetic tool [GHMT]) was also run from 241 mbsf to the seafloor. The Formation MicroScanner (FMS) was run successfully (from 241 m to the seafloor) only after repairing an electronic problem.

The hole was filled with mud and the drill string retrieved, which took longer than usual because of the routine end-of-leg inspection of drill-collar connections in the BHA. The positioning beacon was recalled, and the vessel departed the site for Cape Town at 1130 hr on 26 March. At 1800 hr, the *Polar Duk*e was released in accordance with the contract. The 3660-nmi transit to Cape Town took 13.8 days at an average speed of 11.3 kt. Leg 178 ended when the *JOIDES Resolution* docked in Cape Town at 0900 hr on 9 April 1998.

# LITHOSTRATIGRAPHY

## Site 1100

### Description

The total depth penetrated at Site 1100 was 100.9 mbsf (Hole 1100D), and ~4 m of sediment was recovered (4.3% recovery) from one core (Core 178-1100C-1R, 0–5 mbsf). Recovered sediment consists of poorly consolidated massive diamict (see "Lithostratigraphy," p. 3, in the "Explanatory Notes" chapter), with a diatom-bearing silty clay matrix (Fig. F5). Site 1100 lies at the edge of an area of hummocky, ice-scoured topography underlain by an acoustically transparent facies

F5. Vertical profile of massive, matrix-supported diamict from Hole 1100C, p. 33.

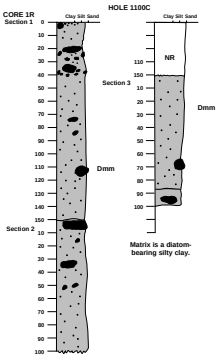

with indistinct layering and numerous point-source diffractions, interpreted by Vanneste and Larter (1995) as till.

### Interpretation

The character of the diamict recovered at this site is consistent with iceberg plowing of underlying till (e.g., Woodsworth-Lynas and Dowdeswell, 1993; Pudsey et al., 1994). Rare, open-shelf marine microfauna are reworked and abraded, consistent with faunal data collected from tills at Site 1097 (see "Biostratigraphy," p. 10). No age inference can be made from any of the material examined because of the poor nature of its preservation.

The core recovered at Site 1100 is compatible with currently available sedimentological data from the Antarctic Peninsula shelf, which are limited. Short (maximum length ~4 m) piston cores were taken from the shelf area by Pudsey et al. (1994) and from the area to the south by Pope and Anderson (1992). Several cores were collected near Site 1097. Sediments from these cores were described as "terrigenous gravelly muds" and interpreted as "compound glacial marine sediments" by Pope and Anderson (1992), meaning marine muds with ice-rafted debris. Such facies contain a low-diversity foraminiferal fauna with reworked sponge spicules and diatoms. Pudsey et al. (1994) also described a "structureless diamicton" transitional to laminated marine muds from a piston core site nearby. All these facies are regarded as the tops of tills reworked postdepositionally by iceberg turbation.

## Site 1103

### Description

Poor core recovery at Site 1103 allows a partial picture of sedimentary history to be established (Fig. F6). The total depth of the hole was 362.7 mbsf. Recovery from the upper 247 m was 2.3% but improved in the lower 115 m, where 38.7 m of sediment was recovered (34% recovery). This sediment consists of diamictites, poorly sorted sandstones, and mudstones that are interpreted as sediment gravity flows. In the absence of a continuous sedimentary record, stratigraphic subdivision is not possible. Nonetheless, several sedimentary facies can be identified. These record deposition of debris flows and poorly sorted turbidites on an active, glacially influenced slope. Biofacies data are insufficient to constrain age, water depths, or position relative to the shelf break.

### Lithofacies

Three lithofacies can be identified at Site 1103. These are massive and chaotically stratified diamictite (50% of recovered core), sandstone (25% of recovered core), and mudstone (25% of recovered interval) (Fig. F7).

## Diamictite

Diamictites are poorly sorted, lithified mixtures of clasts, sand, and mud (see "Lithostratigraphy," p. 3, in the "Explanatory Notes" chapter). At Site 1103, diamictites have a distinctive gray, asphalt-like appearance (Fig. F8A, F8B). Single beds of massive, unstructured, and

F6. Simplified lithostratigraphy showing lithofacies at Site 1103, p. 34.

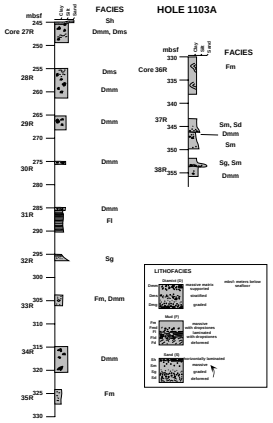


F7. Detailed graphic logs showing each section of recovery for Cores 178-1103A-27R through 29R and 31R through 38R, p. 35.

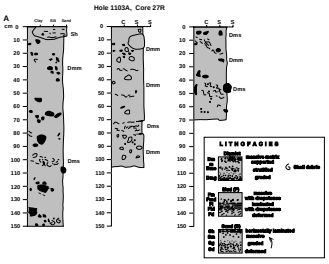


F8. Massive diamict, massive diamict facies, chaotically stratified diamict, and chaotically bedded diamict, p. 45.

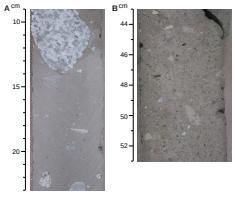

matrix-supported diamictite (Facies Dmm) range from 20 cm to 4.2 m in thickness (e.g., Sections 178-1103A-28R-2 through 28R-5; Fig. F7A, F7B, F7C). Beds are separated by thin (<30 cm) intervals of chaotically stratified facies (Facies Dms) showing highly deformed "flow-banding" (Visser, 1993) defined by "stringers" and "streaks" of mudstone (e.g., Sections 178-1103A-28R-1 and 28R-2; Figs. F7B, F8C, F8D). Diamictites vary from clast rich (>20% gravel) to clast poor (10%–20%), with the latter showing a smaller overall clast size (<2 cm). Gradations between poorly sorted muddy siltstone with dispersed clasts (Facies Fmd) and diamictite (Dmm) occur in several cores (Cores 178-1103A-33R and 37R; Fig. F7E, F7I). The largest clast size observed is 10 cm, and clast shape varies from angular to rounded. Measurements of clast long-axis dip angle show a wide variation from flat-lying to steeply dipping clasts (Fig. F9); preferred orientation of clasts and matrix is apparent in some thin (<20 cm) intervals that show a "flow fabric." Clasts are supported by a poorly sorted muddy sand matrix (ranging from 60% sand, 30% silt, and 10% clay to 30% sand, 50% silt, and 20% clay). The sand fraction is compositionally immature, with >40% lithic fragments.

A distinctive feature of diamictites at Site 1103 is the presence of large amounts of reworked marine mud in the form of discrete clasts and deformed matrix. Small mudstone clasts (<2 cm diameter) (variably termed "intraclasts," "rip-up clasts," "silt clasts," or "chips" in the literature [Pickering et al., 1989; Eyles et al., 1993]) are a ubiquitous component of diamictite facies (Fig. F8C) and in some intervals form as much as 20% of the total clast population, resembling the "clast breccias" of Pickering et al. (1989). In addition, a common component of these diamictites are irregular patches and stringers of dark mudstone. Examination of thin sections of chaotically stratified diamictite suggests that as much as 20% of the diamictite matrix consists of reworked mudstone. Mudstone clasts contain reworked Miocene marine biota and Cretaceous radiolarians (see "Biostratigraphy," p. 10). Shell fragments are common and include a complete barnacle valve in Section 178-1103A-28R at 120 cm.

F9. Distribution plots of clast long-axis dip angles for diamictites from Site 1103, p. 47.

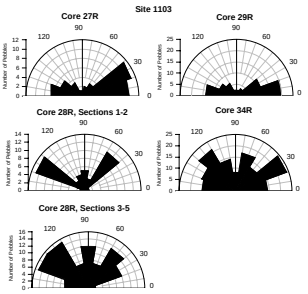


## Chaotically Stratified and Massive Sandstones

Beds of chaotically stratified and massive muddy sandstone (Sd and Sm, respectively; Figs. F7, F10A) are from 2 cm to 3 m thick (Cores 178-1103A-37R and 38R; Fig. F7I, F7J). Sandstones are very poorly sorted (65% sand, 25% silt, and 10% clay) and gray in color. Bed bases are sharp and erosional; bed tops were not recovered. Chaotically stratified sandstones show extensive soft-sediment deformation and incomplete mixing of different grain sizes (Fig. F10A). Thin (up to 2 cm) graded intervals of conglomerate and mud clasts are present at bed bases (Fig. F7J). Section 178-1103A-32R-1 (Fig. F7D) consists of a thin (38 cm) interval of parallel-laminated sandstone, with successive laminations fining upward and showing small-scale "convolute" soft-sediment deformation. Thin beds of steeply dipping sandstone occur in Core 178-1103A-33R interbedded with mudstone and diamict (Figs. F7E, F10B). Floating granules, gravel, and mud clasts are present throughout the sandstone facies, and shell fragments are present in all cores.

F10. Chaotically bedded sandstone and thin sandstone bed, p. 48.

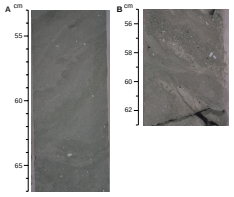

## Mudstone

Fine-grained sediments at Site 1103 are very poorly sorted silty mudstones. The dominant facies is massive (Facies Fm; Fig. F11A), with a

F11. Massive mudstone facies and weakly laminated mudstone facies, p. 49.

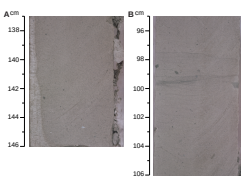

subordinate weakly laminated facies (Facies Fl; Fig. F11B, F11C). Laminations have no systematic structure but are defined by thin (<1 mm) streaks and sheared-out "blebs" of siltstone and mudstone. Mudstones show transitions from massive to laminated facies with no systematic trends upcore (Core 178-1103A-31R; Fig. F7D). Mudstones are very poorly sorted (5%–20% sand, 35%–70% silt, and 10%–60% clay), with the same gray color as diamictites and sandstones. "Floating" clasts are present in massive and laminated mudstones (Facies Fmd and Fld respectively; Fig. F7). Bioturbation is absent. Deformation structures, such as small-scale normal faults (e.g., intervals 178-1103A-34R-1, 127–130 cm; 35R-1, 45–50 cm, and 36R-3, 20–30 cm; Fig. F7) and dewatering structures (Fig. F7), are present throughout. Section 178-1103A-37R-3 shows pillow structures and associated downward-penetrating dikes below a thin (4 cm) bed of medium-grained massive sandstone (Fig. F7I). Section 178-1103A-31R-1 is composed of interbedded laminated and massive mudstone, with dispersed clasts, and diamictite (Fig. F7D). In other cores (Core 178-1103A-33R; Fig. F7E), there are gradations among diamictite facies, mudstone with dispersed clasts, and mudstone lacking any clasts.

## Environmental Interpretation

Massive diamict(ite) is not diagnostic of any one depositional environment and can be deposited in a wide range of settings. Interpretation relies on examination of other related facies to provide a context for deposition. Diamictites at Site 1103 are associated with massive sandstones and siltstones. The former can be identified as "disorganized muddy sands" of Pickering et al. (1989), deposited either by very high density turbidity currents or very fluid sand-mud debris flows. A muddy matrix creates sufficient buoyancy to enable clasts to be freighted within the flow, and grading is absent, except for thin "coarse-tail" graded intervals at bed bases (e.g., Fig. F7J). Chaotically bedded and massive, poorly sorted sandstones record very rapid deposition and rapid "freezing" of concentrated dispersions transported by sediment gravity flows. Horizontally laminated sandstones in Core 178-1103A-32R represent the B division of turbidites (Pickering et al., 1989).

Massive and irregularly laminated siltstones also record rapid deposition from dense turbidity currents or muddy debris flows; lamination is probably generated when the flow progressively "freezes" from the bed base to the top during deposition. Widespread soft-sediment deformation structures attest to rapid deposition and local fluidization generated by rapid dewatering. Additional deformation, such as faults, may result from downslope creep.

Stratigraphic successions of diamictites interbedded with poorly sorted massive sandstones and siltstones are classically associated with downslope resedimentation of poorly sorted debris by sediment gravity flows. Beds of massive diamictite at Site 1103 (Facies Dmm; as much as 4.2 m thick) that show variation in clast content and contain large amounts of reworked sediment such as silt clasts and mudstone are, consequently, identified as debris flows (debrites). Successive flows are probably recorded by the interbedding of massive facies with thin zones (<30 cm) of crudely stratified diamict with mud stringers (Facies Dms; Fig. F7). Muds were probably deposited on bed tops between flow events and were subsequently reworked and incorporated in later flows and deposited as chaotically stratified diamict facies (Dms) that show flow banding (Visser, 1993). The absence of bioturbation and the lack of

any in situ marine biota from mudstones suggest short recurrence intervals between flows. Relatively coarse-grained turbidites, such as those recovered at Site 1103, are deposited rapidly; high overall sedimentation rates are indicated by common water-escape structures and soft-sediment deformation.

Sediments recovered at Site 1103 record an active slope close to a source of poorly sorted glacial debris, such as till. In common with other widely reported debrite/turbidite facies associations (e.g., Walker, 1992), diamictite, sandstone, and mudstone probably represent an evolutionary sequence recording progressively better sorting downslope and the loss of the coarse fraction (clasts) from debris flows in response to increasing water content and nonlinear processes. Consequently, these facies are intimately interbedded and show upcore transitions from clast-rich to clast-poor diamictite and from diamictite to pebbly mudstone to mudstone (e.g., Core 178-1103A-33R; Fig. **F7E**). Protracted downslope transport results in rapid expulsion of mud and the generation of well-sorted graded conglomerates, sandstones, and siltstone turbidites (e.g., Pickering et al., 1989; Walker, 1992; Eyles et al., 1993). Such facies are limited at Site 1103 to thin (<10 cm) sandstone beds in Cores 178-1103A-32R, 33R, and 37R (Fig. **F7D, F7E, F7I**). Because of the very poor overall sorting in turbidites at this site, an upper slope setting close to an area of active slumping is suggested. Biofacies data are limited and suggest an outer shelf setting (see **"Biostratigraphy,"** p. 10). Unfortunately, age-specific material was not recovered. The abundance of reworked mudstone and marine biota is similar to the characteristics noted for deformation tills recovered at Site 1097 (see **"Lithostratigraphy,"** p. 3, in the "Site 1097" chapter) and indicates a till source for debrites at Site 1103.

The sedimentary record at Site 1103 is consistent either with an upper continental slope setting or with deposition on the shelf, such as within an overdeepened trough or along an ice margin. Glaciation of continental shelves results in large subglacial fluxes of sediment to the outer shelf edge and the remobilization of muddy debris and existing shelf edge sediments downslope as slumps, debris flows, and turbidity currents. Such facies have been described from the modern Antarctic continental shelf and slope by Anderson et al. (1979, 1980, 1984). Detailed facies descriptions of debrite and turbidite associations from other settings have been presented by several workers (e.g., Visser, 1983; Hill, 1984; Miall, 1985; Young and Gostin, 1991; Eyles, 1990, 1993; Eyles et al., 1993; Gipp, 1993). It is possible that the debrite/turbidite facies association recovered at Site 1103 provides insight into sedimentary processes operating on the present continental slope and the probable composition of slope "foresets" underlying the present continental slope. Alternatively, such facies may be representative of the "till deltas" argued to be forming at the grounding line of Ice Stream B of the Ross Ice Shelf (Alley et al., 1989). The existence of similar till deltas on the continental shelf of the Antarctic Peninsula has been proposed by Vanneste and Larter (1995) on the basis of interpretation of deep-tow boomer profiles.

## Seabed Observations, Site 1102

While waiting for the swell to subside at the continental shelf edge, *JOIDES Resolution* scientists undertook a survey of the seabed close to Site 1102, using the camera usually lowered around the drill string in order to effect reentry. The survey covered an area ~50 m × 50 m and

took ~2 hr to complete. Two short sections of this survey (23:58:00 to 00:00:00 and 00:19:00 to 00:22:20) are presented as a QuickTime video (Movie M1). The view is of the seabed, illuminated by camera lighting; the drill bit (~28 cm diameter) and lower BHA remain a constant distance from the camera but move with respect to the seabed as a result of slow, regular ship heave and horizontal ship motion. The heave compensator was turned off during the survey; ship heave was estimated (from the acoustic signal of a pinger attached to the camera) as 3 m average, 5 m maximum.

The camera survey showed a carapace of coarse, subrounded-to-angular blocks as much as a meter across over much of the seabed. We saw sharp transitions from patches of mainly fine-grained seabed sediment, a few meters across, to larger areas of blocky seafloor (see, for example, 23:59:40). We could not establish shape or orientation of areas of different texture, or any sedimentary structures.

Having failed to spud in at Holes 1102A and 1102B, we used the survey to choose a better place (showing finer grained sediment at the seabed) to spud in at Hole 1102C. Neither of the succeeding holes was successful, however, and we conclude that a layer of coarse, angular blocks also underlies the areas of fine-grained seabed, the total thickness probably exceeding 10 m.

Such a carapace has not been seen or sampled elsewhere on the continental shelf. We speculate that the blocks were transported to the shelf edge within subglacial till at times when the ice sheet was grounded to the shelf edge, with the likely addition of postglacial ice-rafted debris. Subsequent proglacial processes (plowing by iceberg keels, with the suspension of fine-grained sediment and its transport across the nearby shelf edge by tides and currents) have left only a coarse lag deposit on the outermost shelf. We are uncertain if such a coarse, shelf-edge facies is preserved in situ within the geologic record of the glacial prograded wedge or if it is moved onto the upper slope during the next grounding line advance.

## BIOSTRATIGRAPHY

A single hole of 362.7 mbsf was rotary drilled at Site 1103 to obtain glaciomarine and preglacial sediments. The upper part of Hole 1103A (0–247.3 mbsf) and all of Hole 1100D (0–100.9 mbsf) contain intervals of poor recovery: 2.3% and 4.8%, respectively. Recovery at Site 1102 consisted of coarse clasts of hard rock, originally from diamicts or dropstones, with the exception of one small sample of sediment from Hole 1102C. This sediment became a single small paleontological sample (Sample 178-1102C-2R-CC) that was examined only for foraminifers. It was found to contain rare planktonic foraminifers (*Neogloboquadrina pachyderma* sinistral) and was barren of benthic foraminifers. Samples 178-1100D-1R-CC through 12R-CC (0.05–100.9 mbsf) and Samples 178-1103A-1R-CC through 24R-CC (0.2–218.4 mbsf) contain isolated large clasts with small amounts of fine sediment on or between them. Microfossils (radiolarians, diatoms, and foraminifers) are rare to barren in these sediments, and those that are present could be reworked. The presence of late Pliocene and Pleistocene diatoms suggests that the sediments in Hole 1100D and the upper part of Hole 1103A were deposited during or after this time. The lower part of Hole 1103A, between 247 mbsf and the bottom of the hole (Cores 178-1103A-27R [247.3 mbsf] through 38R [362.7 mbsf]), had better core recovery (3% to 67%). It

contains marine diamictite, mudstone, and sandstones (see "Lithostratigraphy," p. 5). The three fossil groups examined were very rare in abundance and provide poor age assignments (pre-Pliocene, possibly late Miocene, based on diatoms).

## Diatoms

### Site 1100

All core-catcher materials from Hole 1100D were examined. However, only poorly preserved, fragmented, rare diatoms were observed from the upper part of this hole. The appearance of *Fragilariopsis kerguelensis* in Samples 178-1100D-1R-CC through 3R-CC suggests that those sediments are younger than the first occurrence age of this species (3.3 Ma). Samples 178-1100D-4R-CC through 12R-CC were barren or contained only unidentifiable diatom fragments.

### Site 1103

At Site 1103, smear slides of all core-catcher samples, and additional samples taken within the split sections of the core, were examined for diatoms. Diatoms were mostly rare at Site 1103. Valves were often fragmented beyond the limit for identification, yet these fragments can be abundant in the material recovered.

Samples 178-1103A-1R-CC through 6R-CC (55.2 mbsf) contain only rare fragments of *F. kerguelensis* (present to 3.3 Ma) (Fig. F12). The absence of Pliocene to early Pleistocene diatoms, which appear in the middle part of this hole, suggests an age younger than early Pleistocene.

The middle part of this hole, Samples 178-1103A-11R-CC (93.7 mbsf) through 24R-CC (228 mbsf), contains low numbers of several biostratigraphic index species. Co-occurrence of *Actinocyclus ingens, Fragilariopsis barronii, Thalassiosira insigna, Thalassiosira inura, Thalassiosira oestrupii,* and *Thalassiosira torokina* suggests that these samples are younger than the first appearances of these species and may be placed into the *Thalassiosira kolbei* Zone or the lower part of the *A. ingens* Zone (Fig. F12). The absence of *Thalassiosira vulnifica* supports this age assignment. The lower portion of Hole 1103A from Samples 178-1103A-31R-1, 22 cm (286 mbsf), to the bottom of the hole at Sample 178-1103A-38R-CC (355.34 mbsf) has a lower abundance of diatoms and no Pleistocene to Pliocene species. The occurrence of *Denticulopsis simonsenii* s.l. suggests that this interval is younger than the first occurrence of this species (14.18 Ma). A trace occurrence of *Nitzschia januaria* and *Rouxia californica* in Sample 178-1103A-31R-1, 63 cm (286.4 mbsf), may allow this sample to be placed in the late Miocene (Fig. F12). The better preservation of *D. simonsenii* s.l. may indicate a close source area, if the specimens are reworked, or an environment with high sedimentation rate (see "Lithostratigraphy," p. 5). Light yellowish gray pebble-sized clasts of soft sediment within the diamict in Core 178-1103A-34R contain a nearly monospecific diatom assemblage dominated by *Stephanopyxis grunowii* and *Thalassionema/Thalassiothrix* fragments. Another clast from the same core has a different diatom assemblage, dominated by *Denticulopsis* spp. but still having a high diversity, including other species (*Thalassiothrix/Thalassionema* spp. and *Fragilariopsis/Nitzschia* spp.). The existence of these well-preserved clasts within the diamictite matrix and the lack of abundant diatom species in the matrix add support for a close source location for the clasts.

F12. Occurrence of diatoms, radiolarians, and planktonic foraminifers at Site 1103, p. 51.

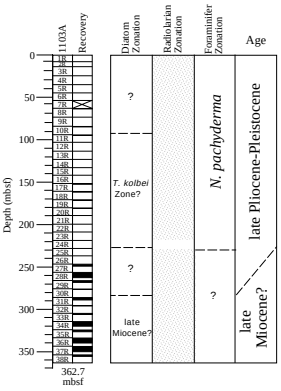

## Radiolarians

### Site 1100

Trace amounts of radiolarians were observed at Site 1100. Most of the skeletons were reworked or recrystallized. No age-diagnostic in situ specimens were found.

### Site 1103

Radiolarians are sparse with poor to moderate preservation in core-catcher samples from Site 1103, making biostratigraphic determinations nearly impossible (Fig. F12). Radiolarians are present in Samples 178-1103A-1R-CC (10.8 mbsf), 6R-CC (55.2 mbsf), 13R-CC (122.6 mbsf), 23R-CC (218.4 mbsf), and 24R-CC (228.0 mbsf). Reworked Cretaceous radiolarians were present in all but Sample 178-1103A-1R-CC. Sample 178-1103A-24R-CC (228.0 mbsf) contained an assemblage indicative of the Upsilon Zone, but considering the age based on diatoms, this is probably reworked. Marker species were not encountered in any other samples.

## Foraminifers

Foraminifers are absent to rare in core-catcher samples from Sites 1100 and 1103. In Samples 178-1103A-1R-CC through 24R-CC (0.2–218.4 mbsf) and Samples 178-1100D-1R-CC through 12R-CC (0.05–100.9 mbsf), the fauna contains rare, well-preserved, and white *Neogloboquadrina pachyderma* sinistral along with older, reworked, darker colored benthics and planktonics. In addition, *Inoceramus* prisms, sponge spicules, and recrystallized radiolarians are found. In Samples 178-1103A-27R-CC through 35R-CC (250.58–326.49 mbsf), the foraminiferal fauna was rare, with more evidence of reworking. Samples 178-1103A-31R-CC and 33R-CC contain the most abundant assemblages, with well-preserved specimens of *Cassidulinoides parkerianus* along with a substantial reworked component. The lowest three samples, 178-1103A-35R-CC through 38R-CC (338.77–355.34 mbsf), are barren of foraminifers.

# PALEOMAGNETISM

## Split-Core Measurements

Archive halves of rotary-cored sections recovered at Sites 1100 and 1103 were measured at 5-cm intervals. Only a few small rocks were recovered at Site 1102; therefore, no sections were measured. The sensor velocity on the magnetometer was set at 10 cm/s to avoid saturation of the magnetometer electronics. This saturation results from high-amplitude variations of the magnetic flux induced by the rapid motion of highly magnetized material. Sections of cores containing pebbles and cobbles (dropstones or rocks from glacial units) were not measured because their magnetization is unrelated to the ambient geomagnetic field at the time of deposition and cannot be used to construct a magnetostratigraphic record. In addition, many dropstones have a very high intensity of magnetization, which causes saturation in the cryogenic magnetometer electronics.

## Discrete Samples

Measurement of discrete samples from the working halves of cores and subsequent data analysis followed the methods described in **"Paleomagnetism,"** p. 16, in the "Site 1095" chapter. Stepwise alternating field (AF) demagnetization of samples revealed that the drill-string overprint was dominantly vertically down, showing the behavior observed at all previous sites during Leg 178. The drill-string overprint was mostly or wholly removed by partial AF demagnetization of the natural remanent magnetization (NRM) at the 10-mT level. Samples from intervals identified as diamictites (see **"Lithostratigraphy,"** p. 5) had unstable directions of magnetization (Fig. **F13A**). After removal of the drill-string overprint, the intensity of the signal was within the noise level of the magnetometer, and no characteristic remanent magnetization could be identified (Fig. **F13B, F13C, F13D**). These observations, combined with the extremely high values of magnetic susceptibility (see **"Physical Properties,"** p. 15, and **"Downhole Measurements,"** p. 19), are consistent with a magnetic mineral assemblage dominated by coarse-grained magnetite, termed "multidomain," which is not an effective geomagnetic field recorder (see **"Paleomagnetism,"** p. 11, in the "Site 1097" chapter).

The diamictites at Site 1103 were unsorted, and the possibility exists that finer grained magnetic minerals are present. To examine whether the signals from effective (1- to 10-µm magnetite) and ineffective magnetic recorders (>10-µm magnetite) could be separated, low-temperature demagnetization (LTD) was employed to erase signals carried by multidomain grains. LTD uses the crystal structure transition that occurs in magnetite at 110–120 K, termed the "Verwey transition." At this crystallographic transition, the magnetocrystalline anisotropy goes to zero, which allows a reordering of magnetic moments within domains and domain walls. Cooling through this transition and subsequent warming is performed in zero magnetic field, which eliminates even the slightest magnetic bias. Domain walls, originally formed in response to the mineral's previous thermal history (thermal remanence) and exposure to the Earth's magnetic field through time (viscous remanence), reform in such a way that the vector sum of the magnetic moments is near zero. Fine-grained magnetite (0.03–10 µm) is unaffected by LTD because the shape anisotropy of magnetite is sufficient to keep the magnetic moments locked to the long axis of the mineral grain during the Verwey transition. By using LTD to remove the signal carried by multidomain grains, the residual signal can be examined more closely.

Three pairs of discrete samples were collected from Site 1103 for LTD. In each pair, both samples were taken from the same 2-cm interval, when possible. Two pairs were taken from diamictites, one pair from Core 178-1103-27R and one from Core 178-1103-28R, and the third pair from a finer grained interval in Core 178-1103-28R. One member of each pair was subjected to the regular AF demagnetization. The second member of each pair was measured at the 0 mT (NRM) level and was then subjected to LTD. The LTD samples were placed inside a triple-layer mu-metal shield, which reduces the intensity of the ambient laboratory field by several orders of magnitude. The samples were covered in liquid nitrogen (77 K) and then thermally re-equilibrated to room temperature for 1 hr while remaining inside the mu-metal shield. The samples were remeasured at the 0-mT step and then subjected to stepwise AF demagnetization. The sample from Core 178-1103-27R lost

F13. AF demagnetization of discrete Sample 178-1103A-27R-1, 13–15 cm, **p. 52.**

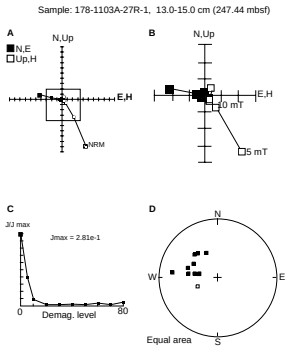

75% of its signal as a result of LTD (Fig. F14A), which suggests that multidomain minerals dominate the magnetic mineral assemblage. The residual signal of the sample was very weak and dropped into the noise level of the magnetometer at the 10-mT demagnetization level. The measurable signal was oriented vertically downward, the direction of the drill-string overprint (Fig. F14B). In addition, the positive inclination measured in Sample 178-1103A-27R-1, 14 cm, is the opposite of the reversed polarity measured in this same interval in the archive half of the core. The second pair of samples from a diamictite (Section 178-1103A-28R-4) had stable directions during regular AF demagnetization and LTD. The sample from this pair lost only 30% of its signal during LTD.

The sample from the finer grained lithology lost 60% of its intensity after LTD, the same percentage of signal that its twin lost at the 10-mT demagnetization level. In this instance, LTD removed the drill-string overprint. The finer grained sample retained a strong, stable remanence after LTD, and the direction had a steep negative inclination. These observations suggest that effective geomagnetic field recorders are not consistently present in the diamictites, and the polarities measured in that lithology are not trustworthy.

F14. AF demagnetization of discrete Sample 178-1103A-27R-1, 15–17 cm, following LTD, p. 53.

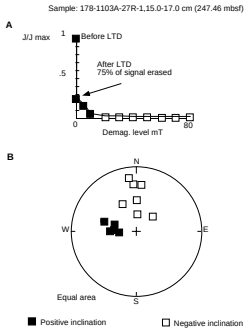


## Magnetostratigraphy

One goal of the leg was to date glacial events using one of several dating methods. Unfortunately, the intermittent nature of deposition on the continental shelf, the inability of coarse-grained magnetic minerals (common in diamictites) to record the paleomagnetic field, and sparse recovery together prohibit any reasonable age assignment from magnetostratigraphic constraints alone. First, the deposition of diamictites and turbidites, the two main lithologies (see "Lithostratigraphy," p. 5), is discontinuous. Diamictite units are probably deposited in a very short time with no clear mechanism for acquisition of a depositional remanence. Turbidites also are rapidly deposited, and some have given shallower than expected remanence directions at other Leg 178 sites (see "Paleomagnetism," p. 11, in the "Palmer Deep [Sites 1098 and 1099]" chapter). A hiatus between each change in lithology is possible. A more severe interpretation limitation comes from the large gaps in recovery, even within the interval with highest recovery (247–356 mbsf). Within this interval, the gaps are one to three times the size of the recovered intervals. A smaller problem is that the position of the recovered core is not known within the cored interval.

Finally, the magnetic minerals in the core have been shown to be ineffective paleomagnetic field recorders. For example, Core 178-1100C-1R is from the upper 10 m of the hole but has a reversed polarity magnetization at the 30-mT demagnetization level, contrary to the expected Brunhes normal polarity (Fig. F15). For Hole 1103A, AF demagnetization and LTD experiments show that no stable component is present in the diamictites other than a drill-string overprint. In addition, logging data from the GHMT show that the induced magnetization dominates the signal in Hole 1103A, which is consistent with a coarse-grained magnetic mineral assemblage (see "Downhole Measurements," p. 19). The GHMT signal in Hole 1103A contrasts strongly with that seen in Hole 1095B, where the induced component was negligible and the polarity signal clear.

Finer grained lithologies (silty clays, rather than diamictites) at Site 1103 gave stable paleomagnetic results (Fig. F16). However, given the

F15. Inclination vs. depth and intensity of magnetization vs. depth after AF demagnetization at 30 mT for Hole 1100C, p. 54.

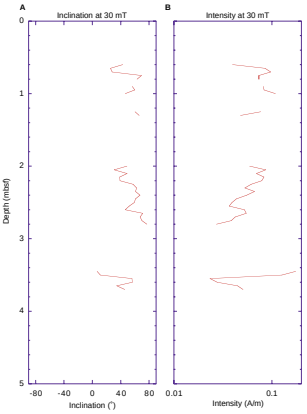


F16. AF demagnetization of discrete Sample 178-1103A-31R-3, 3–5 cm, p. 55.

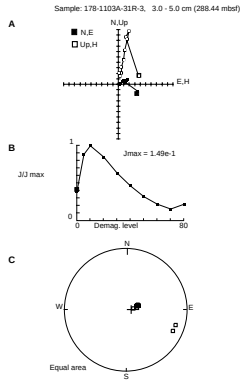

above uncertainties and that the finer grained lithologies comprise only ~15 m of the recovery from Hole 1103A, a magnetostratigraphic interpretation would be unfounded. Cores 178-1103-27R through 37R may provide a sequence of two normal and two reversed polarities (Figs. F17, F18), but this interpretation ignores the complications discussed above. Furthermore, even with a short sequence of reversals in an undated stratigraphic section with unknown sedimentation rates, a unique interpretation is impossible.

# ORGANIC GEOCHEMISTRY

No samples were collected from Sites 1100 or 1102. At Site 1103, routine monitoring of hydrocarbon gases was performed on every core recovered on deck. Methane was identified in all headspace samples, and ethane occurred at a concentration of 1 ppm in the last sample of the hole (Table T2).

# INORGANIC GEOCHEMISTRY

## Interstitial Water Chemistry

We could not obtain interstitial water samples at Sites 1100, 1102, and 1103 along the shelf transect because of the lithified nature of most material recovered, except for one sample from 2.95 mbsf in Hole 1100C (Table T3). The interstitial water chemistry of this diatom-bearing silty clay shows evidence of bacterial degradation of organic matter and silica dissolution comparable to that observed in the uppermost few meters of sediment at Sites 1095, 1096, and 1101 on the continental rise. The sulfate concentration (29 µM) does not differ significantly from seawater, so active sulfate reduction must occur at greater depths. The high concentration of manganese (29 µM), however, reflects dissolution of Mn oxides under suboxic conditions. Slightly increased alkalinity (3.56 mM), ammonium (77 µM), and phosphate (9.5 µM) relative to seawater also reflect moderate amounts of organic-matter decay. Dissolved fluoride (62 µM) has decreased slightly from its seawater concentration and suggests fluoride uptake by the sediment, whereas the high dissolved silica concentration (0.57 mM) indicates that biogenic opal begins dissolving above 3 mbsf. All other dissolved constituents (e.g., calcium, magnesium, potassium, and strontium) have concentrations similar to seawater and thus show no signs of either organic or inorganic diagenesis.

# PHYSICAL PROPERTIES

## Whole-Core Measurements

### Multisensor Track (MST)

Natural gamma-ray activity (NGR), magnetic susceptibility, and gamma-ray attenuation porosity evaluator (GRAPE) density were measured on whole-round samples (see "Physical Properties," p. 20, in the "Explanatory Notes" chapter). Because of the low recovery at the shelf sites (Sites 1100, 1102, and 1103), only a few cores were available for MST measurement. At Site 1100, all the MST measurements were made

F17. Inclination vs. depth after AF demagnetization at 30 mT for the shelf transect sites, p. 56.

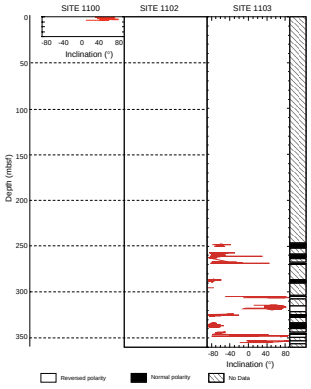


F18. Inclination vs. depth and intensity of remanence vs. depth after AF demagnetization, p. 57.

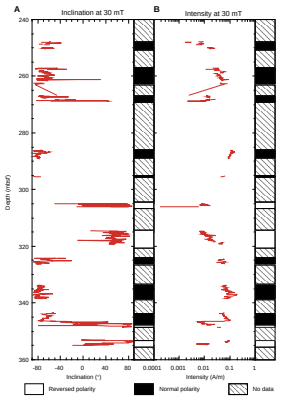


T2. Summary of gas concentrations for Hole 1103A, p. 81.

T3. Profiles of interstitial water chemistry at Hole 1100C, p. 82.

on one core (Core 178-1100C-1R). No measurements were made from Site 1102. At Site 1103, GRAPE density, magnetic susceptibility, and NGR activity were measured from 247.33 to 355.80 mbsf (Cores 178-1103A-27R through 38R). No *P*-wave measurements were made on the cores because of the many air gaps in the whole-core sections.

## Magnetic Susceptibility

Whole-core magnetic susceptibility was measured at 2-cm intervals (averaged over 2 s). The raw data for Site 1100 are provided **on CD-ROM and the World Wide Web** and are presented in Figure **F19.** Limited recovery in the upper sections of other shelf sites renders comparison impossible. The raw data for Site 1103 are provided **on CD-ROM and the World Wide Web** and are presented in Figure **F20.** The data show no discernibly consistent relationship with the described sediment column (see **"Lithostratigraphy,"** p. 5, and discussion below).

## GRAPE Bulk Density

Density was measured by gamma-ray attenuation at 2-cm intervals (averaged over 2 s at each point). The raw data for Site 1100 are provided **on CD-ROM and the World Wide Web** and are presented in Figure **F19.** Again, limited recovery in the upper sections of other shelf sites renders comparison impossible. The raw data for Site 1103 (**on CD-ROM and the World Wide Web;** Fig. **F20**) show no obvious correlation with lithostratigraphic variation.

## *P*-wave Velocities

The raw data for Site 1100 are provided **on CD-ROM and the World Wide Web** and are presented in Figure **F19.** Limited recovery in the upper sections of other shelf sites renders comparison impossible.

## Natural Gamma Radiation

Whole-core NGR emissions (averaged over 15 s) were counted at 15-cm intervals. The raw data for Site 1100 are provided **on CD-ROM and the World Wide Web** and are presented in Figure **F19.** The raw data for Site 1103 are provided **on CD-ROM and the World Wide Web** and are presented in Figure **F20.** The data show no obvious correlation with lithostratigraphic variation.

## Cross-Comparison

In the absence of a continuous record and any obvious downhole correlation between the MST data sets and the lithostratigraphy, the data were cross-plotted by facies to determine whether relationships existed. Cross plots of magnetic susceptibility and NGR data for the upper and lower diamicts are shown in Figure **F21A.** From the plot it can be seen that the diamict sequences between 246 and 286 mbsf (upper diamict) and 304 and 321 mbsf (lower diamict) form two distinct populations. This may suggest that the diamicts are derived from different source materials or may reflect the differences in grain size or packing between the two materials. Smear-slide analysis (see **"Site 1103 Smear Slides,"** p. 37) shows that the clay and silt contents in the matrix of the upper diamict average ~67.6% and 37.2%, respectively; in the lower diamict, the values are 29% and 15%. Low clay and silt con-

F19. Raw NGR, GRAPE density, magnetic susceptibility, and *P*-wave velocity data for Site 1100, **p. 58.**

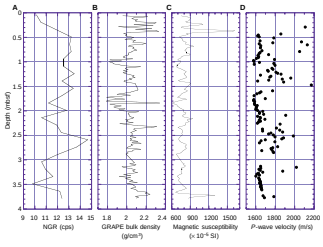


F20. Raw NGR, GRAPE density, and magnetic susceptibility data for Site 1103, **p. 59.**

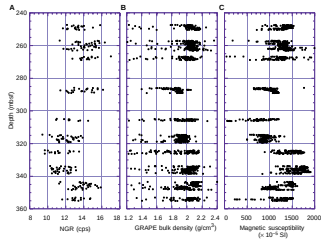


F21. Lithofacies from Site 1103 in magnetic susceptibility vs. NGR space, **p. 60.**

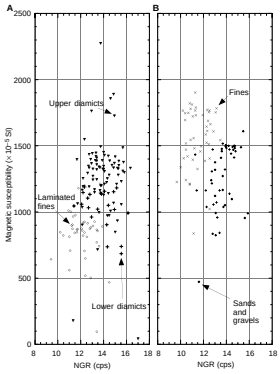

tents in the lower diamict might be expected to reduce the NGR and susceptibility signals. However, the other nondiamict lithofacies form clusters of values in susceptibility-NGR space (Fig. F21A, F21B), with no consistent relationship with grain size. The sands and gravels show two populations (not size dependent), which are coincident with the upper diamict and the laminated sediments.

## Split-Core Measurements

### Index Properties

Gravimetric and volumetric determinations of index properties were made for two samples from each of Holes 1100C and 1100D and 18 samples from Hole 1103A. One sample was taken from Hole 1103A every first and third section per core, where possible. Wet mass, dry mass, and dry volume were measured, and from these measurements, percentage water weight, porosity, dry density, bulk density, and grain density were calculated (see "Physical Properties," p. 20, in the "Explanatory Notes" chapter). The raw data for Site 1100 are provided on CD-ROM and the World Wide Web and are presented in Figure F22. The raw data for Site 1103 are provided on CD-ROM and the World Wide Web and are presented in Figure F23.

Bulk density for Site 1103 correlates well with GRAPE density (Fig. F23A), although the two measurements of density are offset as at other sites. This offset shows a slight decrease with depth, which may reflect the effects of lithology and compaction on core disturbance.

Porosity values at Site 1103 show a pattern similar to that at Site 1097. The diamicts between 245 and 285 mbsf show a porosity of ~20% (Fig. F23B), ~10%–15% lower than the laminated sediments directly below them. The diamicts between 300 and 320 mbsf show no drop in porosity and are 5%– 15% more porous than the diamicts 15 m higher in the sequence. Porosity is related to sediment sorting, cementation, and the stress history of the sediments. The lower levels of clay and silts in the lower diamict (see "Lithostratigraphy," p. 5) suggest that they are better sorted and may maintain a higher porosity under stress (horizontal or vertical). Thin-section analysis ("Micromorphology," p. 18) also suggests cementation in the sediments, although there is little difference between the upper and lower diamicts. Alternatively, the upper material may have undergone shear or overburden compaction to a greater extent than the lower material (see "Lithostratigraphy," p. 3, and "Physical Properties," p. 15, both in the "Site 1097" chapter, for further details). However, if the porosity is shear dependent, this shear cannot have occurred in a turbulent debris flow, as the open upper surface would have ensured mixing. Any shear reduction must therefore be a subglacial relic that survived in a plug-flow mass movement, or imply plug-flow layers within any debris flow (to have prevented turbulence).

### Discrete *P*-wave Velocities

Discrete *P*-wave velocity measurements were made on cores of Sites 1100 and 1103 for the depth interval 0–3.5 mbsf (Site 1100) and 75–355 mbsf (Site 1103) using the Hamilton Frame sensor pair (PWS3) of the velocity-strength system. All measurements were done using single unfractured matrix or matrix-supported pieces placed directly (without the liner) between the Hamilton Frame heads. The data for Site 1100

F22. GRAPE and MAD bulk density, grain density, and porosity from Site 1100, p. 61.

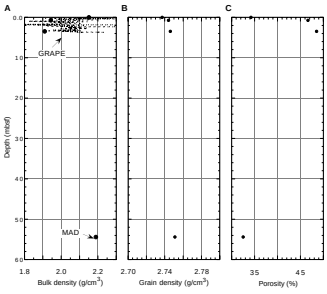


F23. GRAPE and MAD bulk density, grain density, and porosity from Site 1103, p. 62.

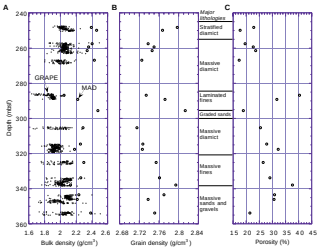

(five values) are provided **on CD-ROM and the World Wide Web.** The data for Site 1103 are provided **on CD-ROM and the World Wide Web** and are given in Figure **F24**.

The low recovery zone (0–240 mbsf) of Site 1103 is covered by only nine data values, one of which is from a granite clast. With the exception of the clast, the velocities vary between 1760 and 2660 m/s. In Cores 178-1103A-27R through 38R (247–355 mbsf), the data coverage is much better, with an average spatial resolution of 2.3 m. The lower lithified part of the site shows *P*-wave velocities between 2000 and 3700 m/s. The diamictite layers with pebble size clasts (3000–3500 m/s) contrast sharply in *P*-wave velocity with the poorly sorted sandy units (2000–2700 m/s).

Although measurements from Site 1100 samples are limited, they provide the only direct *P*-wave velocity information collected near the seafloor for all shelf sites.

F24. PWS3 data for Site 1103, **p. 63.**

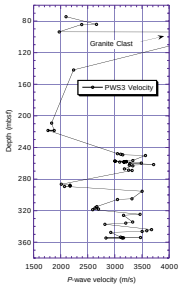


## Micromorphology

Samples were taken from Cores 178-1103A-28R and 34R for impregnated thin-section analysis to determine the structural composition of the diamicts and their response to their stress history. The latter often gives information on the physical properties of the sediment in the past.

Sample 178-1103A-28R-1, 85 cm, is a sand-rich (40% sand) diamict that contains a lens of fines, matching the lithostratigraphic assignment of the material as a stratified matrix-supported diamict. The fines and diamict all show a strong grain alignment at 10° from the horizontal, which suggests shear after the materials were deposited. Such a morphology may indicate subglacial deposition and shear. The alternative, matching the lithostratigraphic interpretation, is that the materials were deposited as flow bodies (presumably at the angle of repose) and were then reactivated at some later point as a whole unit.

Sample 178-1103A-28R-2, 27 cm, is a less sand-rich material (15% sands) than that above, with a subhorizontal grain fabric and bands of stronger alignment suggesting subhorizontal shear. This fabric was then disrupted by low-strain shear zones mirrored at ~30° around the horizontal and bands of fines in the same directions. These later fabrics probably indicate subhorizontal compression and dewatering, which might be expected in both flow deposits and a clast-rich diamict (where material can be trapped in a pure shear geometry between clasts).

Thus, the micromorphology of Core 178-1103A-28R gives only ambiguous evidence for the origin of the material. The material also shows moderate iron mineral precipitation, which may explain the low porosity of the sediments (see discussion above).

Sample 178-1103A-34R-1, 107 cm (Fig. **F25**), was taken across the boundary between a thick diamict and a thin (<3 cm thick) clay-rich bed. The thin section suggests that the diamict is at least partially composed of reworked diamicts from two sources with different levels of iron staining and silt. Rounded clay intraclasts were incorporated into the diamict from the clay layer, and the boundary with the clay layer is pervasively mixed over a distance of ~75 µm. This mixing morphology probably indicates a low effective pressure ("fluid" conditions) and an unconfined, high-energy mixing environment. After the material was mixed, it gained a fabric in two directions. First, the material pervasively aligned at 48° (dipping right in the slide), and then numerous shears formed at 25° (dipping left).

F25. Photomicrograph of Sample 178-1103A-34R-1, 107 cm, **p. 64.**

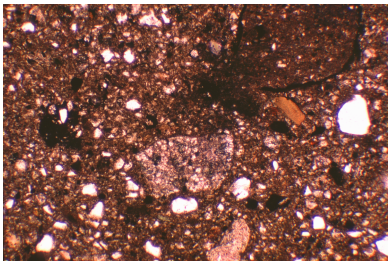

Several of these shears can be traced into the remnants of the clay layer where they join the Riedel shears of a principal displacement zone (PDZ). The PDZ shows a lensed, infinite shear geometry and dips left at 10°. Although the true dip angles are unknown, it is highly likely that the initial pervasive fabric alignment was in the thrust shear direction of the PDZ and formed during the early shearing of the material. Such a development is strongly suggestive of material that has not been overconsolidated (Tchalenko, 1968), which suggests that the diamict had lost any subglacial overconsolidation signature before the shear event.

Where the clays are in a single body or in the form of a large intraclast, they display a remnant domainal fabric in patches at various high angles to the initial pervasive reorientation at 48° (dipping right). Strong domainal fabrics have not been found in subglacial materials or subglacially reworked materials, and the fabric is strongly suggestive of marine material that has not been subjected to subglacial conditions. Thus, the stress response and general micromorphology of the material backs a mass flow reworked origin for the diamict in Core 178-1103A-34R (see "Lithostratigraphy," p. 5).

# DOWNHOLE MEASUREMENTS

## Logging Operations

After coring had reached maximum depth at 367 mbsf, Hole 1103A was reamed, the RCB bit was released, and the pipe was pulled up to 84 mbsf. We ran the TC (natural gamma, porosity, density, and resistivity), GHMT (natural gamma, magnetic susceptibility, and total magnetic field), and FMS-sonic tool strings (see Fig. F26 and "Downhole Measurements," p. 25, in the "Explanatory Notes" chapter). The last core arrived on deck at 0710 hr on 25 March, and logging operations finished at 0700 hr on 26 March (Table T4). The wireline heave compensator was used for all passes.

During the TC run, we encountered a hole blockage at 242 mbsf that the tool string could not pass. The hole was then logged up to pipe, with no repeat section. Apart from the initial blockage, hole conditions were good, and no further constrictions were met. After logging the open hole, the TC was initially unable to pass into the base of the pipe and came free only after 2 hr (see "Operations," p. 3). Once the tool had returned to the ship, the accelerator porosity sonde (APS) bow-spring (a 1.5-m-long strip of metal) was found to be missing. The GHMT logged both on the way down to 241 mbsf and up to the pipe and seafloor. The FMS-sonic tool string was run without its normal centralizer unit (comprising three 1-m-long bow-springs) to prevent it from becoming entangled with the APS bow-spring, left downhole after the first run. The FMS tool failed at 148 mbsf on the first upward pass and at 180 mbsf on the second.

## Log Quality

Hole 1103A was a good hole for logging, apart from the blockage at 242 mbsf. The borehole width varied between 30 and 41 cm, and <1 m of fill accumulated between the first and last logging runs. Most logs give reliable values (Figs. F27, F28), although we could not confirm this from comparison with core data because core recovery was only significant below 247 mbsf. Anomalous values in the total magnetic field and

F26. Graphic summary of downhole logging operations at Hole 1103A, p. 65.

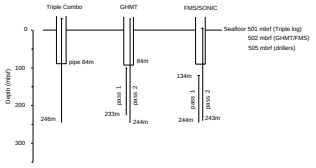


T4. Summary of logging operations, p. 83.

F27. Downhole logs of hole diameter, HSGR, RHOM, IPLC, SGR, sonic velocity, and RMGS from Hole 1103A, p. 66.

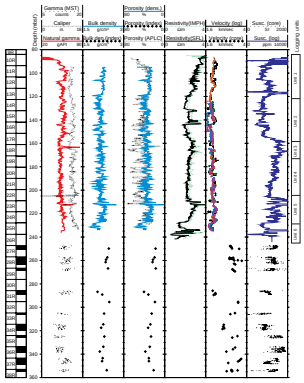

F28. Downhole logs of natural gamma, uranium, thorium, thorium/potassium ratio from NGT, PEF, and magnetic susceptibility in Hole 1103A, p. 67.

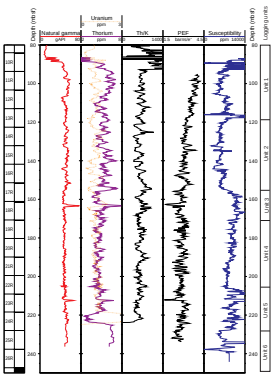

susceptibility logs near 117 mbsf may be caused by the APS bow-spring, which had been lost in the hole.

The sonic first-arrival traveltimes (autopicked during logging) are of poor quality. Those from the lower of the two digital sonic tool (SDT) transmitters (LTT3 and LTT4) are completely unusable, and those from the upper transmitter (LTT1 and LTT2) are often underestimates because the first arrival was sometimes incorrectly picked in the noise preceding the true first arrival. These traveltimes were converted to velocities by dividing the transmitter-receiver separation by the traveltimes, and then adding 10% to approximate the extra path length and slower water velocities traversed by the sonic wave between the tool and borehole wall. Normally, this correction is not necessary, as velocities are calculated using one traveltime subtracted from another (e.g., the 3.0 m minus the 2.4 m separation traveltime) so that the wave path in the borehole fluid is common to both and is canceled out. We cannot use this method because there are so few depth intervals in which both LTT1 and LTT2 are good. Even using our approximate method, the resulting velocity log shows variations consistent with expectations from the porosity and density logs, and velocity values (~2.1 km/s) comparable with those derived from seismic-survey stacking velocities. Figure F27 shows the velocities derived from the LTT1 and LTT2 traveltimes from the two FMS-sonic passes. Additionally, coherency analysis, performed on the Schlumberger Maxis computer, promises to provide intervals of velocity log with more accurate absolute values. The sonic velocities are discussed further in "Seismic Stratigraphy," p. 22.

Up until the points where the FMS failed, good images were obtained. About half the buttons on the fourth pad failed to function.

## Logging Units

### Unit 1: 84 (Base of Pipe)–118 mbsf

Unit 1 is characterized by low (25%–35%) porosity and high resistivity, density, and velocity. Magnetic susceptibilities are variable. This unit seems to have a distinct lithologic character and may contain more chlorite than the underlying units (Fig. F29).

F29. PEF vs. potassium in Hole 1103A, p. 68.

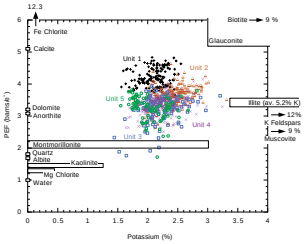


### Unit 2: 118–155 mbsf

Unit 2 generally has 35%–50% porosity but contains a subunit (130–145 mbsf) of lower porosity (25%–40%). Susceptibilities are low. The subunit is bounded at the top and bottom by thin (2 m) beds of distinctly higher resistivity and lower susceptibility, in contrast to the similarity of resistivity and magnetic susceptibility in other parts of the logs.

### Unit 3: 155–172 mbsf

Unit 3 has high susceptibilities, and the FMS images show that clasts are quite common.

### Unit 4: 172–206 mbsf

Unit 4 contains fewer clasts than Units 3 and 5, and there is a reduction in magnetic susceptibility and resistivity.

### Unit 5: 206–228 mbsf

Unit 5 is similar to Unit 3 but with lower porosities and higher resistivities. A 30-cm-thick layer (or flat boulder?) of very low (0%–10%) porosity occurs at 212 mbsf, and a 1-m-thick layer of ~20% porosity lies at 210 mbsf, the only level in which layering is evident in the FMS images.

### Unit 6: 228 mbsf–Base of Logging (242 mbsf)

Unit 6 is marked by a distinct jump to higher porosity (50%) and lower density, resistivity, and velocity. Porosity reaches 60% in a zone of highly variable log behavior (233–242 mbsf). The logs end at 242 mbsf, but Unit 6 cannot extend much deeper, as the first core with significant recovery (178-1103A-27R), characterized by a porosity of 20% and velocities of ~3 km/s, begins at 247 mbsf. The transition between the base of Unit 6 and the top of Core 178-1103A-27R thus represents the largest physical properties contrast observed in the hole, probably caused by induration.

## FMS

FMS images from the two passes are good, which can be attributed in part to favorable borehole conditions. Some buttons of one pad failed, which led to a high-resistivity trace that will be corrected by further processing postcruise. In places, the images are affected by tool stick and slip. The images are repeatable between the two runs. In Units 3 and 5, the FMS images are characterized by the presence of resistive spots (light colored in the image), which are caused by pebbles, because they have a much lower porosity than the surrounding sand, silt, and clay matrix. One of the biggest pebbles, observed in the traces of two of the FMS pads, can be identified at 157 mbsf (Fig. F30). Some conductive (dark) spots are also apparent and could be caused by bad pad contact caused by the seawater-filled depression in the wall left by pebbles plucked during drilling.

Layering is observed only rarely in these images (Fig. F30). The clearest layer is highly resistive and is located at 211.5 mbsf. Its shape, and presence of layered sediment nearby, indicates that it is probably a planar layer; however, the almost zero porosities suggest that the "layer" might be a boulder perforated by coring. This feature corresponds to high resistivity, high gamma ray, and high susceptibility in the logs.

## GHMT

The total magnetic field (MAGB) log (Fig. F31) contains many positive spikes that are grouped in distinct intervals. They are most probably caused by large clasts located close to the borehole wall and are most abundant in Units 1, 3, and 5.

As the first stage in the procedure to recover a polarity stratigraphy (see **"Downhole Measurements,"** p. 25, in the "Explanatory Notes" chapter), the clast-affected intervals were manually removed from the log, along with the modeled pipe effect. The magnetic anomaly in the borehole caused by the sediment's induced magnetization was calculated from the magnetic susceptibility log. The similarity between the total anomaly and the anomaly resulting from the induced magnetization shows that in the sediment, the induced magnetization dominates

F30. FMS resistivity images from Hole 1103A, **p. 69.**

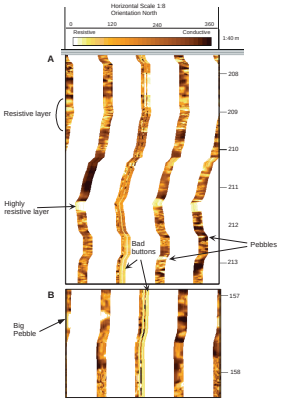


F31. Magnetic field logs from Hole 1103A, **p. 70.**

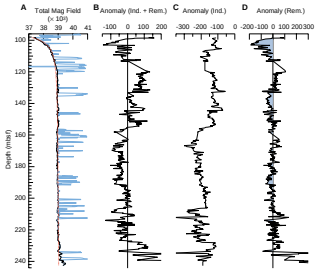

the remanent magnetization. This is what would be expected from coarse-grained sediment: neither the large size of the magnetite particles nor the environment of deposition are ideal for recording the geomagnetic field with any fidelity. Hence a magnetic polarity stratigraphy could not be derived from the GHMT logs aboard ship but may be possible for the clast-free intervals after postcruise processing.

### Temperature Log

The Lamont-Doherty temperature-logging tool recorded the temperature of the fluid in Hole 1103A during the TC run. The curve has a temperature gradient of ~16°C/km (Fig. F32). The downhole and uphole curves show a constant offset of ~0.6°C because the borehole continued to re-equilibrate during acquisition. These temperatures do not represent in situ formation temperatures.

F32. Temperature log from Hole 1103A, p. 71.

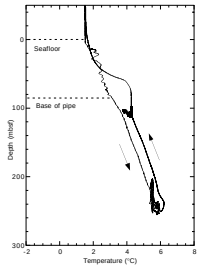


## SEISMIC STRATIGRAPHY

Previous seismic stratigraphic interpretations on the Antarctic Peninsula continental shelf are based on single-channel and multichannel seismic profiles (Larter and Barker, 1989, 1991b; Larter and Cunningham, 1993; Bart and Anderson, 1995; see "Background and Scientific Objectives," p. 1). During Leg 178, existing MCS profiles across Sites 1100, 1102, and 1103, collected by the Osservatorio Geofisico Sperimentale and the British Antarctic Survey (see Fig. F3; "Seismic Stratigraphy," p. 29, in the "Explanatory Notes" chapter; and "Appendix," p. 24, and Fig. AF1, p. 59, both in the "Leg 178 Summary" chapter), were examined to establish the seismic stratigraphy described below. Sonic log velocities and individual laboratory (Hamilton Frame) measurements of *P*-wave velocity on cores recovered at Sites 1100 and 1103 have been used to estimate velocities and to assign depths to reflectors in all three sites along the shelf transect.

### Acoustic Parameters

#### Density/Velocity Model

Bulk densities for Site 1103 have been derived from MST measurements (with a GRAPE, 2-cm spatial resolution), index property measurements (1.5-m spatial resolution), and lithodensity logging data (hostile environment lithodensity sonde, measurement separation ~15 cm; Fig. F33). Densities from downhole logging are available between 84 and 240 mbsf. The MST data used below 247 mbsf are discontinuous because of low recovery (34%). Also, the index properties measurements and the MST-density data are significantly offset. No density information is available within the depth interval 0 to 84 mbsf.

Two differently derived velocities are available. Discrete Hamilton Frame (PWS3) measurements provide high-quality data for the better recovered part of the hole (247 to 355 mbsf). Small matrix pieces occasionally recovered from 70 to 220 mbsf provide some velocity information (see "Physical Properties," p. 15). The sonic velocity data collected with the SDT at Site 1103 is of low quality because many of the recorded waveforms are often noisy; hence, picking the first arrival for the traveltime was difficult. However, several waveforms are recorded at each depth, and after removing noisy waveforms and

F33. Comparison of different density data sets available for Site 1103, p. 72.

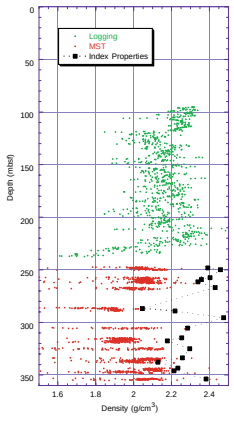

changing tracking and window parameters for the velocity analysis, the data quality improved considerably. The final selection of sonic velocity data was based on six independent quality criteria (e.g., agreement of second and first run, agreement between values obtained by analogue picking, and coherence tracing). The velocity log constructed in this way is given in Figure F34 (see "Downhole Measurements," p. 19, for a comparison with velocities derived from analogue picking). Near the seafloor, data points have been added from Site 1100. This seems to be appropriate because seismic tomography velocities show similar values near the seafloor for Site 1103 (Tinivella et al., 1996).

## Traveltime/Depth Function

The gap in velocity data between 10 and 70 mbsf was closed by a linear interpolation (connecting the two last known data points with a straight line), and a two-way traveltime/depth function was calculated (Fig. F35). The curve has an approximately linear central part (80–240 mbsf, from logging data) and a sharp bend toward higher velocities below 250 mbsf.

## Digital Seismic Section

Forty-two traces of the profile crossing Site 1103 (profile I95-152) have been filtered, statically corrected, gain-recovered, and displayed in Figure F36. The most important reflectors are marked and named. The seafloor (time = 0) has been placed at the maximum of the first positive reflection, instead of at the first onset of energy (the time difference would be ~6–7 ms), to facilitate comparison to traveltimes taken from the conventional printouts. Traveltimes to reflectors below are given from maximum to maximum. The proposed traveltime/depth relationship is necessarily speculative but ties reflectors well in depth to major changes in the lower part of the logging data (Reflectors a, b) and to observed sedimentological changes within the recovered part of Site 1103 (Reflectors c, d, and e).

## Seismic Units

We identify three seismic units, which correspond to Sequence Groups S1, S2, and S3 described by Larter and Barker (1989) (Fig. F3).

### Sequence Group S1

Sequence Group S1 is characterized by nearly flat-lying topset reflectors in the inner and middle shelf that seaward become steeply dipping foreset reflectors (Fig. F3). Topset reflectors are marked by lateral changes in reflector amplitude (i.e., from high to moderate), whereas foreset reflectors have lower amplitudes. S1 has an external wedge geometry. The lower boundary of S1 is a high-amplitude reflector that truncates reflectors from underlying Sequence Groups S2 and S3 (Fig. F3).

Sequence Group S1 at Site 1102 consists of an upper thin (~60 m) package of high-amplitude flat-lying topset reflectors and a lower thick sequence of steeply dipping (foreset) reflectors (Fig. F37). Truncation and downlap relationships within the foresets suggest that S1 comprises several individual prograding sequences (Larter and Barker, 1989).

F34. Downhole logging and Hamilton Frame velocities for Site 1103, p. 73.

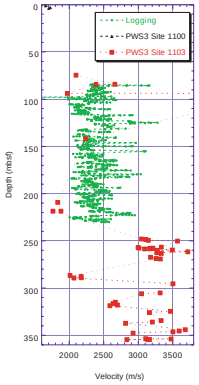


F35. Traveltime/depth function for Site 1103, p. 74.

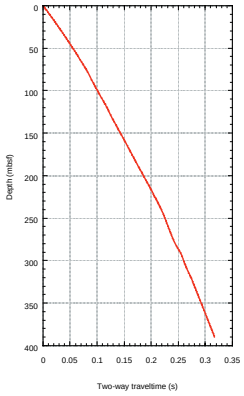


F36. Seismic profile I95-152 over Site 1103 with reflectors marked, p. 75.

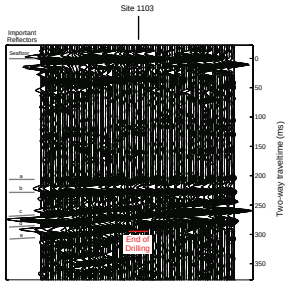

Sequence Group S1 at Site 1100 is characterized by a thick (i.e., 350 ms/402 m) unit of flat-lying parallel and subparallel topset reflectors (Fig. F38). High amplitudes are common in the uppermost topset reflectors, whereas the lower section has alternating high- and moderate-amplitude reflectors. The topset section was drilled with very low recovery at Site 1100, to a depth of 110.5 mbsf.

Sequence Group S1 at Site 1103 (0–255 mbsf) consists of horizontally stratified topset reflectors (Figs. F3, F39). The entire topset section was drilled, with very low recovery. From this site and toward the mid-shelf high (MSH), Sequence Group S1 decreases in thickness to about 57 m. The estimated 255 m thickness of Sequence Group S1 at Site 1103 is based on a velocity model, but it is clear from Figure F34 and from the recovered core that a change in sediment properties, most probably coincident with the sequence boundary, lies above 255 m, perhaps at 242–247 mbsf, where logging was disrupted and recovery improved (see "Operations," p. 3).

## Sequence Group S2

Sequence Group S2 is typified by low-angle dipping reflectors that become more steeply dipping seaward (Fig. F3). Strata from S2 are truncated at the top by the erosional unconformity that marks the boundary between S1 and S2. At Site 1100, Sequence Group S2 consists of steeply dipping foreset reflectors that downlap onto a lower deeper reflector, indicating a prograding sequence (see "Appendix," p. 24, and Fig. AF1, p. 59, both in the "Leg 178 Summary" chapter). Internal truncations and downlap relationships in the foreset section are common, which implies the existence of many individual prograding sequences. Sequence Group S2 is not found at Site 1103, where an unconformity separates reflectors from Sequence Group S1 above from reflectors of Sequence Group S3 below (Fig. F39).

## Sequence Group S3

Sequence Group S3 (255 mbsf and continuing below the cored section) is characterized by a series of reflectors that dip gently seaward from the MSH, a structural high located landward of Site 1103 (Larter and Barker, 1989, 1991b) (see "Background and Scientific Objectives," p. 1). Reflectors of Sequence Group S3 at Site 1103 are parallel or subparallel throughout the section. In tracing the reflectors away from the site, however, we can distinguish two reflector packages separated by a group of three high-amplitude reflectors (Reflectors c, d, and e in Fig. F36). Above these three reflectors, S3 is characterized by parallel and subparallel gently dipping reflectors that are truncated landward by the unconformity that bounds Sequence Group S1 and Sequence Group S3 (Fig. F39 and Reflectors a and b in Fig. F36). Below the three high-amplitude reflectors, S3 reflectors diverge seaward and pinch out landward (Fig. F36). The three strong reflectors (c, d, and e) separating the two reflector packages correspond to changes in the density and variations in the velocity of sedimentary formations (i.e., from 3300 to 2100 m/s between 270 and 285 mbsf) (Figs. F33, F34). All reflector packages in S3 have lower amplitudes landward and increase in amplitude seaward of the site location.

F37. MCS profile I95-152 across Site 1102, p. 76.

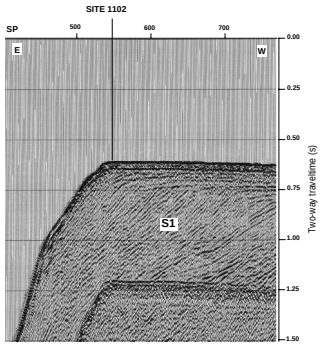


F38. MCS profile I95-152 across Site 1100, p. 77.

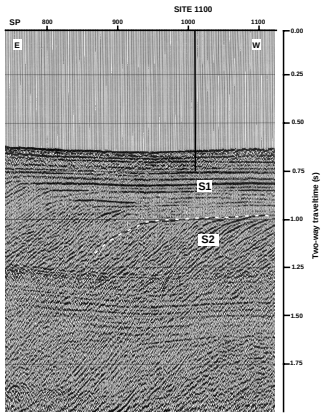


F39. MCS profile I95-152 across Site 1103, p. 78.

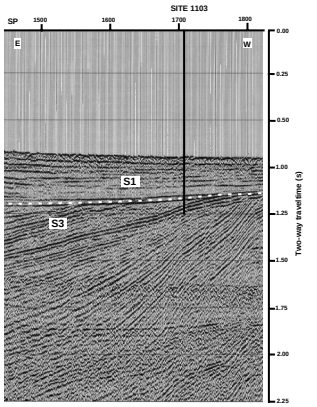

## Interpretation

Sediment recovered from Sequence Group S1 at Sites 1100 and 1103 (see "Lithostratigraphy," p. 5) indicates that during the development of S1, a grounded ice sheet regularly extended across the continental shelf. Individual prograding sequences recognized by truncation and downlap of reflectors in Sequence Group S1 also suggest repeated episodes of ice advance and retreat.

Sequence Group S3 was recovered at Site 1103. The top of this sequence corresponds roughly to an improvement in sediment core recovery at 247 mbsf. The upper part of S3, above the three strong Reflectors c, d, and e (Fig. F36), consists of massive diamict (see "Lithostratigraphy," p. 5). Below these reflectors, sediments are poorly sorted sandstones and mudstones. S3 has been interpreted as sediment gravity flows and turbidites deposited on a very active, glacially influenced second-order slope (see "Lithostratigraphy," p. 5).

Drilling results from Sites 1100, 1102, and 1103 indicate that the three Sequence Groups S1, S2, and S3 were deposited under a glacial regime. The glacial section drilled in the shelf transect of the Antarctic Peninsula is interpreted as changing upward from deposits representing a proximal glaciomarine environment (Sequence Group S3) to principally subglacial strata deposited beneath the base of a grounded ice sheet on the shelf (Sequence Group S1). During deposition of S2 and S1, glacial sequences are characterized by low-angle topsets and steep foresets that prograde the margin by 20 km (along the line of Fig. F3). The differences in acoustic character and geometry of glacial sequences between S3 and S2 indicate an important change in the style of sedimentation, which is probably linked to a change in the glacial regime of this part of the Antarctic margin.

## REFERENCES

Alley, R.B., Blankenship, D.D., Rooney, S.T., and Bentley, C.R., 1989. Sedimentation beneath ice shelves: the view from Ice Stream B. *Mar. Geol.,* 85:101–120.

Anderson, J.B., Brake, C.F., and Myers, N.C., 1984. Sedimentation on the Ross Sea continental shelf, Antarctica. *Mar. Geol.,* 57:295–333.

Anderson, J.B., Kurtz, D.D., Domack, E.W., and Balshaw, K.M., 1980. Glacial and glacial marine sediments of the Antarctic continental shelf. *J. Geol.,* 88:399–414.

Anderson, J.B., Kurtz, D.D., and Weaver, F.M., 1979. Sedimentation on the Antarctic continental slope. *In* Doyle, L.J., and Pilkey, O.H. (Eds.), *Geology of Continental Slopes*. Spec. Publ. Soc. Econ. Paleont. Mineral., 27:265–283.

Bart, P.J., and Anderson, J.B., 1995. Seismic record of glacial events affecting the Pacific margin of the northwestern Antarctic Peninsula. *In* Cooper, A.K., Barker, P.F., and Brancolini, G. (Eds.), *Geology and Seismic Stratigraphy of the Antarctic Margin*. Antarct. Res. Ser., 68:75–96.

Eyles, C.H., Eyles, N., and Franca, A.B., 1993. Glaciation and tectonics in an active intracratonic basin: the late Paleozoic Itarare Group, Parana Basin, Brazil. *Sedimentology,* 40:1–25.

Eyles, N., 1990. Late Precambrian "tillites" of the Avalonian-Cadomian belt: marine debris flows in an active tectonic setting. *Palaeogeogr., Palaeoclimatol., Palaeoecol.,* 79:73–98.

Eyles, N., 1993. Earth's glacial record and its tectonic setting. *Earth-Sci. Rev.,* 35:1–248.

Gipp, M.R., 1993. Architectural styles of glacially influenced marine deposits on tectonically active and passive margins. *In* Deynoux, M., Miller, J.M.G., Domack, E.W., Eyles, N., Fairchild, I.J., and Young, G.M. (Eds.), *Earth's Glacial Record:* Cambridge (Cambridge Univ. Press), 109–120.

Hill, P.R., 1984. Sedimentary facies of the Nova Scotia upper and middle continental slope, offshore eastern Canada. *Sedimentology,* 31:293–309.

Larter, R.D., and Barker, P.F., 1989. Seismic stratigraphy of the Antarctic Peninsula Pacific margin: a record of Pliocene–Pleistocene ice volume and paleoclimate. *Geology,* 17:731–734.

Larter, R.D., and Barker, P.F., 1991a. Effects of ridge-crest trench interaction on Antarctic-Phoenix spreading: forces on a young subducting plate. *J. Geophys. Res.,* 96:19583–19607.

Larter, R.D., and Barker, P.F., 1991b. Neogene interaction of tectonic and glacial processes at the Pacific margin of the Antarctic Peninsula. *In* Macdonald, D.I.M. (Ed.), *Sedimentation, Tectonics and Eustasy: Sea-level Changes at Active Margins*. Spec. Publ. Int. Assoc. Sedimentol., 12:165–186.

Larter, R.D., and Cunningham, A.P., 1993. The depositional pattern and distribution of glacial-interglacial sequences on the Antarctic Peninsula Pacific margin. *Mar. Geol.,* 109:203–219.

Larter, R.D., Rebesco, M., Vanneste, L.E., Gamboa, L.A.P., and Barker, P.F., 1994. Seismic reflection investigations on the Pacific margin of the Antarctic Peninsula. *Terra Antarct.,* 1:271–274.

Larter, R.D., Rebesco, M., Vanneste, L.E., Gamboa, L.A.P., and Barker, P.F., 1997. Cenozoic tectonic, sedimentary and glacial history of the continental shelf west of Graham Land, Antarctic Peninsula. *In* Barker, P.F., and Cooper, A.K. (Eds.), *Geology and Seismic Stratigraphy of the Antarctic Margin* (Pt. 2). Antarct. Res. Ser., 71:1–27.

Miall, A.D., 1985. Sedimentation on an early Proterozoic continental margin under glacial influence: the Gowganda Formation (Huronian), northern Ontario. *Sedimentology,* 32:763–788.

Pickering, K.T., Hiscott, R., and Hein, F.J., 1989. *Deep-marine Environments: Clastic Sedimentation and Tectonics:* London (Unwin Hyman).

Pope, P.G., and Anderson, J.B., 1992. Late Quaternary glacial history of the northern Antarctic Peninsula's western continental shelf: evidence from the marine record.

*In* Elliot, D. H. (Ed.), *Contributions to Antarctic Research III.* Am. Geophys. Union, Antarct. Res. Ser., 57:63–91.

Pudsey, C.J., Barker, P.F., and Larter, R.D., 1994. Ice sheet retreat from the Antarctic Peninsula shelf. *Cont. Shelf Res.,* 14:1647–1675.

Rebesco, M., Camerlenghi, A., and Zanolla, C., in press. Bathymetry and morphogenesis of the continental margin west of the Antarctic Peninsula. *Terra Antarct.*

Tchalenko, J.S., 1968. The evolution of kink-bands and the development of compression textures in sheared clays. *Tectonophysics,* 6:159–174.

Tinivella, U., Camerlenghi, A., and Rebesco, M., 1996. Ocean Drilling Program Proposal #452, rev. (Antarctic Peninsula), velocity analyses at Site APSHE L-3A and APSHE L-10A. *Rept. to Site Survey Panel, Oct. 1996, ODP Site Survey Data Bank.*

Vanneste, L.E., and Larter, R.D., 1995. Deep-tow boomer survey on the Antarctic Peninsula Pacific margin: an investigation of the morphology and acoustic characteristics of Late Quaternary sedimentary deposits on the outer continental shelf and upper slope. *In* Cooper, A.K., Barker, P.F., and Brancolini, G. (Eds.), *Geology and Seismic Stratigraphy of the Antarctic Margin.* Am. Geophys. Union, Antarct. Res. Ser., 68:97–121.

Visser, J.N.J., 1983. Submarine debris flow deposits from the upper Carboniferous Dwyka Tillite Formation in the Kalahari Basin, South Africa. *Sedimentology,* 3:511–523.

Visser, J.N.J., 1993. The interpretation of massive rain-out and debris flow diamictites from the glacial marine environment. *In* Deynoux, M., Miller, J.M.G., Domack, E.W., Eyles, N., Fairchild, I.J., and Young, G.M. (Eds.), *Earth's Glacial Record:* Cambridge (Cambridge Univ. Press), 83–94.

Walker, R.G., 1992. Turbidites and submarine fans. *In* Walker, R.G., and James, N. (Eds.), *Facies Models: Response to Sea-Level Change:* St. Johns, Newfoundland (Geol. Assoc. Canada), 239–264.

Woodworth-Lynas, C.M.T., and Dowdeswell, J.A., 1993. Soft-sediment striated surfaces and massive diamicton facies produced by floating ice. *In* Deynoux, M., Miller, J.M.G., Domack, E.W., Eyles, N., Fairchild, I.J., and Young, G.M. (Eds.), *Earth's Glacial Record:* Cambridge (Cambridge Univ. Press), 241–259.

Young, G.M., and Gostin, V.A., 1991. Late Proterozoic (Sturtian) succession of the North Flinders Basin, South Australia: an example of temperate glaciation in an active rift setting. *In* Anderson, J.B., and Ashley, G. (Eds.), *Glacial Marine Sedimentation: Paleoclimatic Significance.* Geol. Soc. Am. Spec. Publ., 261:207–223.

**Figure F1. A.** Bathymetric map (from Rebesco et al., in press) and main morphologic elements of the continental shelf off Anvers Island, including Lobes 1 and 2 (Larter et al., 1994, 1997). (Continued on next page.)

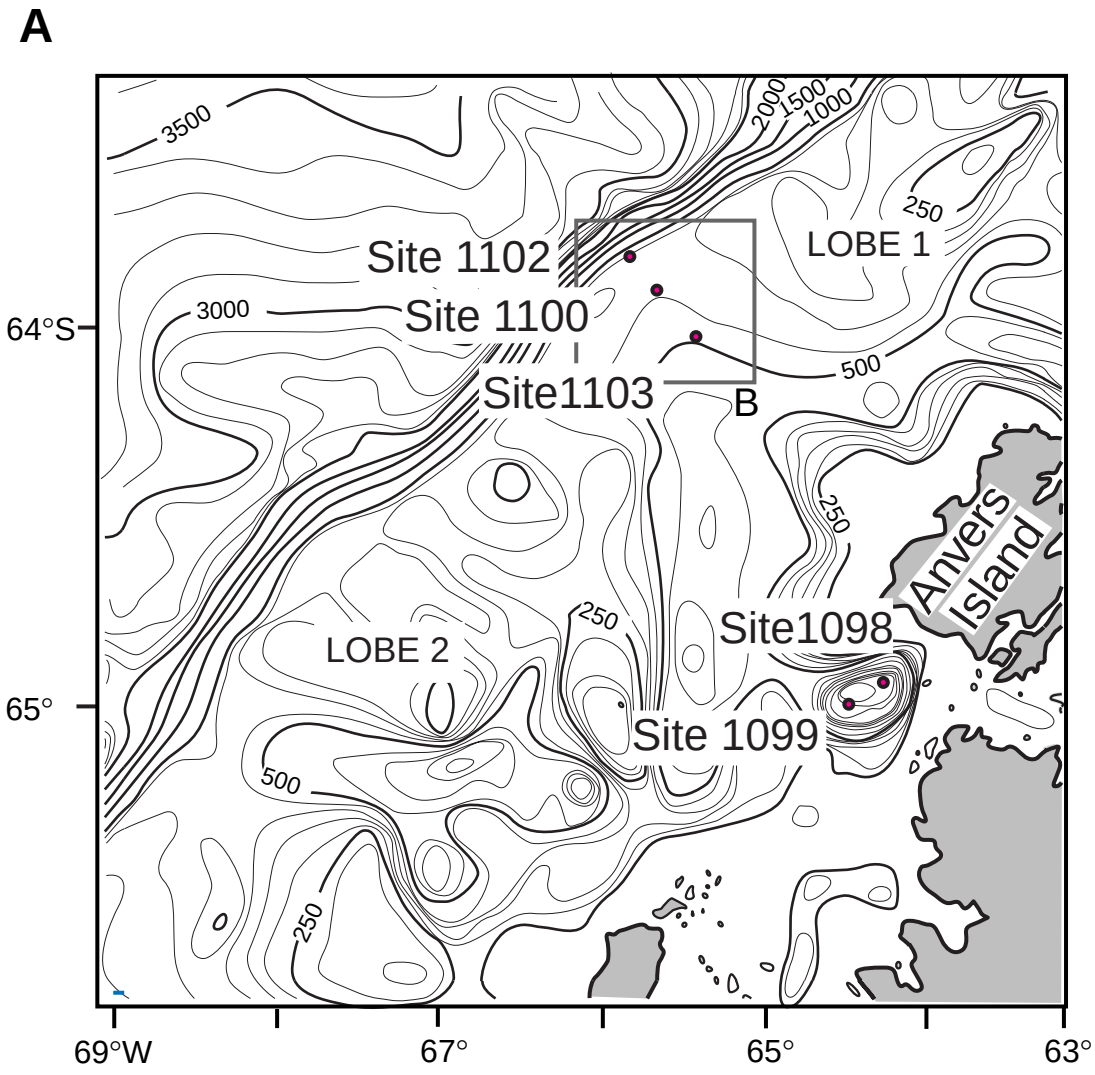

**Figure F1 (continued). B.** Location of site-survey multichannel and single-channel seismic reflection profiles as well as 3.5-kHz sub-bottom profiles acquired during site approach. Leg 178 prospectus sites are indicated for comparison with those sites actually drilled.

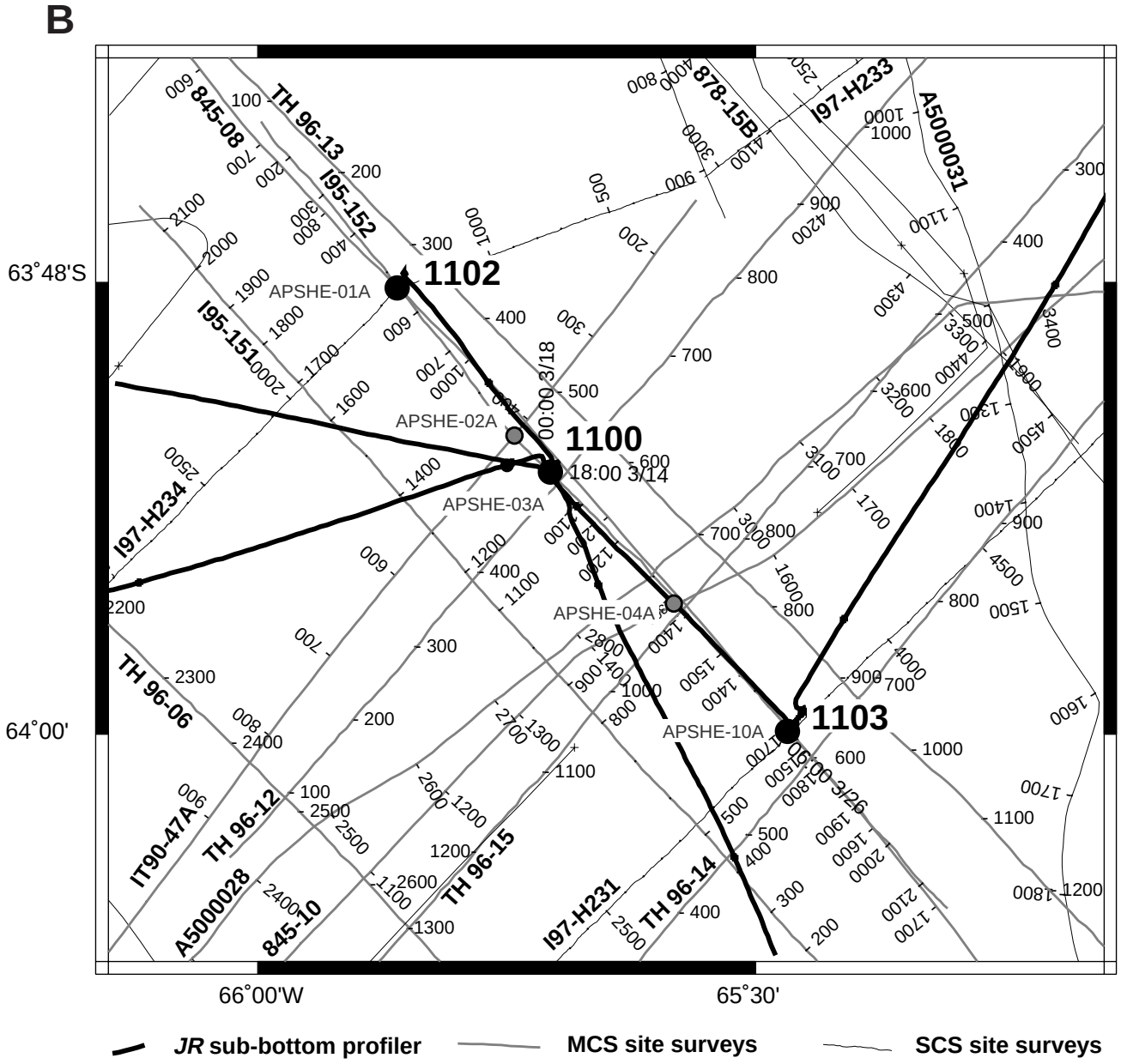

**Figure F2.** Continental shelf transect. Location of Sites 1100, 1102, and 1103 on MCS profile I95-152 across the continental shelf seaward of Anvers Island, Antarctic Peninsula.

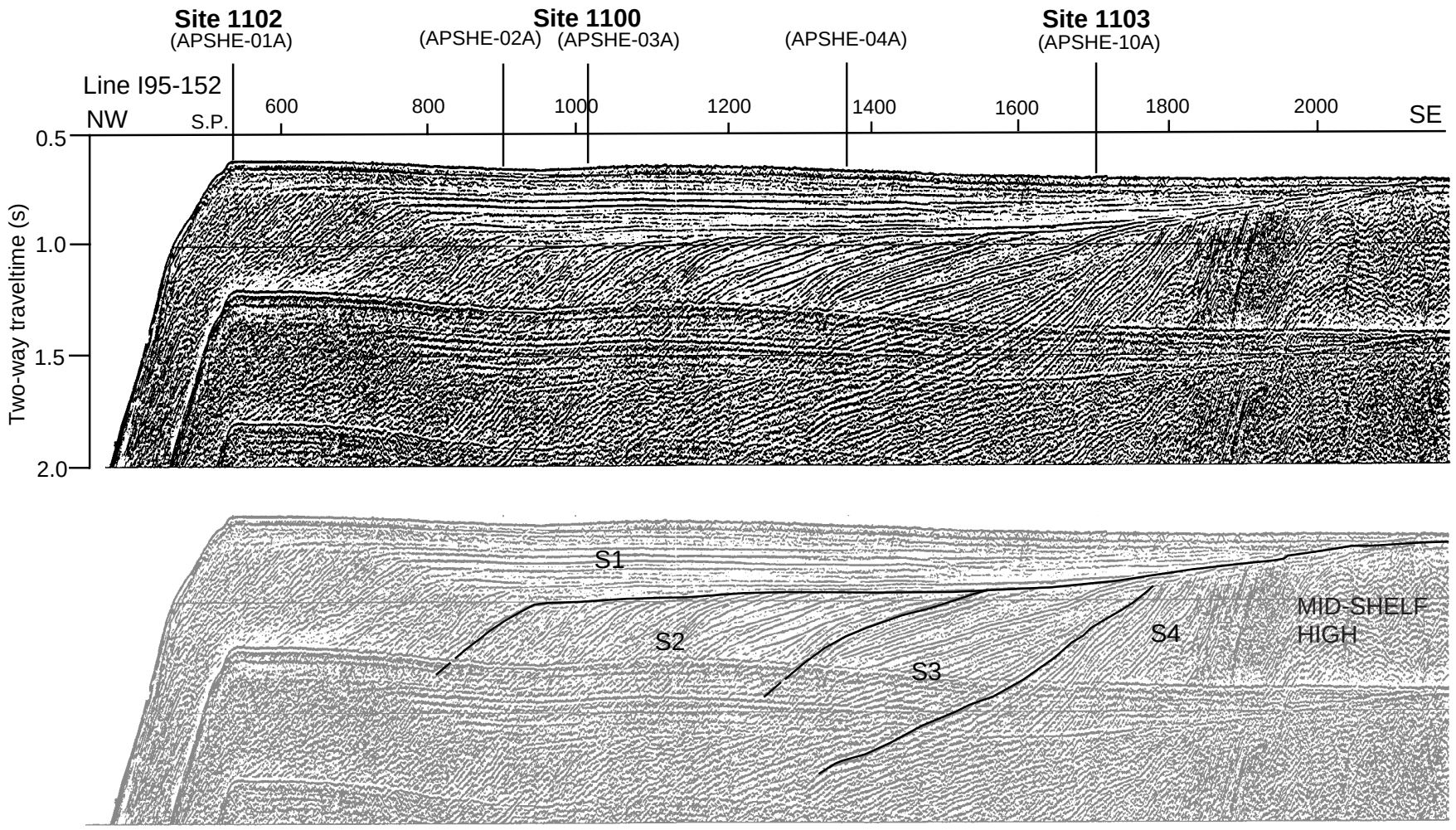

**Figure F3.** Location of Site 1100 on deep-tow boomer profile showing the seaward frontal slope of a young till body and reflections from underlying bodies (Vanneste and Larter, 1995). Vertical black arrows point out small-scale foreset reflectors, indicating the seaward dip of original bedding within the till body.

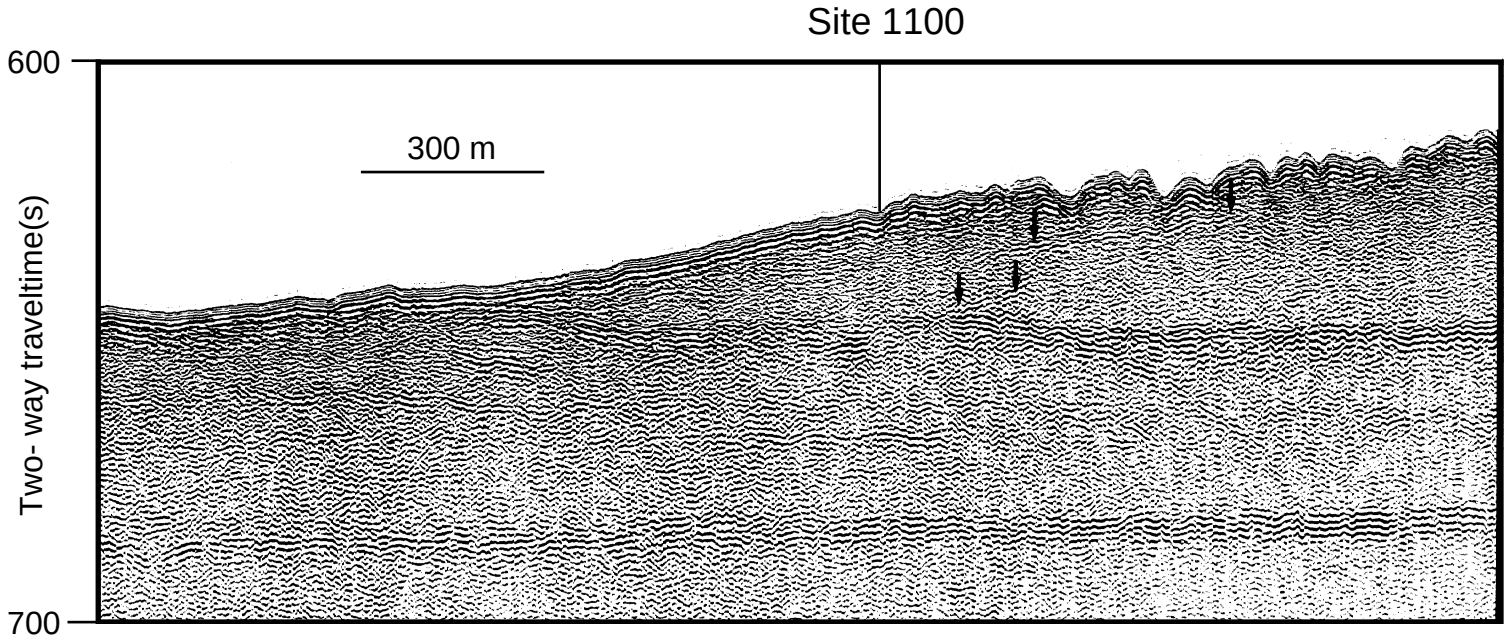

**Figure F4.** Even when weather conditions were excellent on site, a swell from the northwest produced ship heave that often exceeded 2 m at the shelf sites. We attempted to record the size of the heave by using the precision depth recorder (PDR) while fixed over the site. The recorder shows as much as 7.5 m change in water depth, mainly as a result of ship heave, although secondary effects of ship pitch and roll added to the PDR signal.

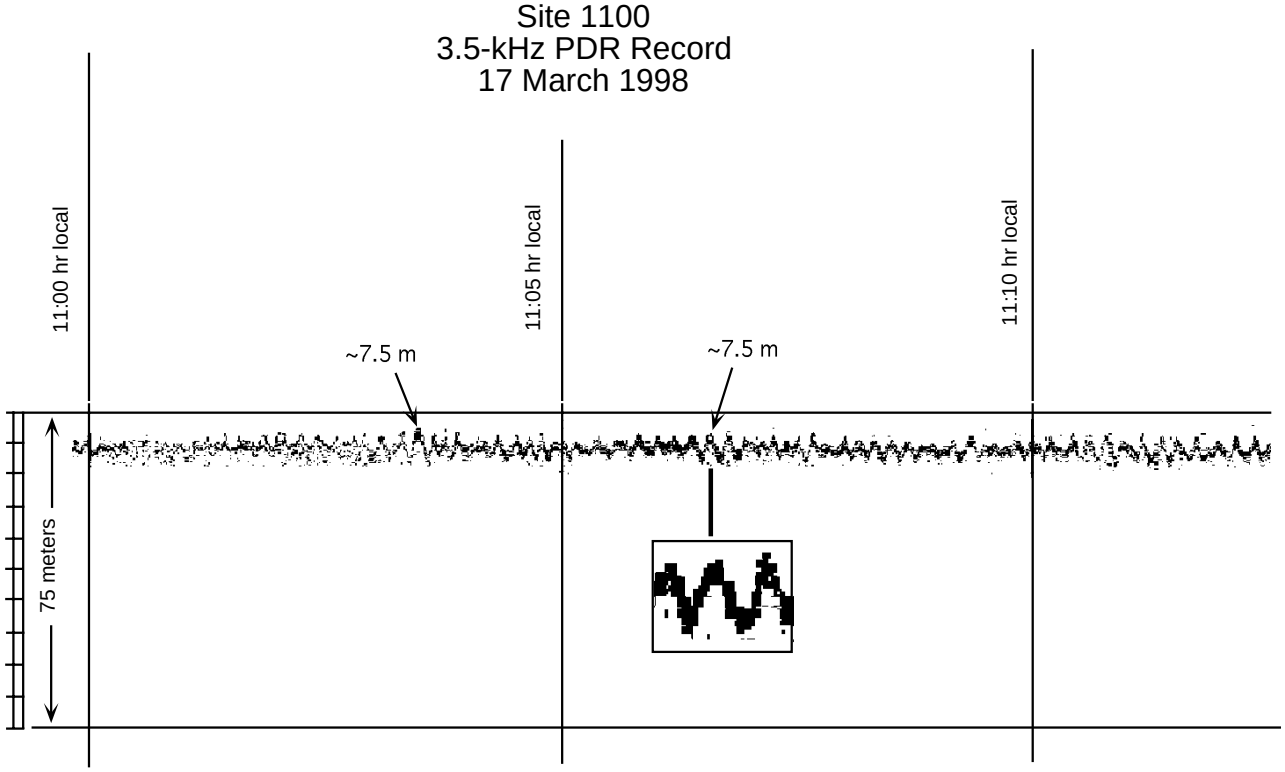

**Figure F5.** Vertical profile of massive, matrix-supported diamict (Facies Dmm) recovered from Hole 1100C (see "Lithostratigraphy," p. 3, in the "Explanatory Notes" chapter, for lithofacies coding). The site lies in an area of iceberg-furrowed till (NR = no core recovery). For position of Site 1100, see Figure F3, p. 31.

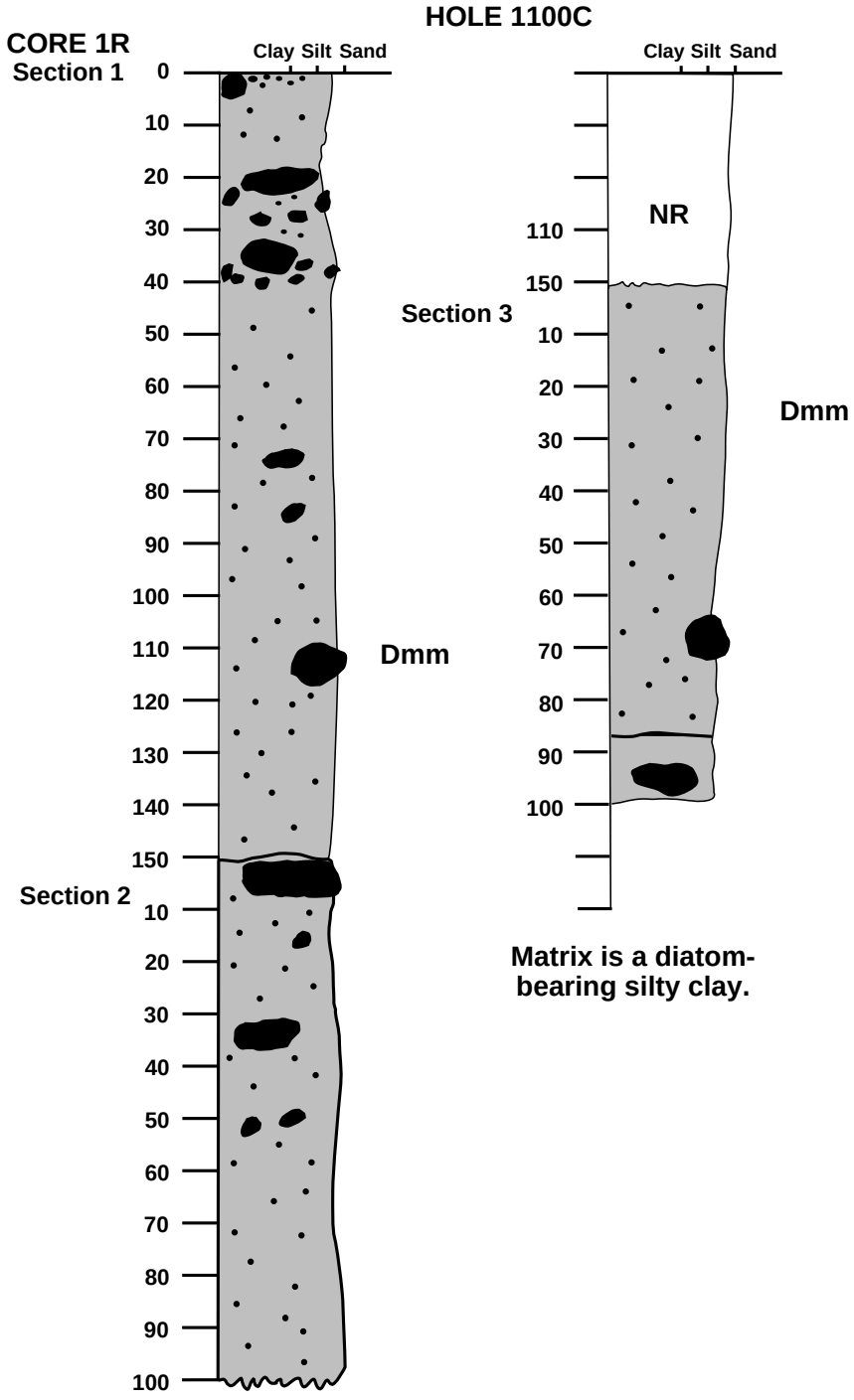

**Figure F6.** Simplified lithostratigraphy showing lithofacies at Site 1103.

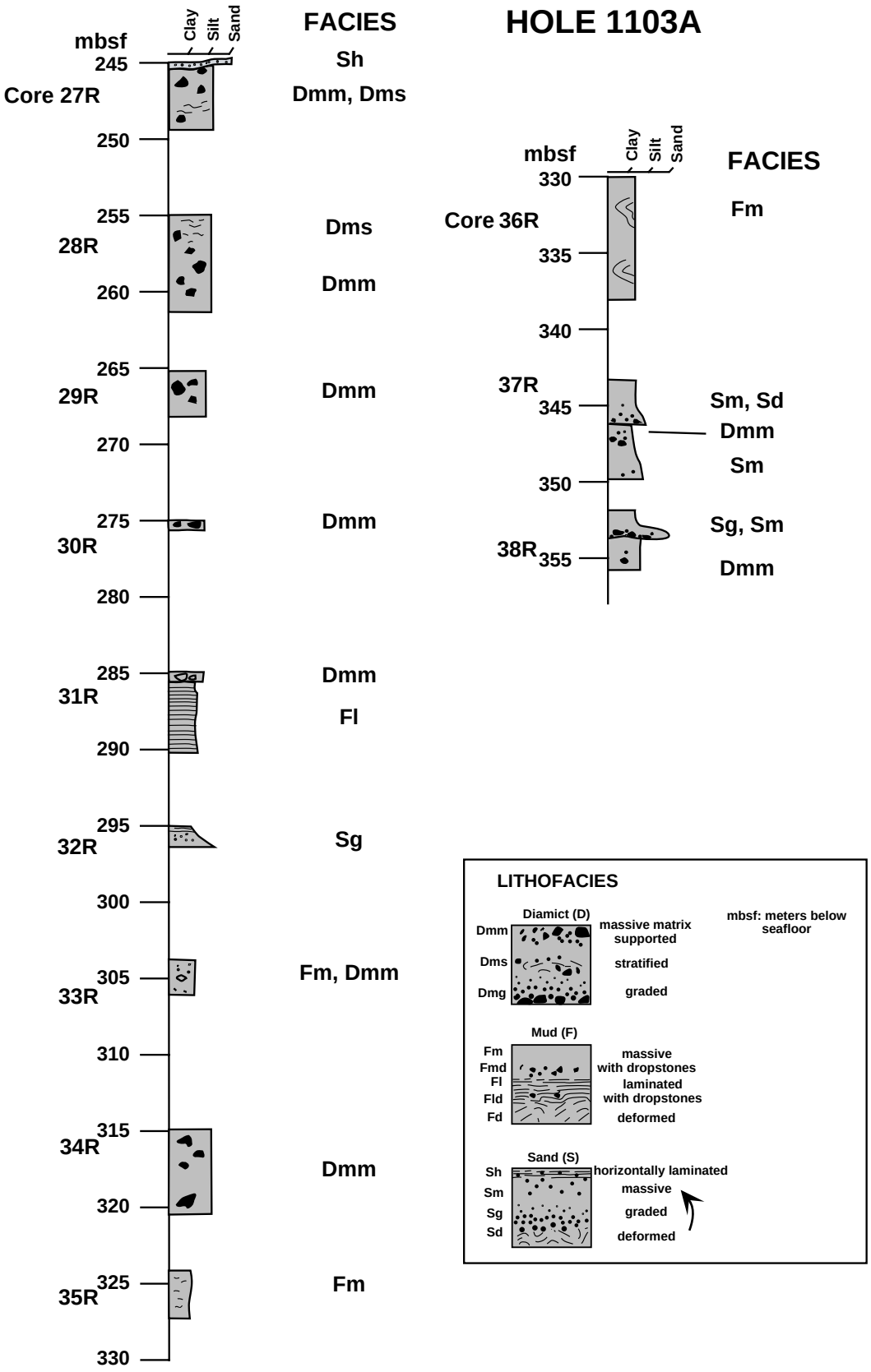

**Figure F7. A.** Detailed graphic logs showing each section of recovery for Core 178-1103A-27R. (Continued on next nine pages.)

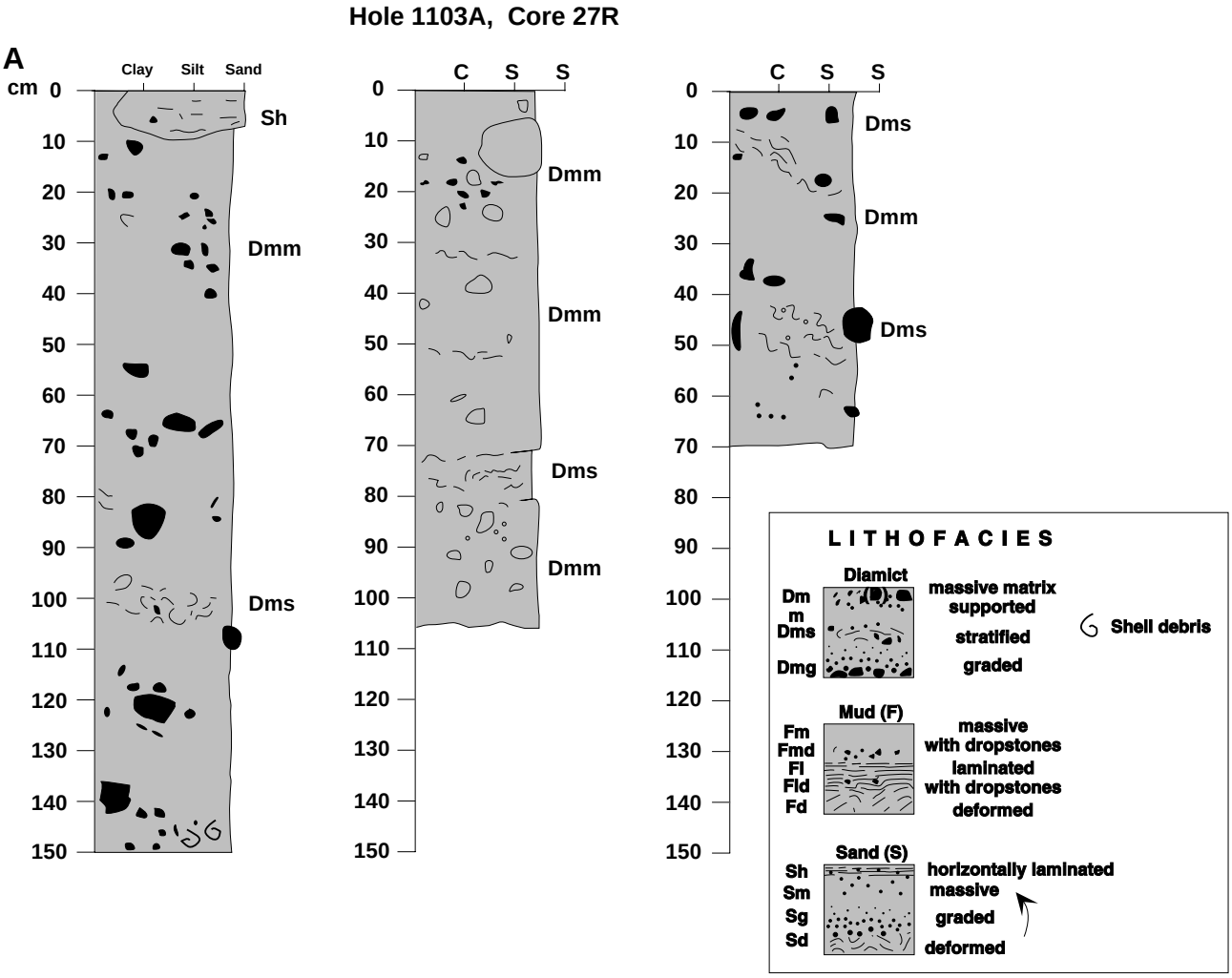

**Figure F7 (continued). B.** Detailed graphic logs showing each section of recovery for Core 178-1103A-28R.

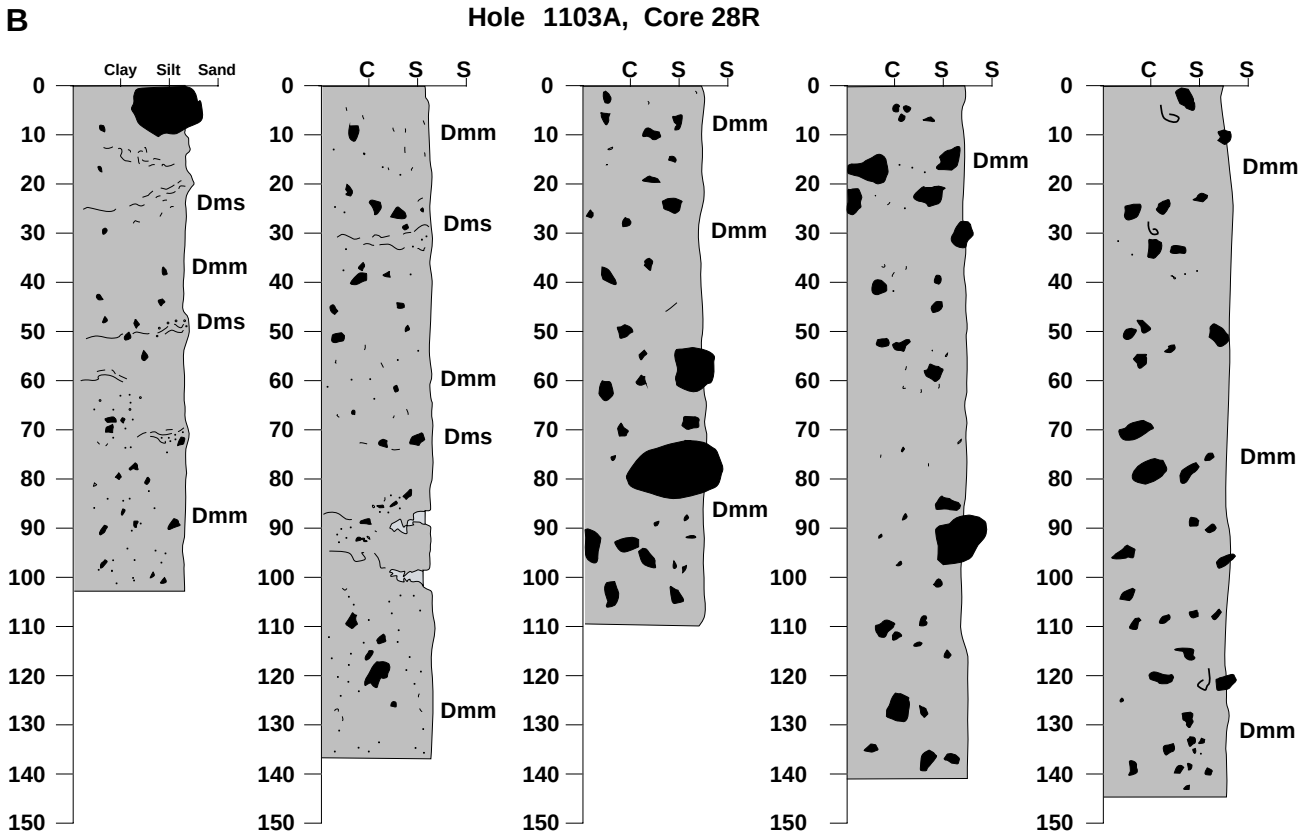

**Figure F7 (continued). C.** Detailed graphic logs showing each section of recovery for Core 178-1103A-29R.

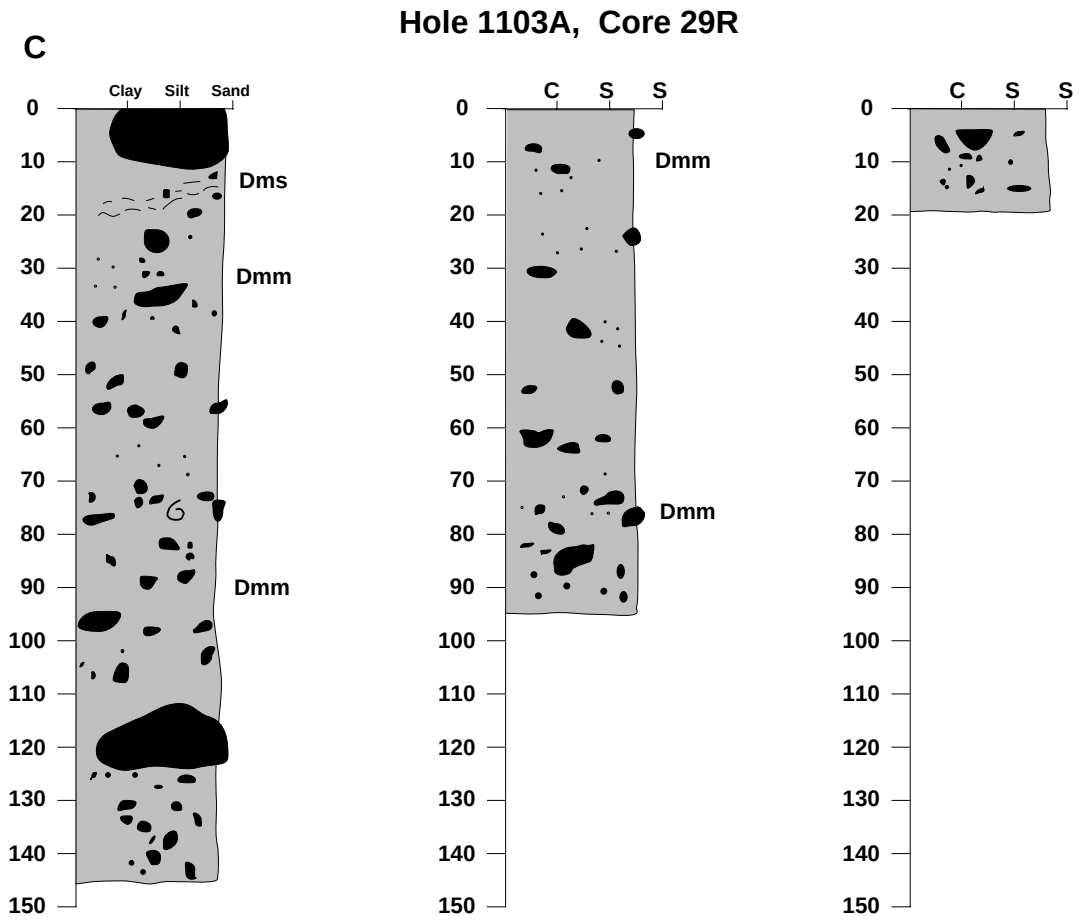

**Figure F7 (continued). D.** Detailed graphic logs showing each section of recovery for Cores 178-1103A-31R and 32R.

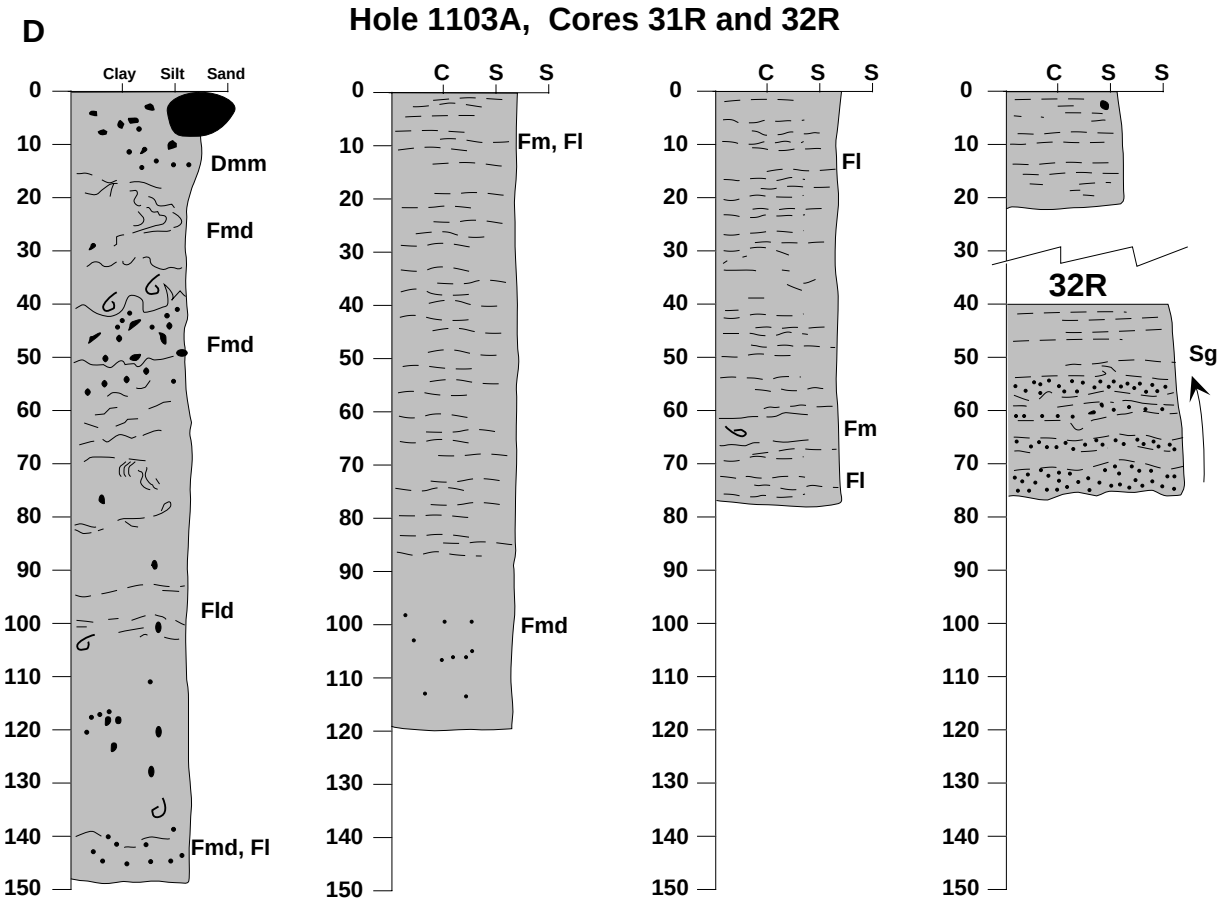

**Figure F7 (continued). E.** Detailed graphic logs showing each section of recovery for Core 178-1103A-33R.

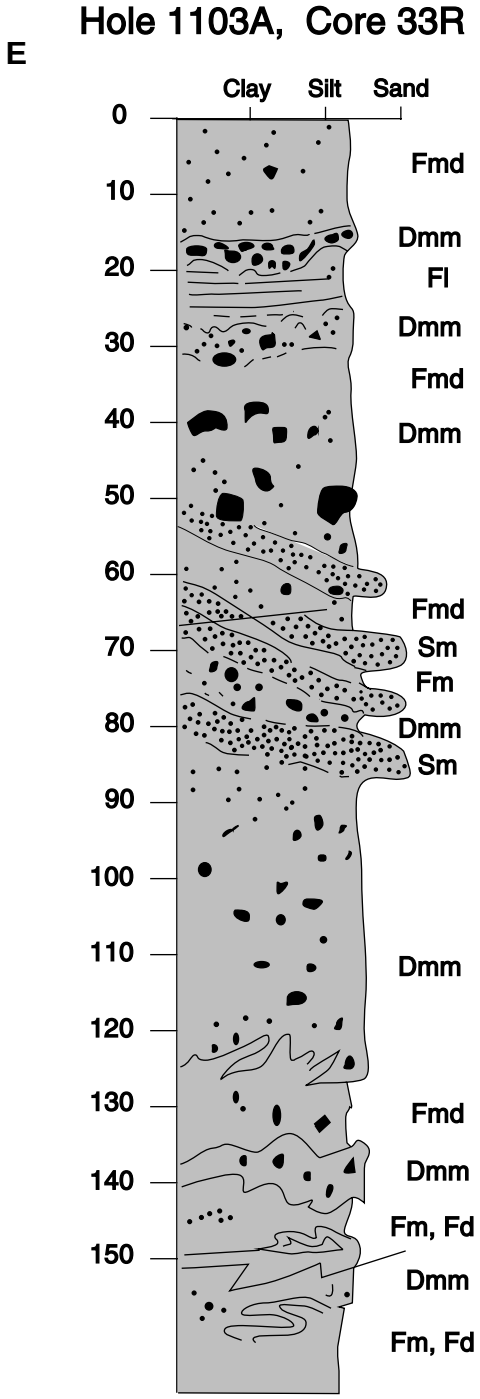

**Figure F7 (continued). F.** Detailed graphic logs showing each section of recovery for Core 178-1103A-34R.

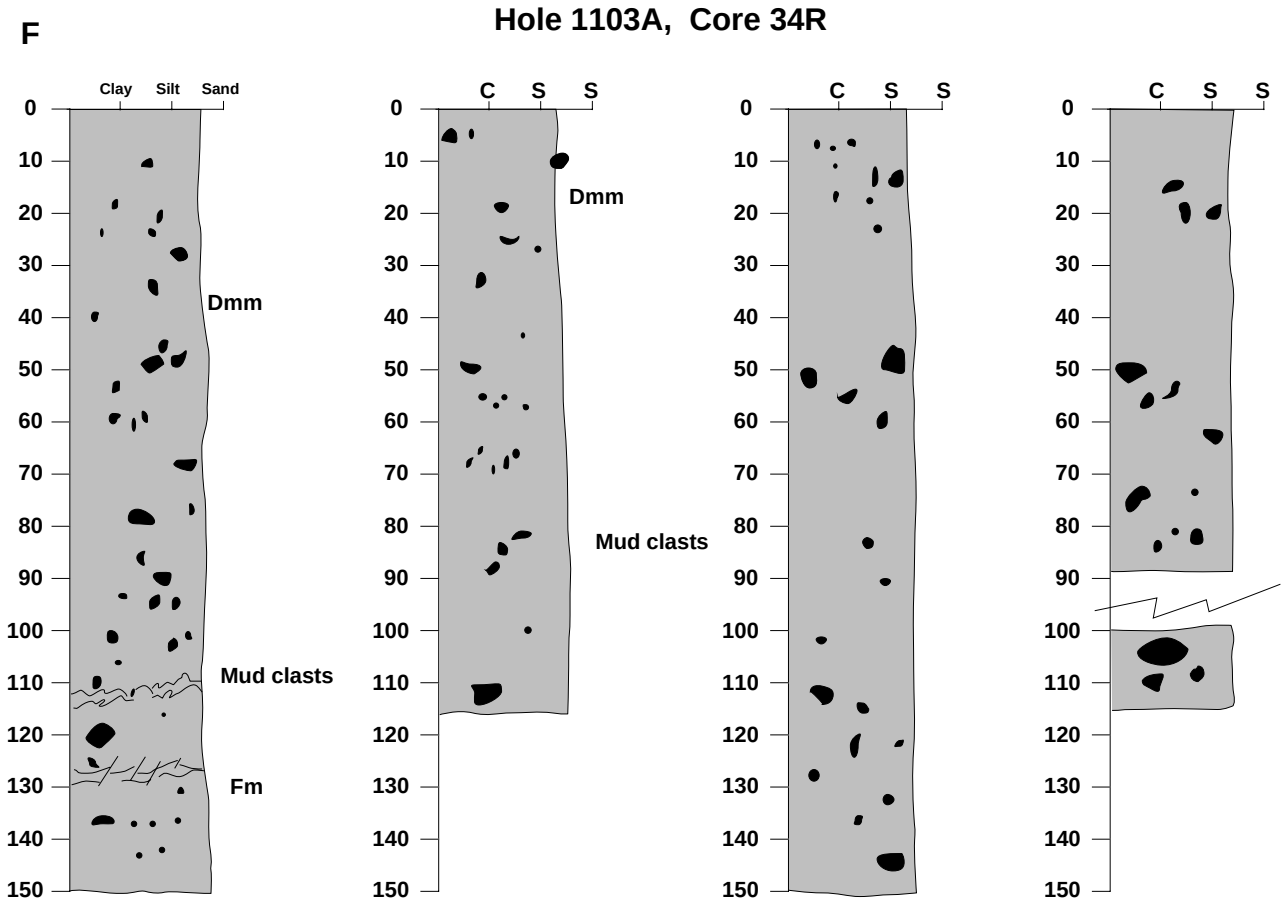

**Figure F7 (continued).** G. Detailed graphic logs showing each section of recovery for Core 178-1103A-35R.

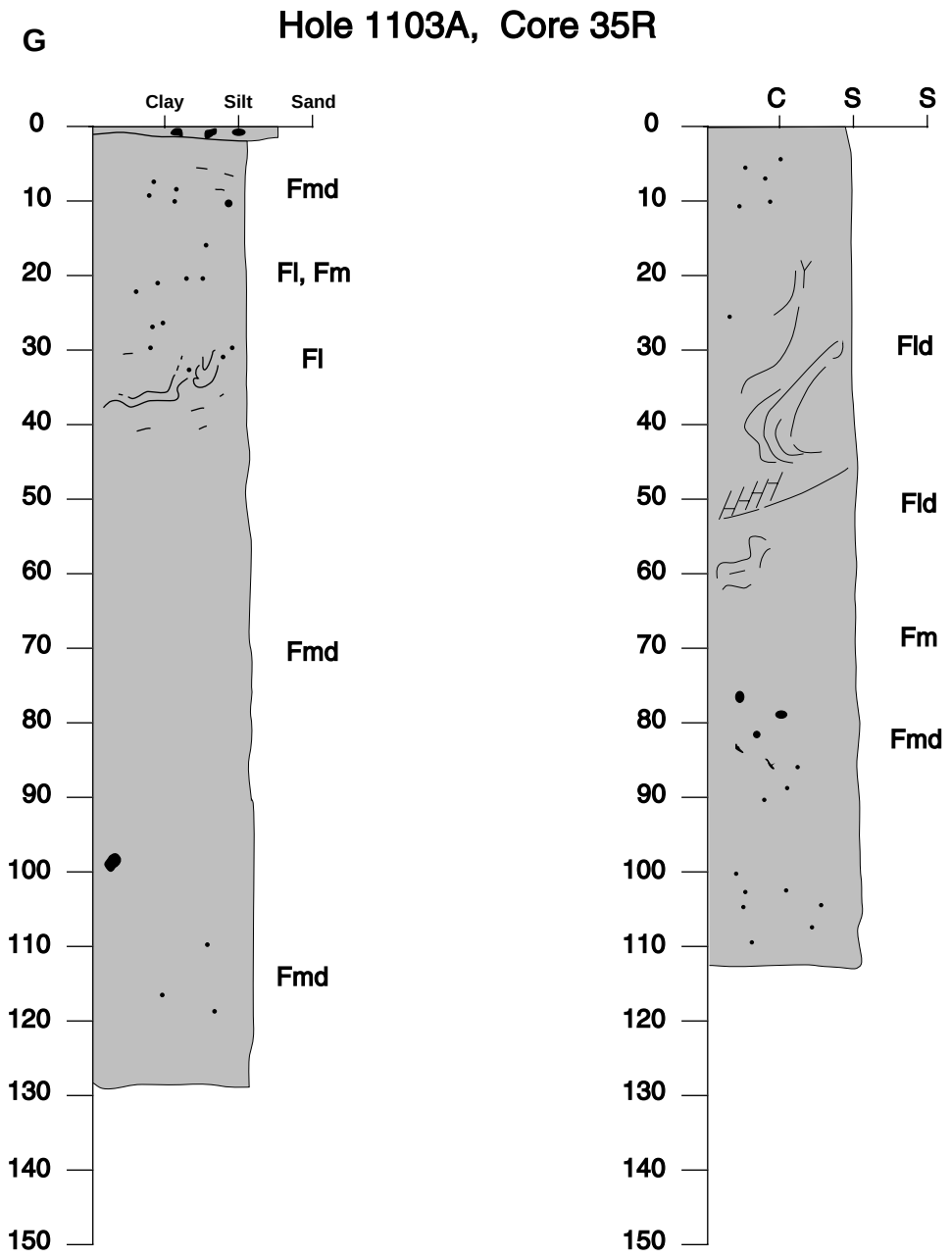

**Figure F7 (continued). H.** Detailed graphic logs showing each section of recovery for Core 178-1103A-36R.

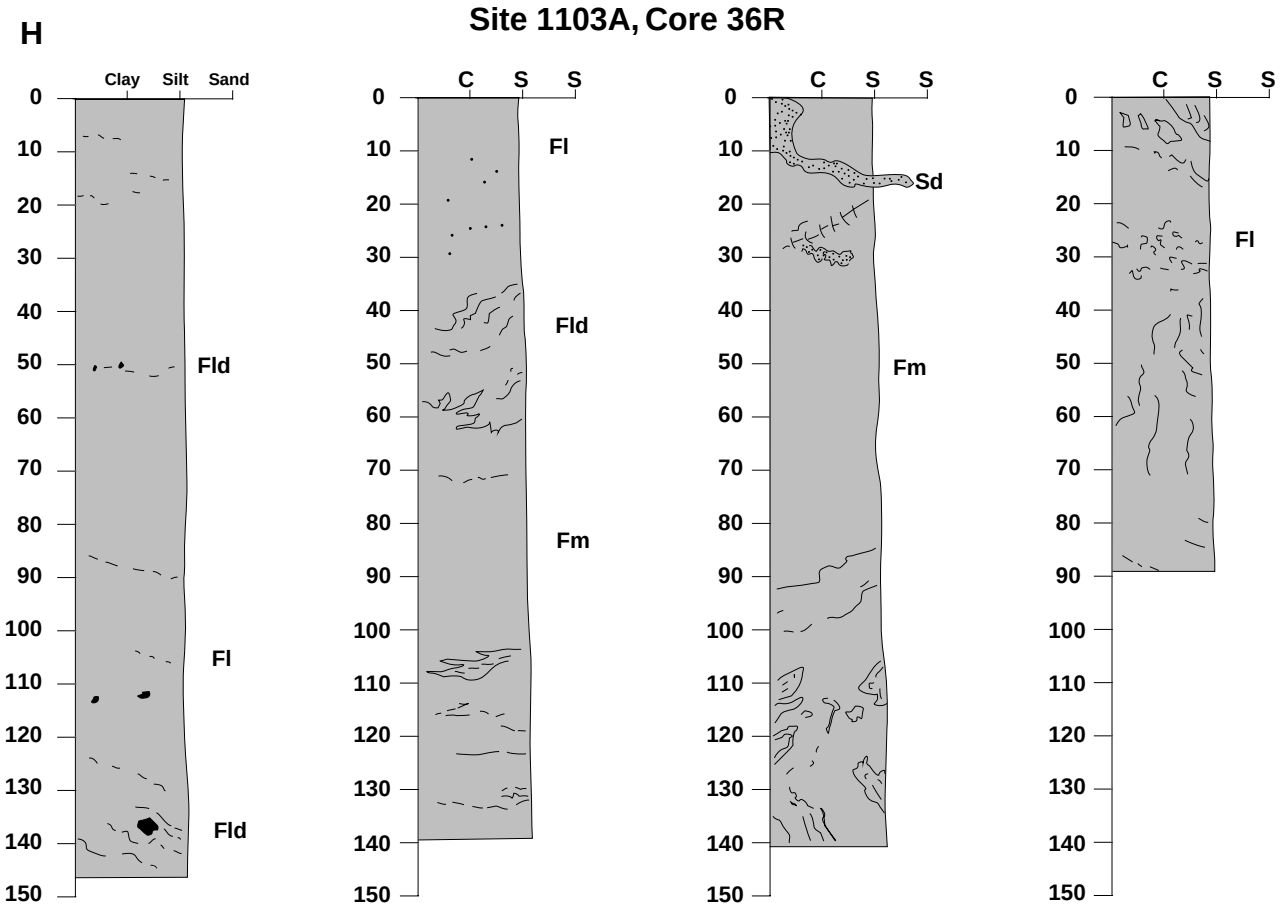

**Figure F7 (continued). I.** Detailed graphic logs showing each section of recovery for Core 178-1103A-37R.

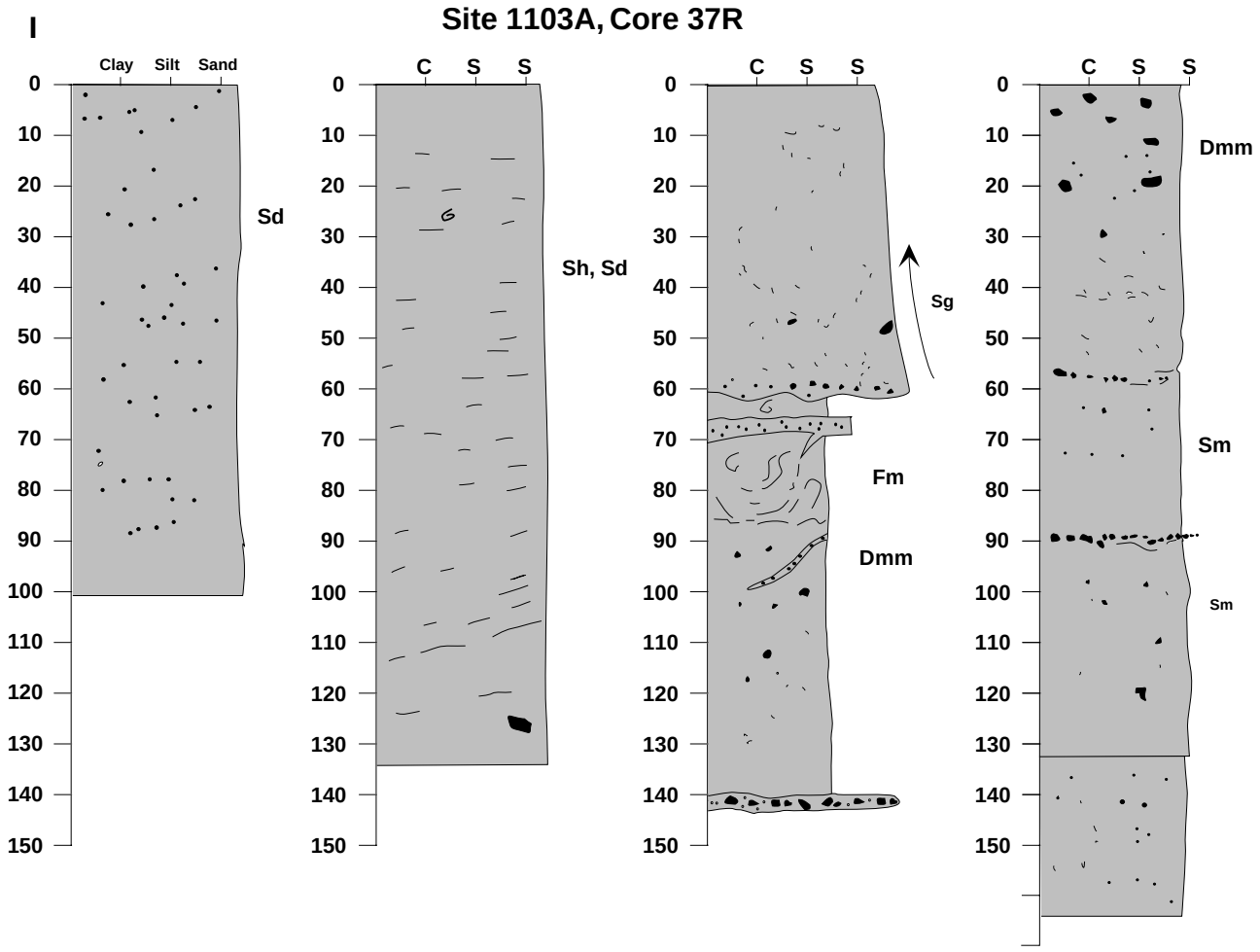

**Figure F7 (continued). J.** Detailed graphic logs showing each section of recovery for Core 178-1103A-38R.

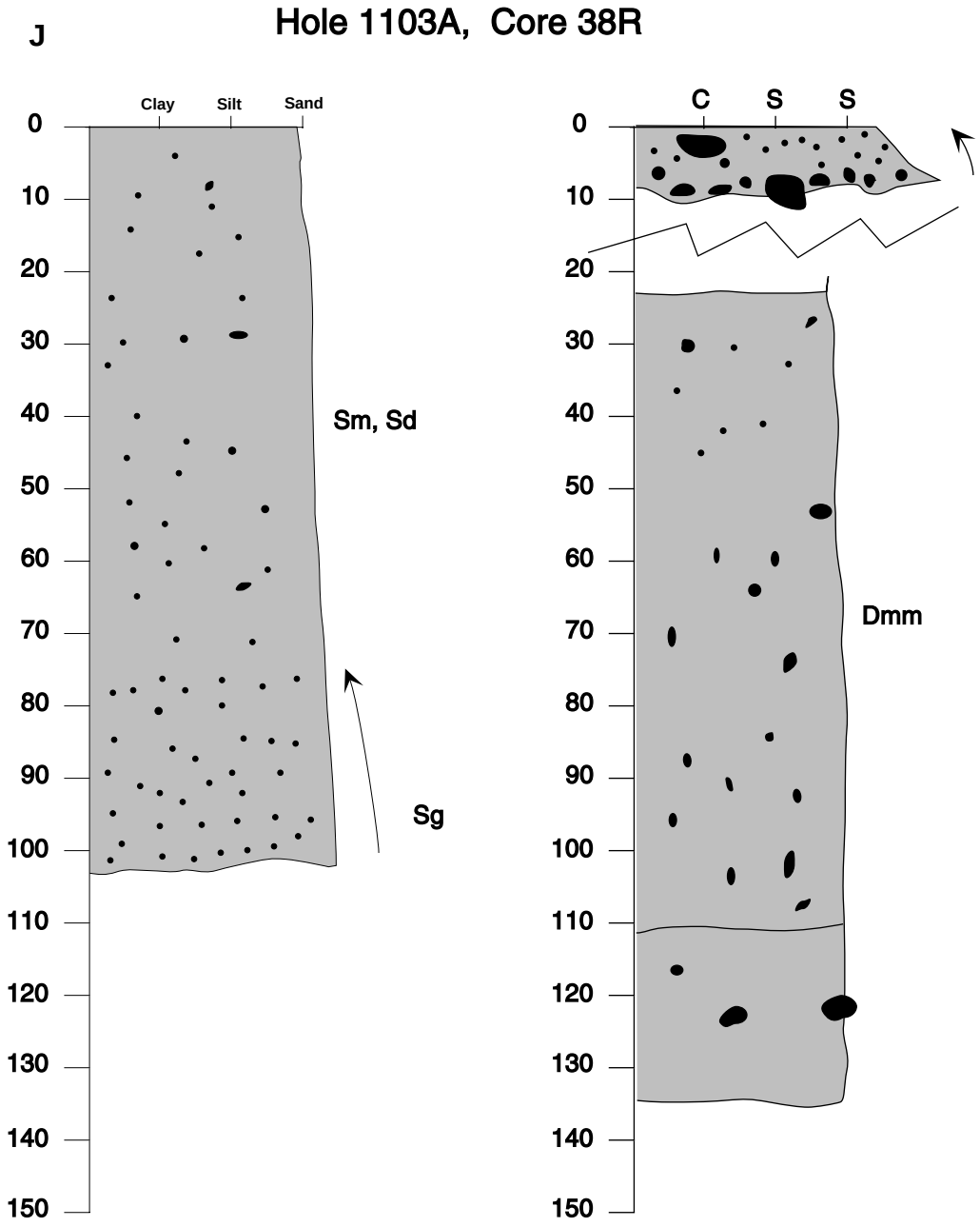

**Figure F8. A.** Massive diamict (Facies Dmm) (interval 178-1103A-27R-2, 9–23 cm). **B.** Massive diamict facies with numerous light-colored silt clasts (interval 178-1103A-34R-4, 43–53 cm). (Continued on next page.)

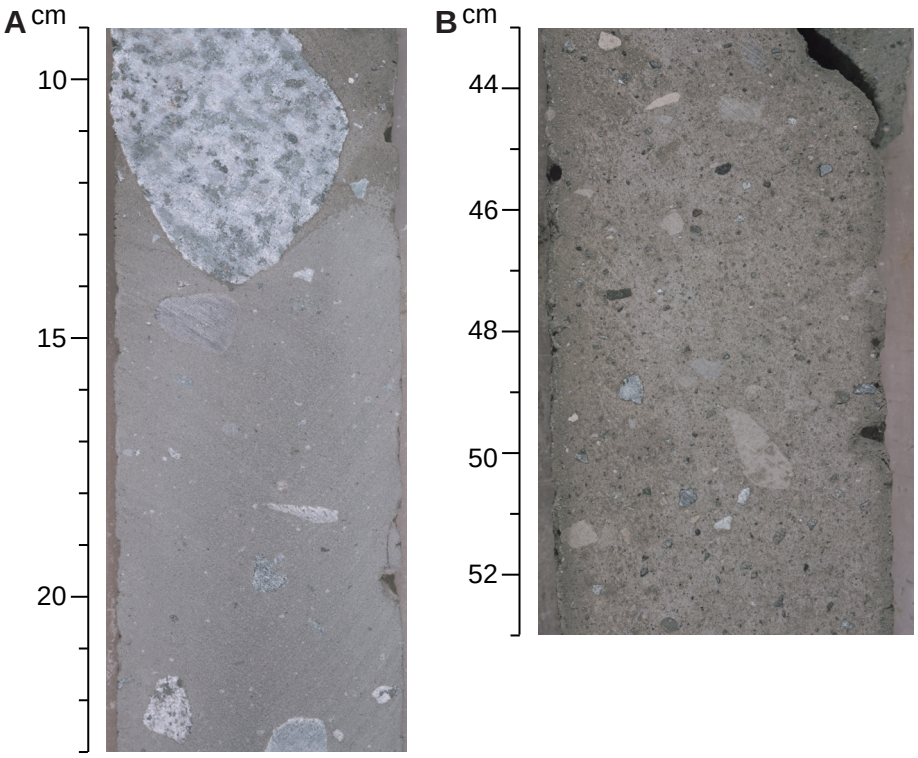

**Figure F8 (continued).** **C.** Chaotically stratified diamict (Facies Dms) (interval 178-1103A-28R-2, 83–92 cm). **D.** Chaotically bedded diamict (interval 178-1103A-28R-2, 24–41 cm).

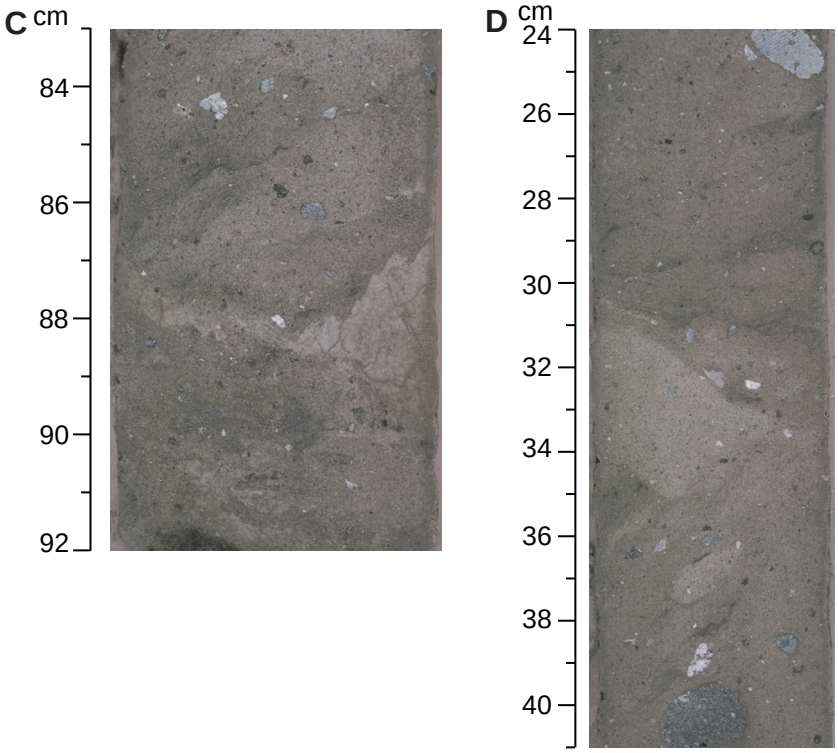

**Figure F9.** Distribution plots of clast long-axis dip angles for diamictites from Site 1103.

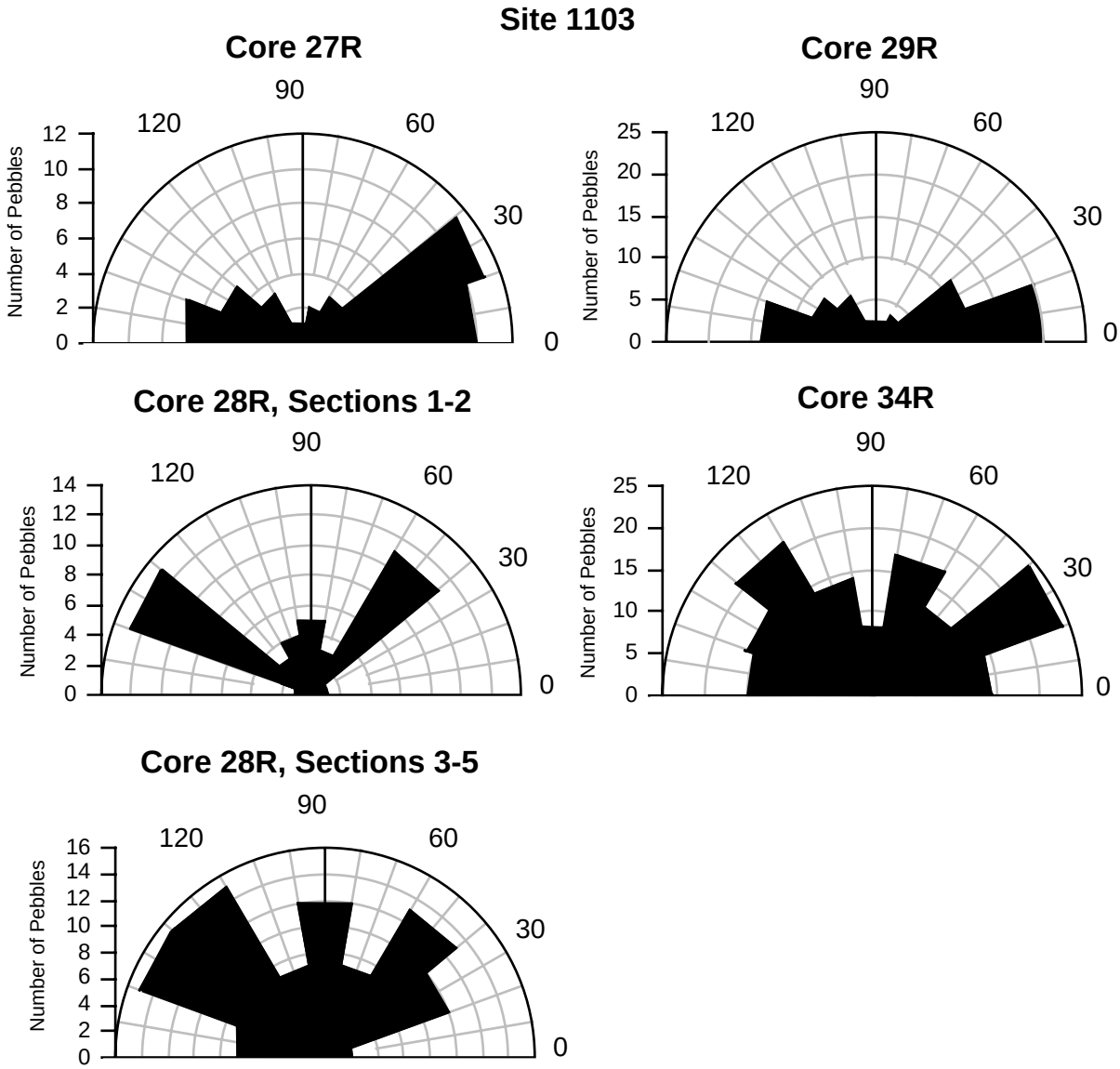

**Figure F10. A.** Chaotically bedded sandstone (Facies Sd) (interval 178-1103A-38R-1, 53–67 cm). **B.** Thin sandstone bed in interval 178-1103A-33R-1, 55–63 cm.

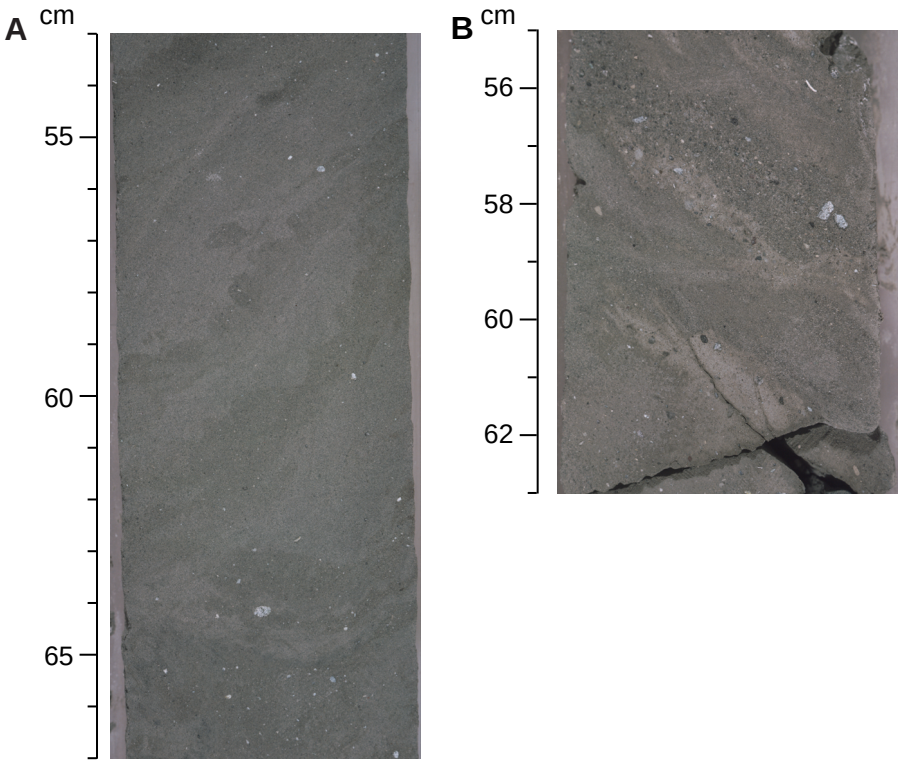

**Figure F11. A.** Massive mudstone facies (Fm) (interval 178-1103A-31R-1, 137–146 cm). **B.** Weakly laminated mudstone facies (Facies Fl) (interval 178-1103A-31R-1, 95–106 cm). (Continued on next page.)

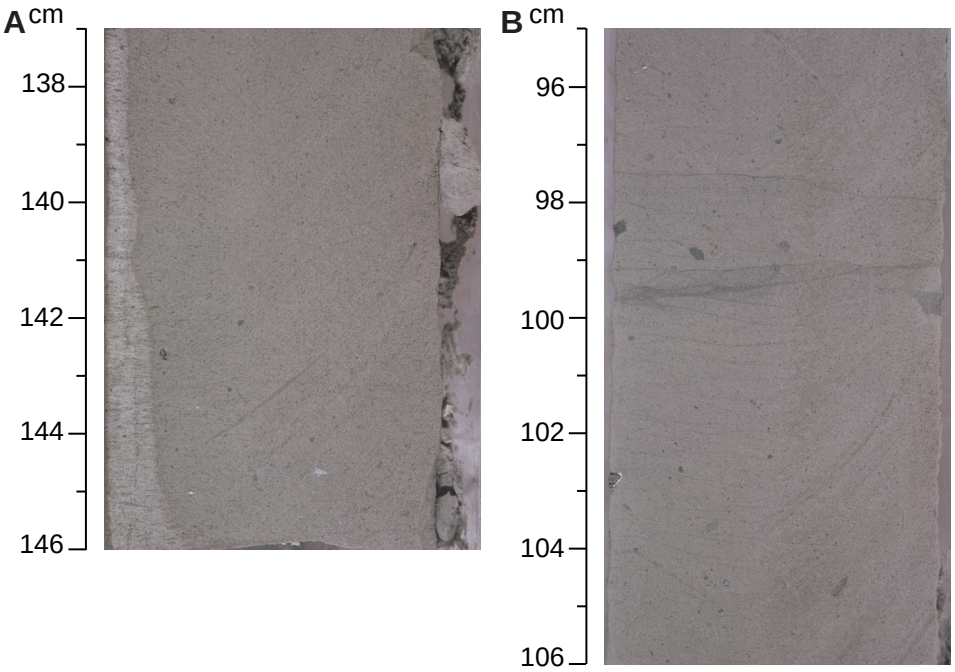

**Figure F11 (continued).** C. Weakly laminated mudstone facies (Facies Fl) (interval 178-1103A-31R-1, 55–67 cm).

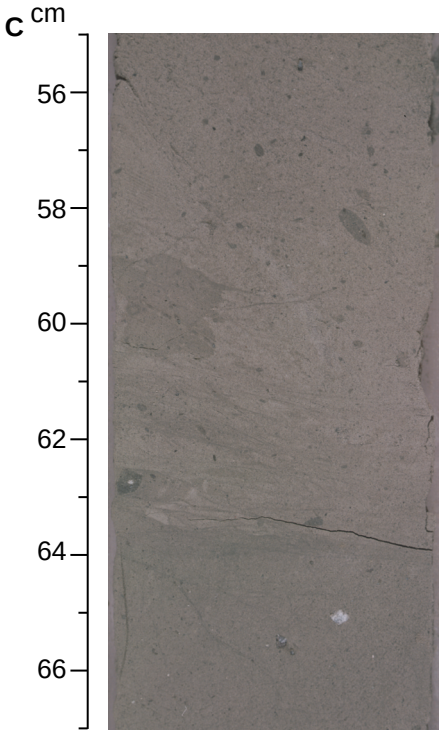

**Figure F12.** A summary of the occurrence of diatoms, radiolarians, and planktonic foraminifers at Site 1103. Stippled intervals = barren of microfossils.

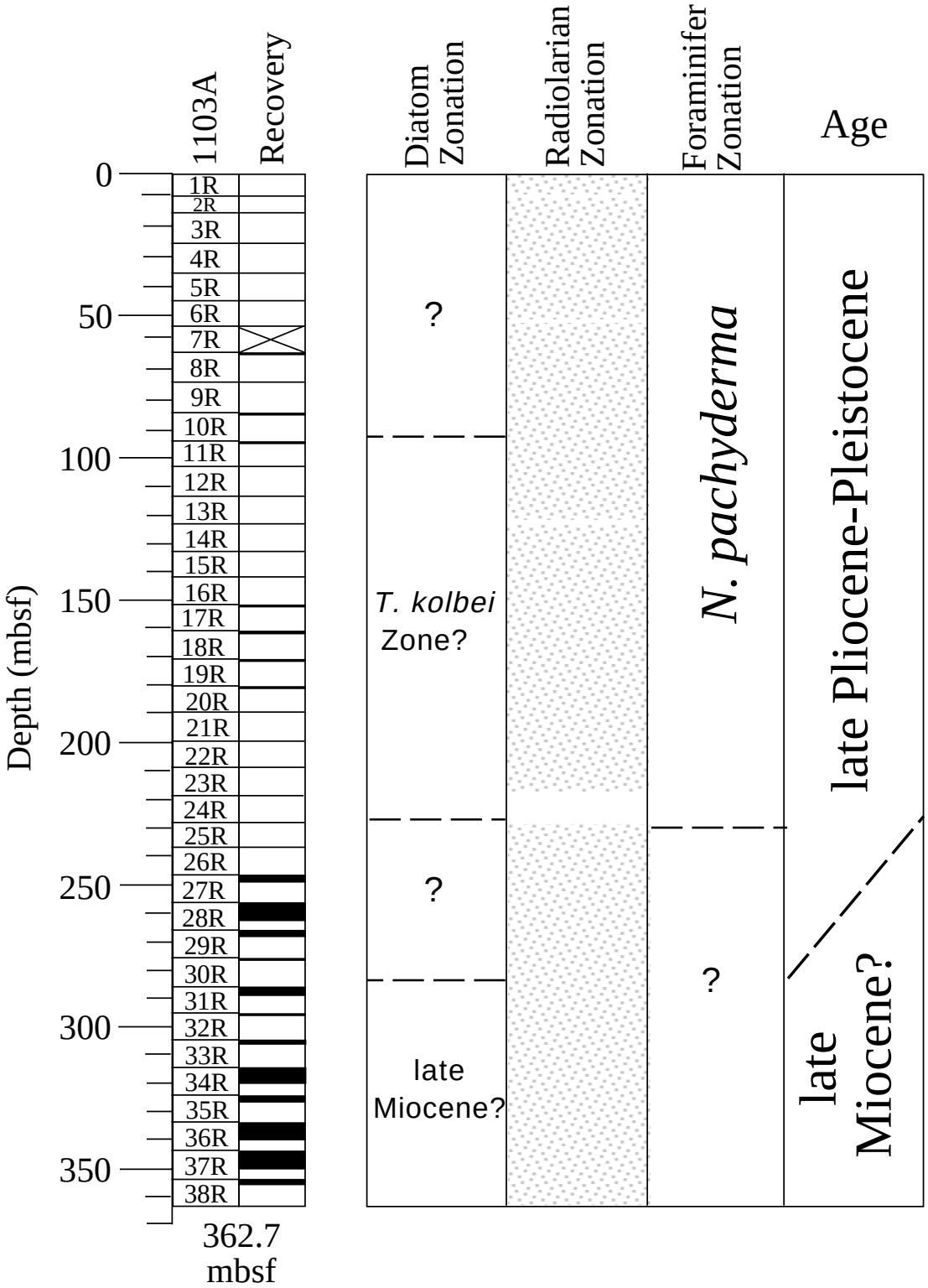

**Figure F13.** AF demagnetization of discrete Sample 178-1103A-27R-1, 13–15 cm. **A.** Orthogonal projection of the end-points of the remanence vector. Open and solid symbols represent the vertical and horizontal projections, respectively. The steeply inclined drill-string overprint was removed after AF demagnetization at 10 mT. **B.** Enlarged view of boxed region in **A**. After removal of the drill-string overprint at 10 mT, the intensity of this sample is in the noise level of the magnetometer. **C.** Change in the intensity of remanence during AF demagnetization. **D.** Equal-area projection of the remanence vector during AF demagnetization. No stable direction can be obtained from this sample.

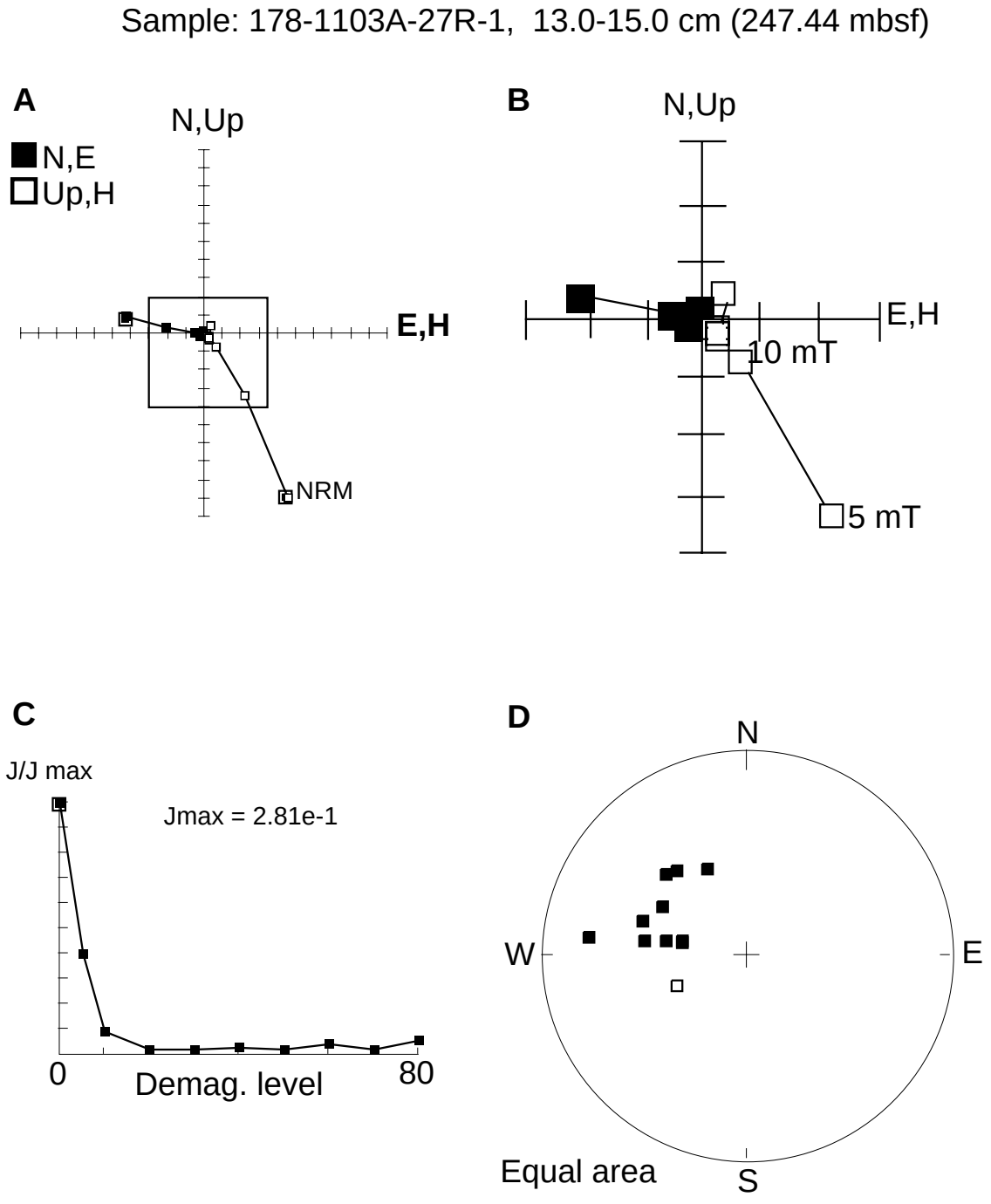

**Figure F14.** AF demagnetization of discrete Sample 178-1103A-27R-1, 15–17 cm, following LTD. **A.** Change in the intensity of remanence at the NRM step before and after LTD and during AF demagnetization. **B.** Equal-area projection of the remanence vector before and after LTD and during AF demagnetization.

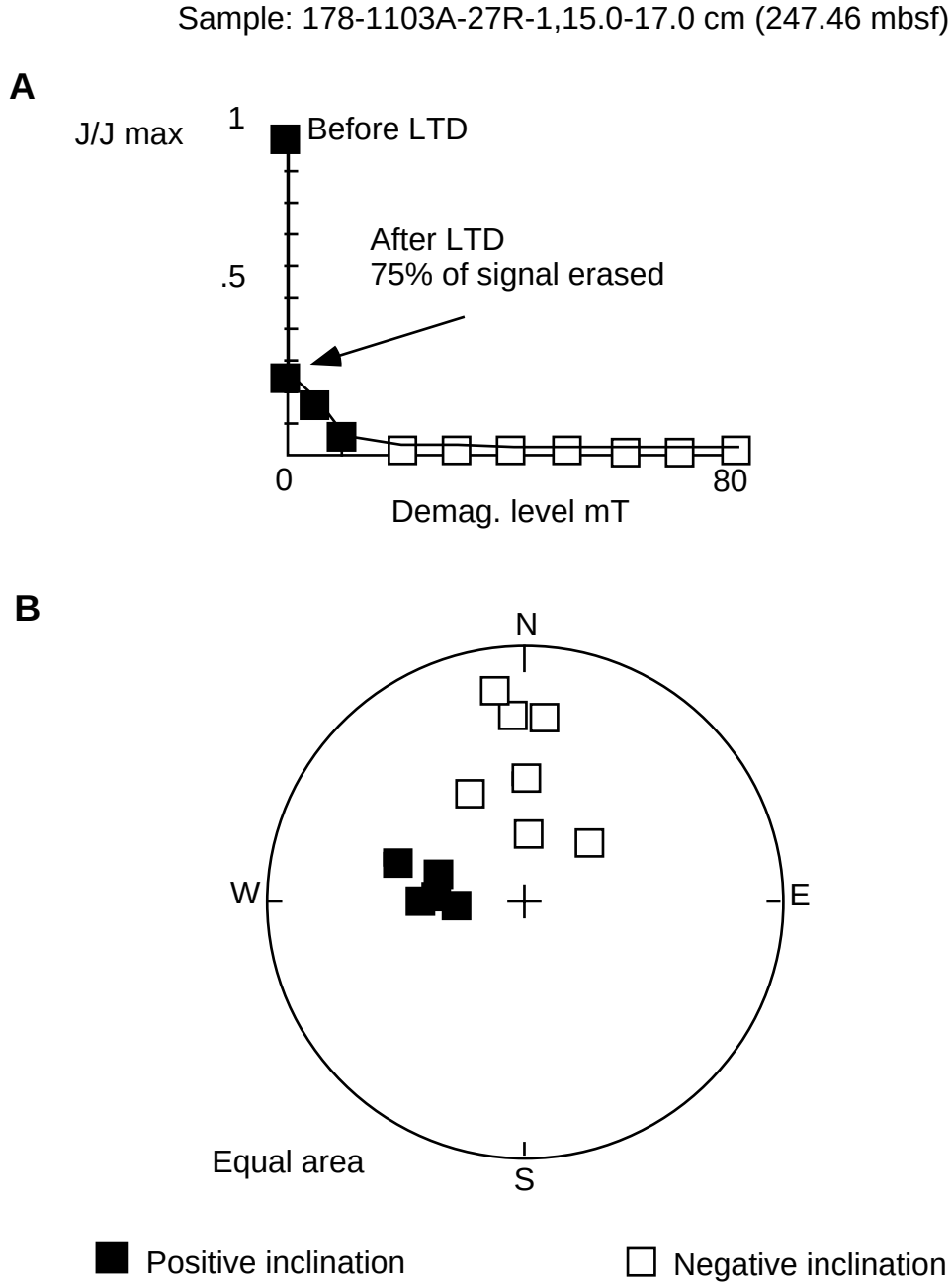

**Figure F15. A.** Inclination vs. depth (mbsf) after AF demagnetization at 30 mT for Hole 1100C. **B.** Intensity of magnetization vs. depth (mbsf) after AF demagnetization at 30 mT for Hole 1100C.

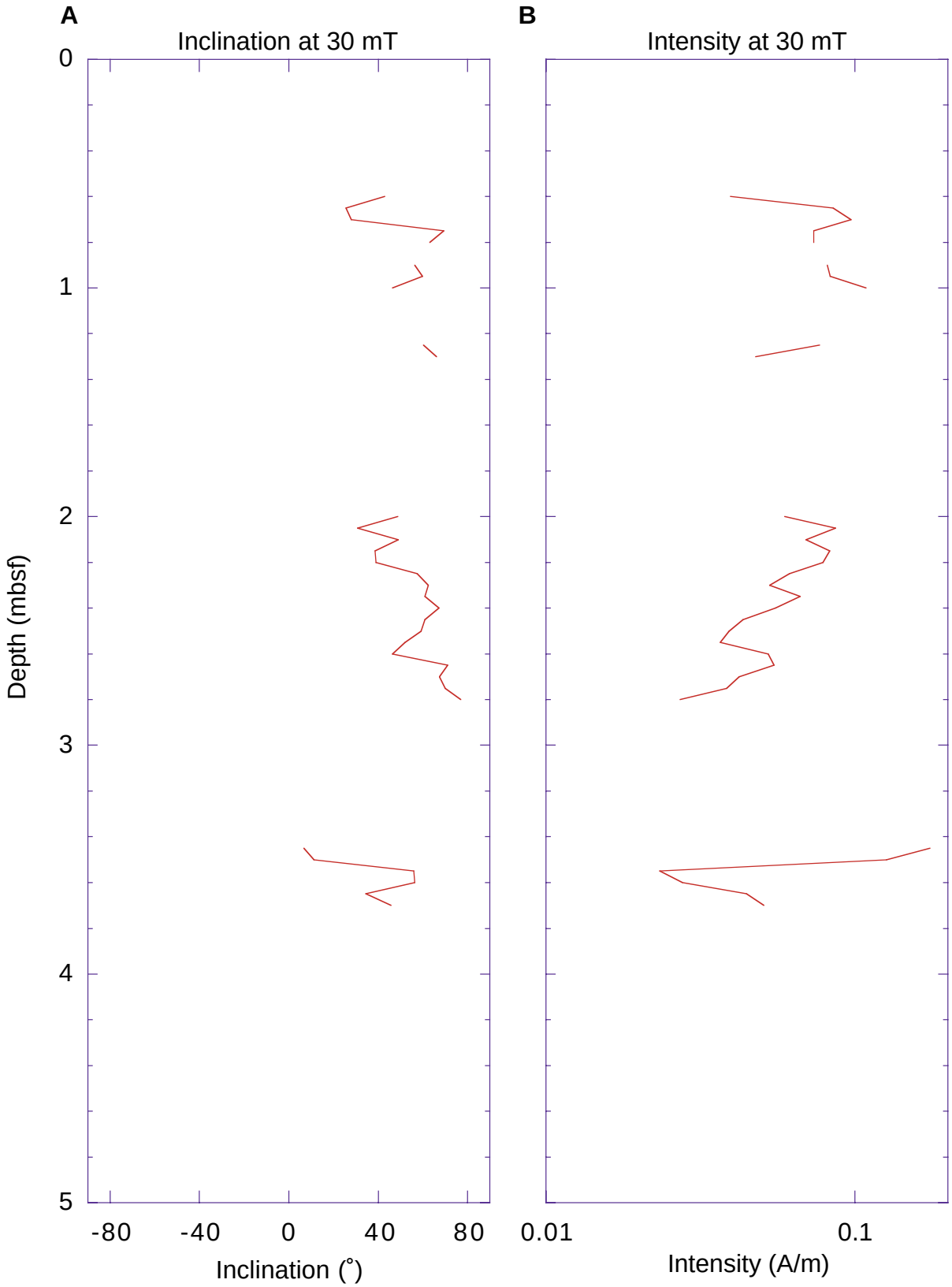

**Figure F16.** AF demagnetization of discrete Sample 178-1103A-31R-3, 3–5 cm. **A.** Orthogonal projection of the end-points of the remanence vector. Open and solid symbols represent the vertical and horizontal projections, respectively. The steeply inclined drill-string overprint was removed after AF demagnetization at 10 mT. **B.** Change in the intensity of remanence during AF demagnetization. **C.** Equal-area projection of the remanence vector during AF demagnetization.

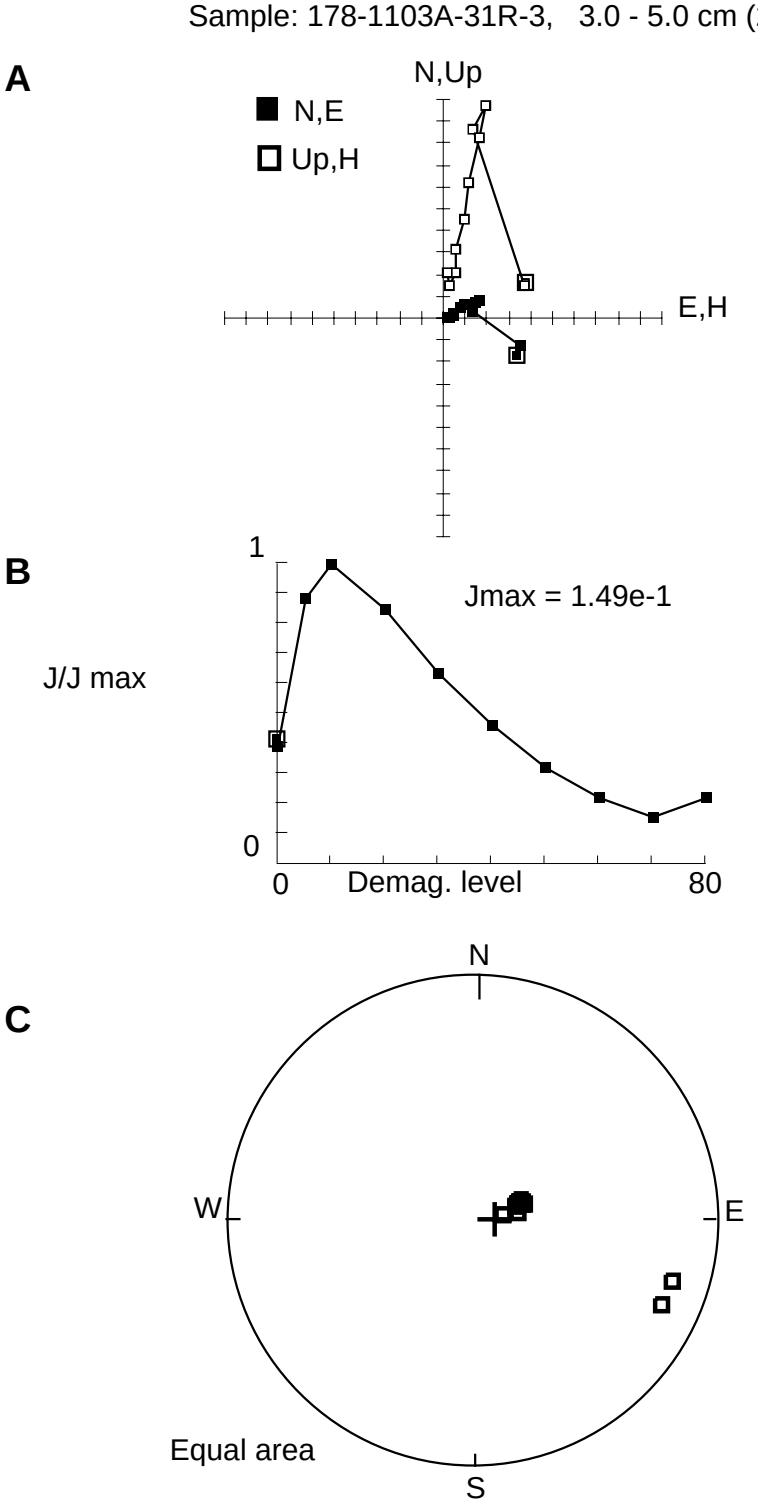

**Figure F17.** Inclination vs. depth (mbsf) after AF demagnetization at 30 mT for the shelf transect sites.

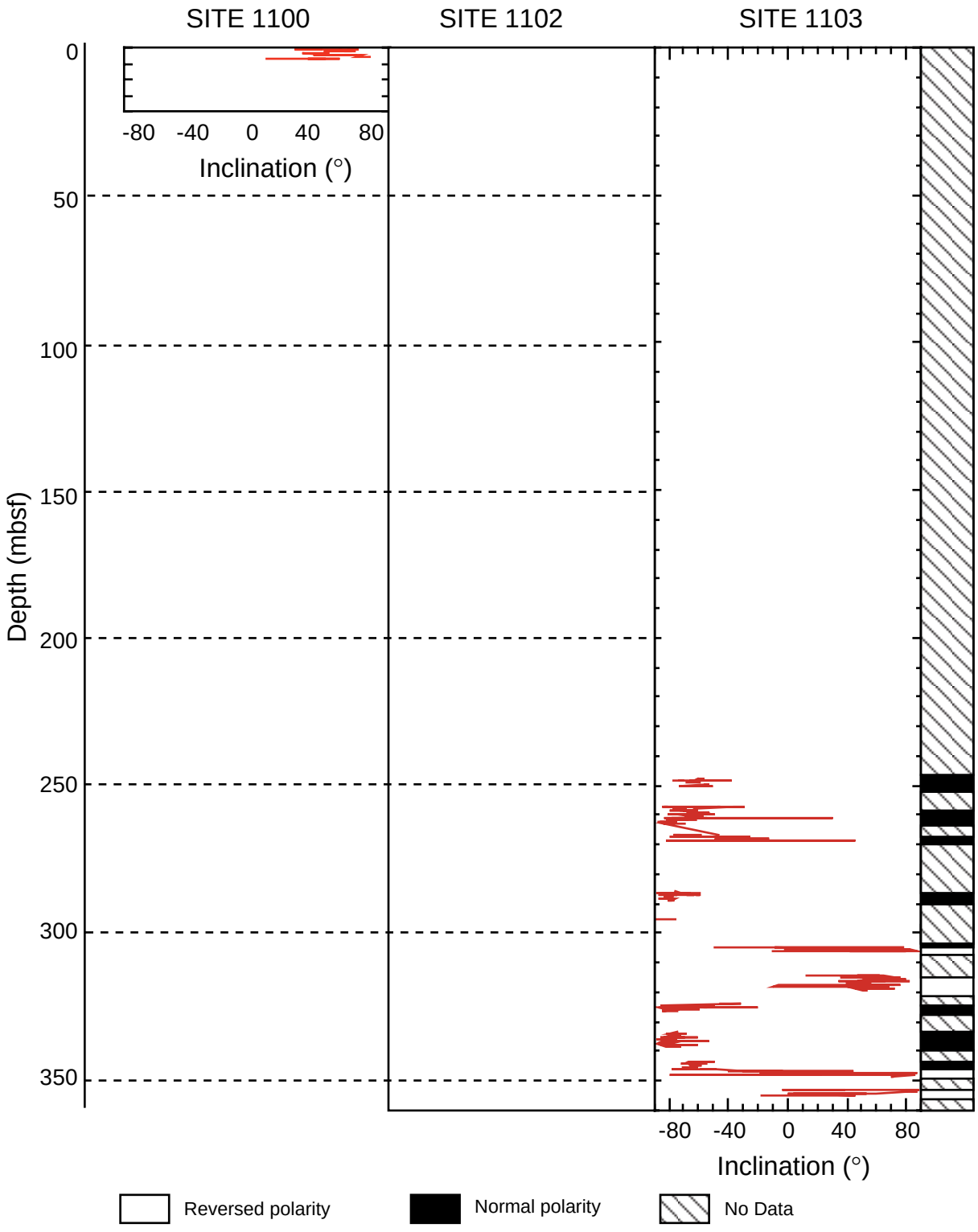

**Figure F18. A.** Inclination vs. depth (mbsf) after AF demagnetization at 30 mT for the high-recovery interval at Site 1103. **B.** Intensity of remanence vs. depth (mbsf) after AF demagnetization at 30 mT for the high-recovery interval at Site 1103.

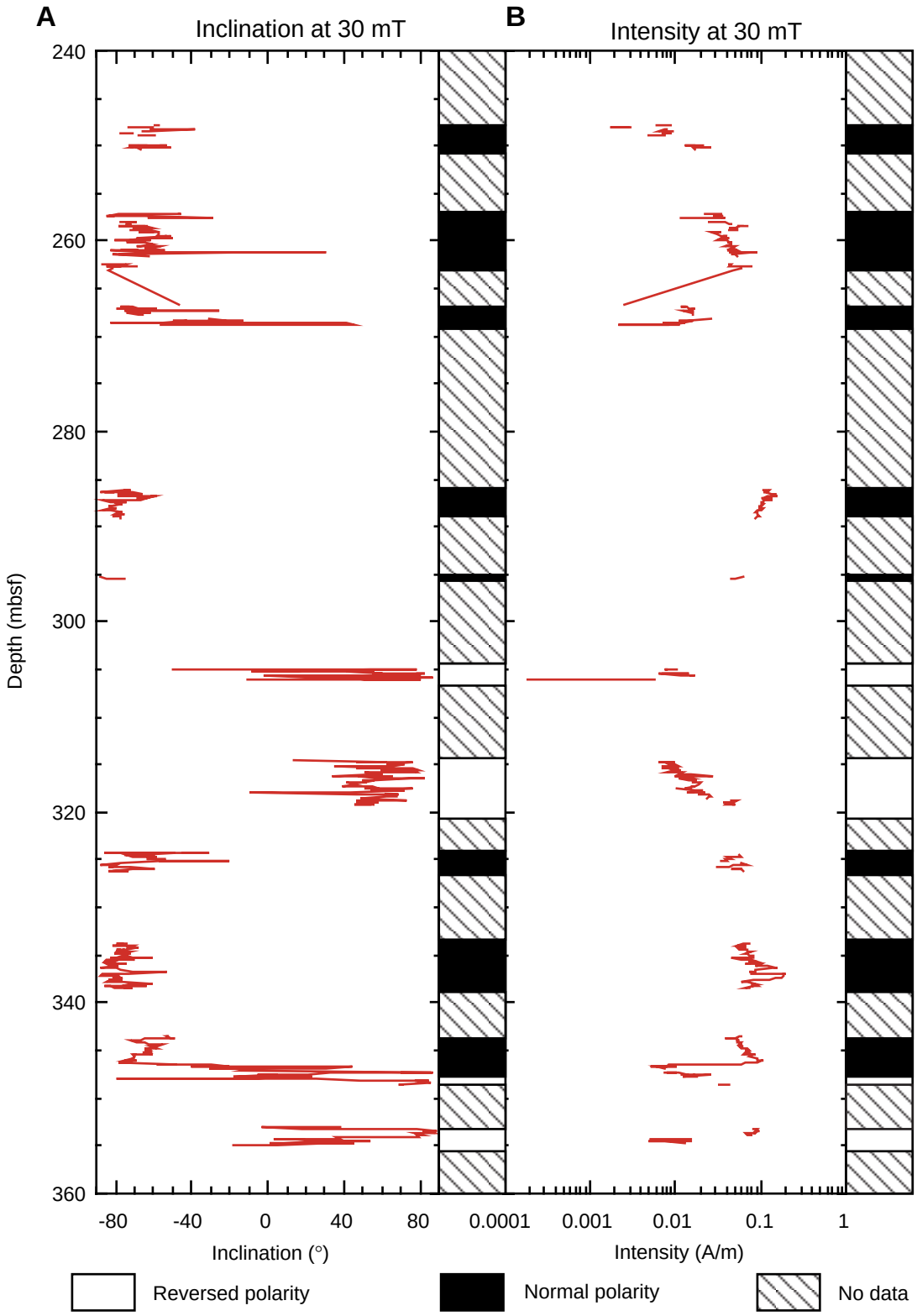

**Figure F19.** Raw (**A**) NGR, (**B**) GRAPE density, (**C**) magnetic susceptibility, and (**D**) *P*-wave velocity data for Site 1100. GRAPE data were truncated at 1.2 g/cm³ and susceptibility at 0 SI to remove equipment noise. *P*-wave data were truncated at 2200 m/s.

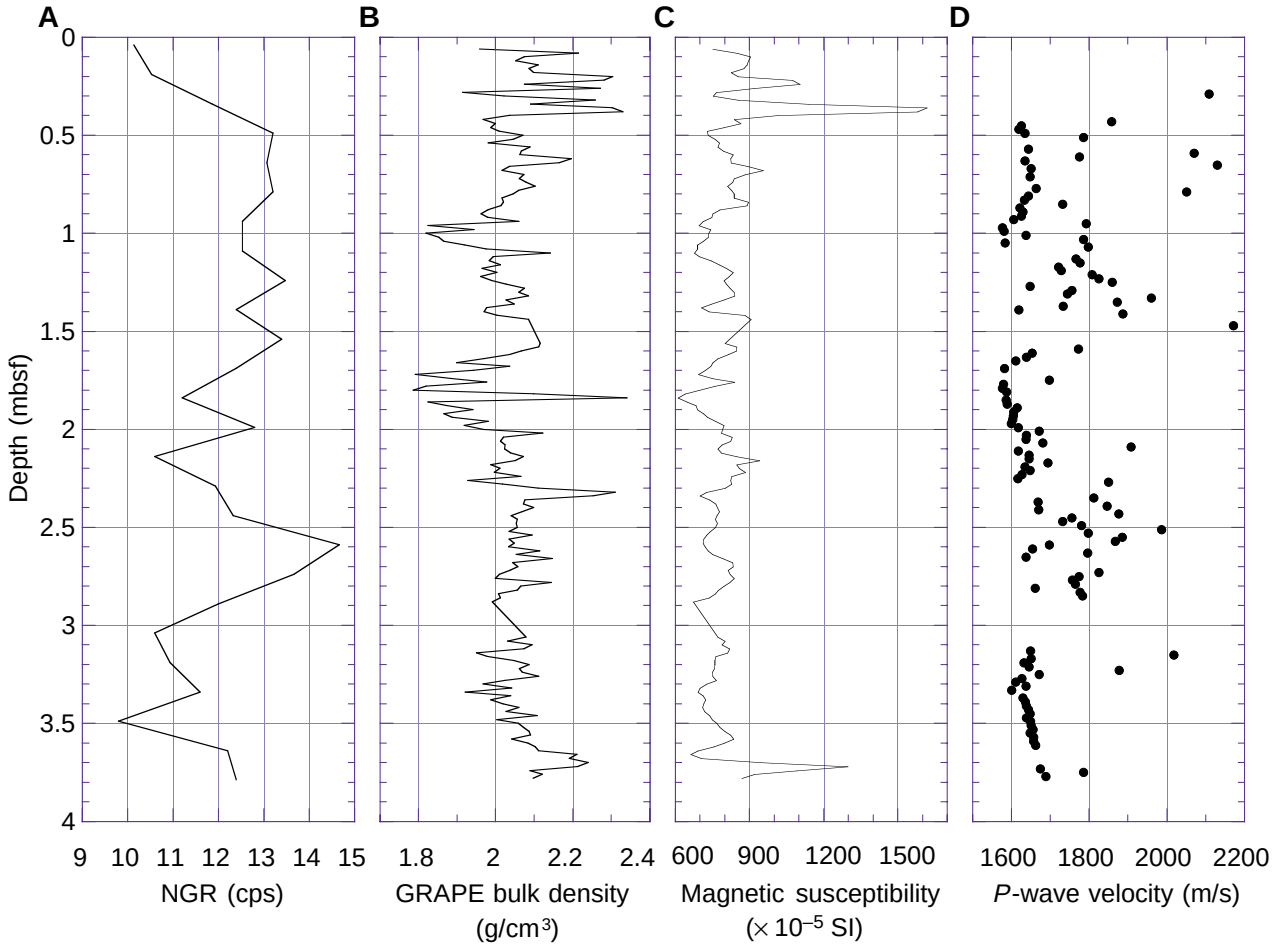

**Figure F20.** Raw (**A**) NGR, (**B**) GRAPE density, and (**C**) magnetic susceptibility data for Site 1103. GRAPE data were truncated at 1.2 g/cm³ and susceptibility at 0 SI to remove equipment noise. *P*-wave data were truncated at 2200 m/s.

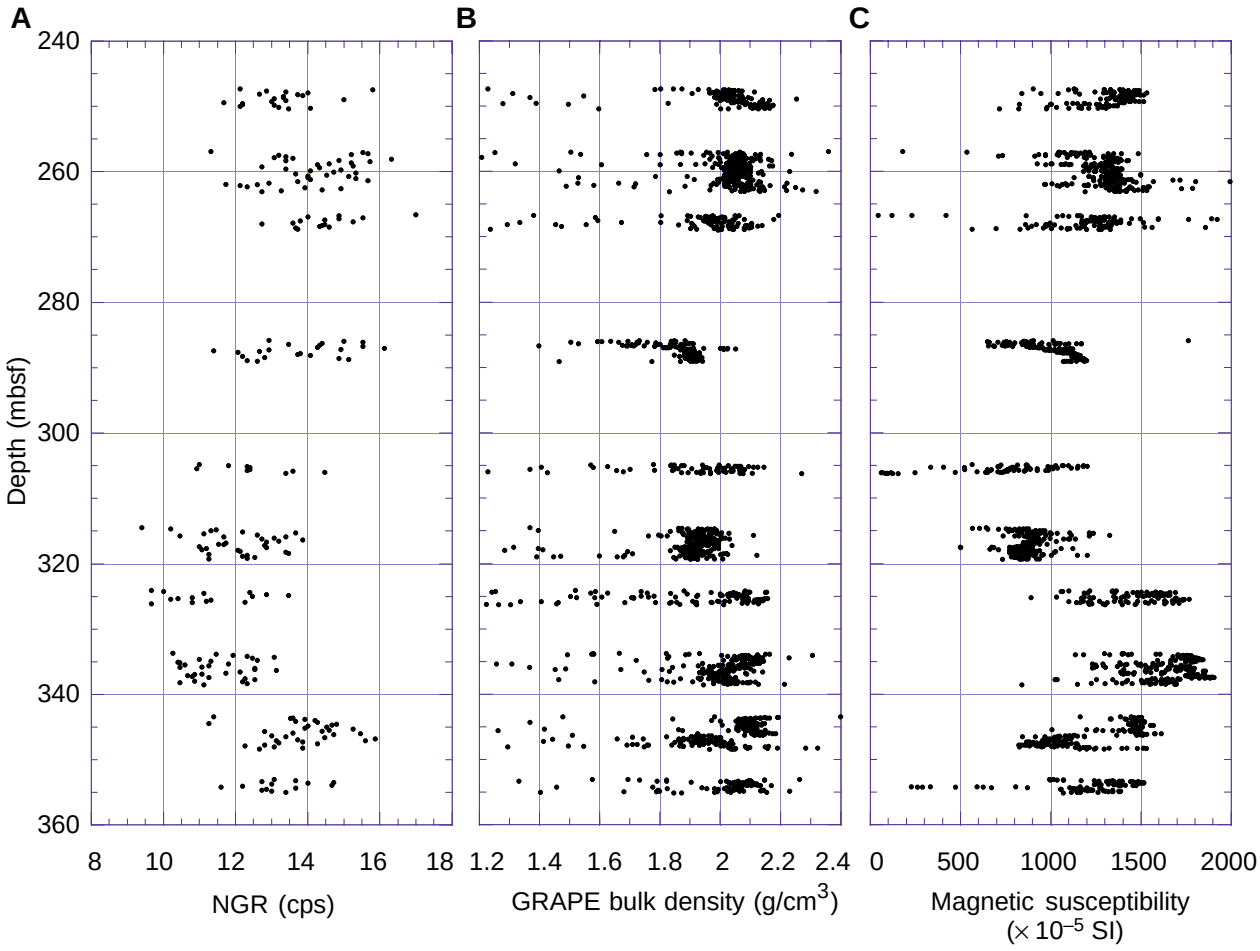

**Figure F21.** Lithofacies from Site 1103 in magnetic susceptibility vs. NGR space.

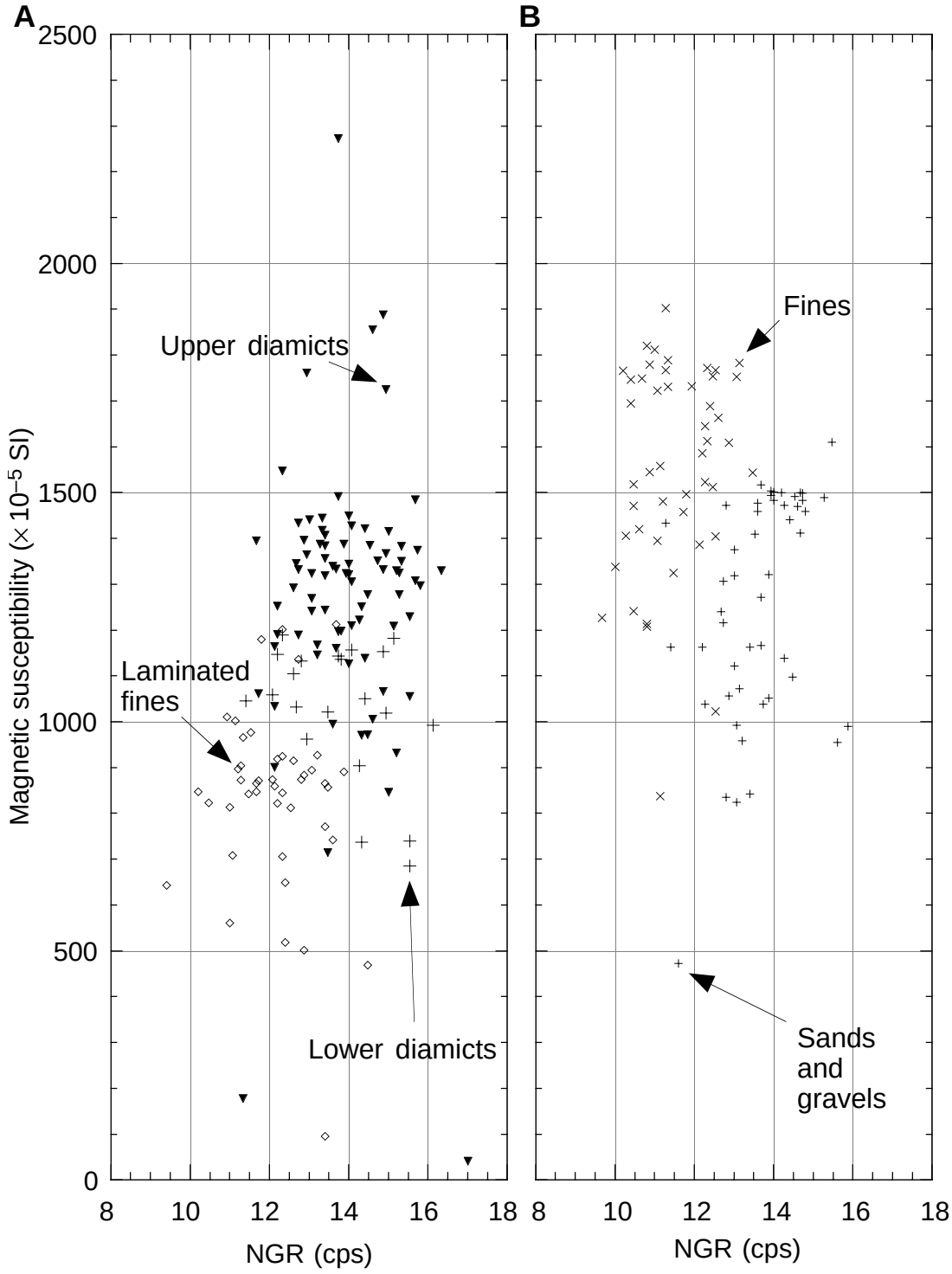

**Figure F22.** (**A**) GRAPE and MAD bulk density, (**B**) grain density, and (**C**) porosity from Site 1100.

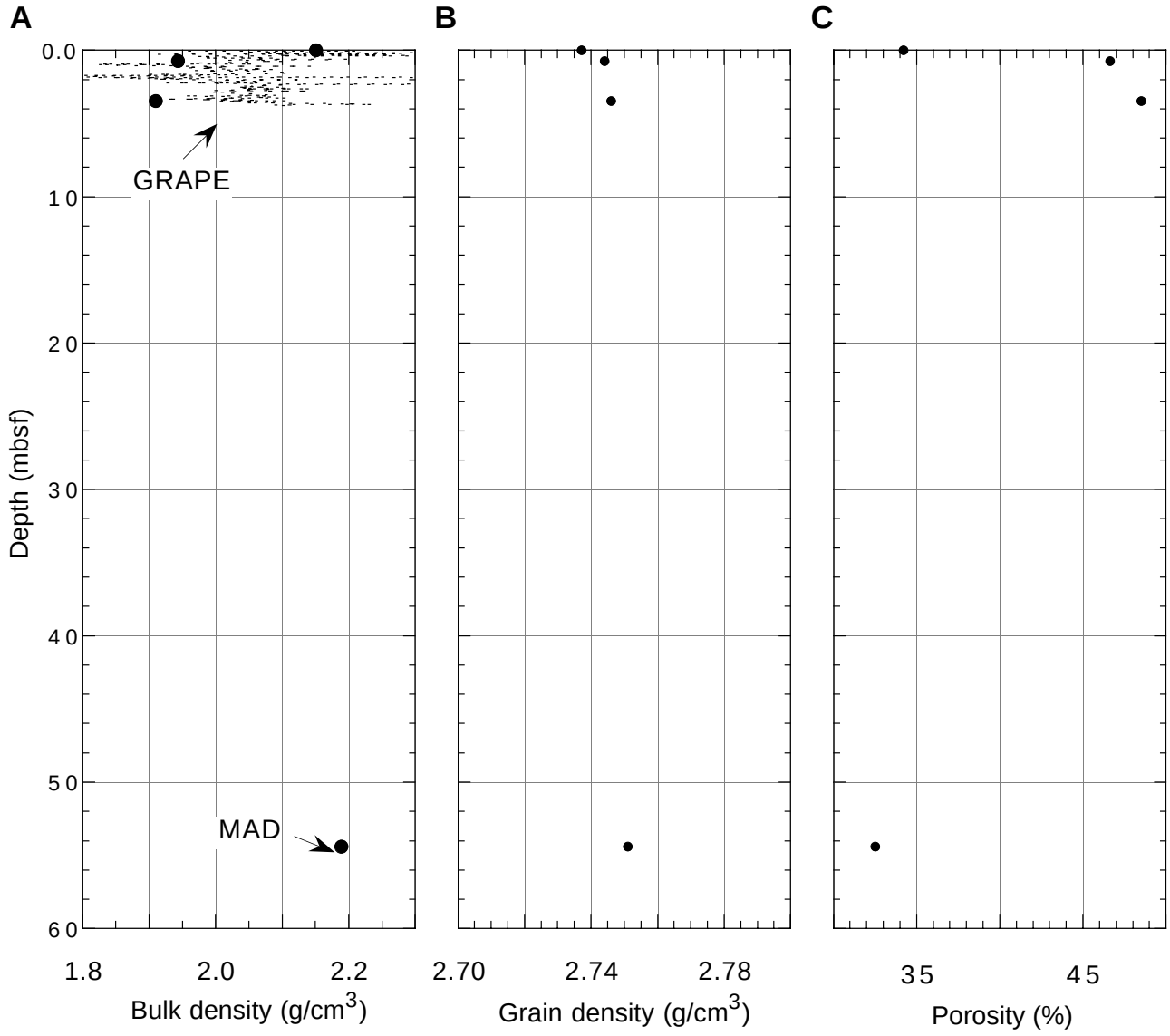

**Figure F23.** (**A**) GRAPE and MAD bulk density, (**B**) grain density, and (**C**) porosity from Site 1103.

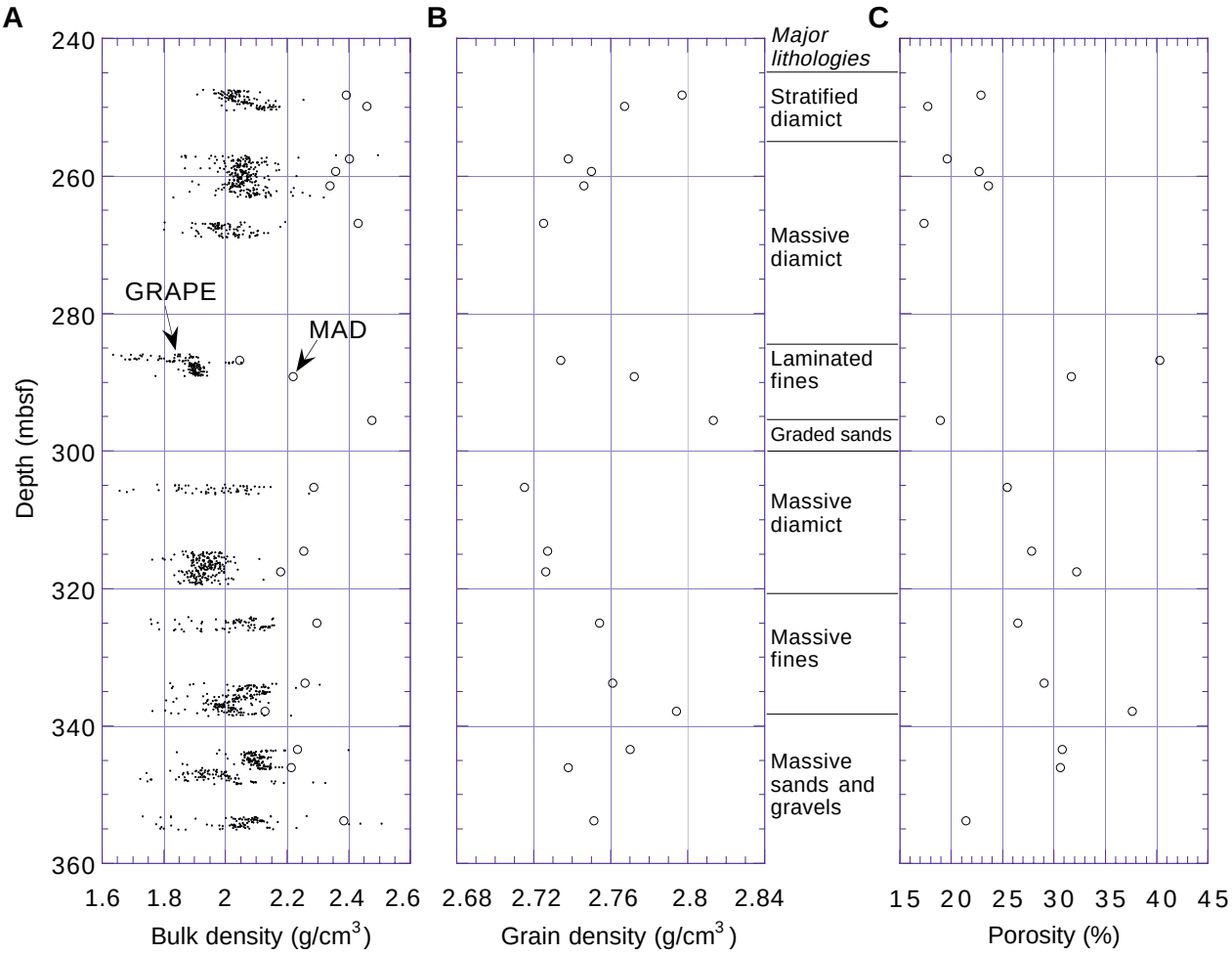

**Figure F24.** PWS3 data for Site 1103.

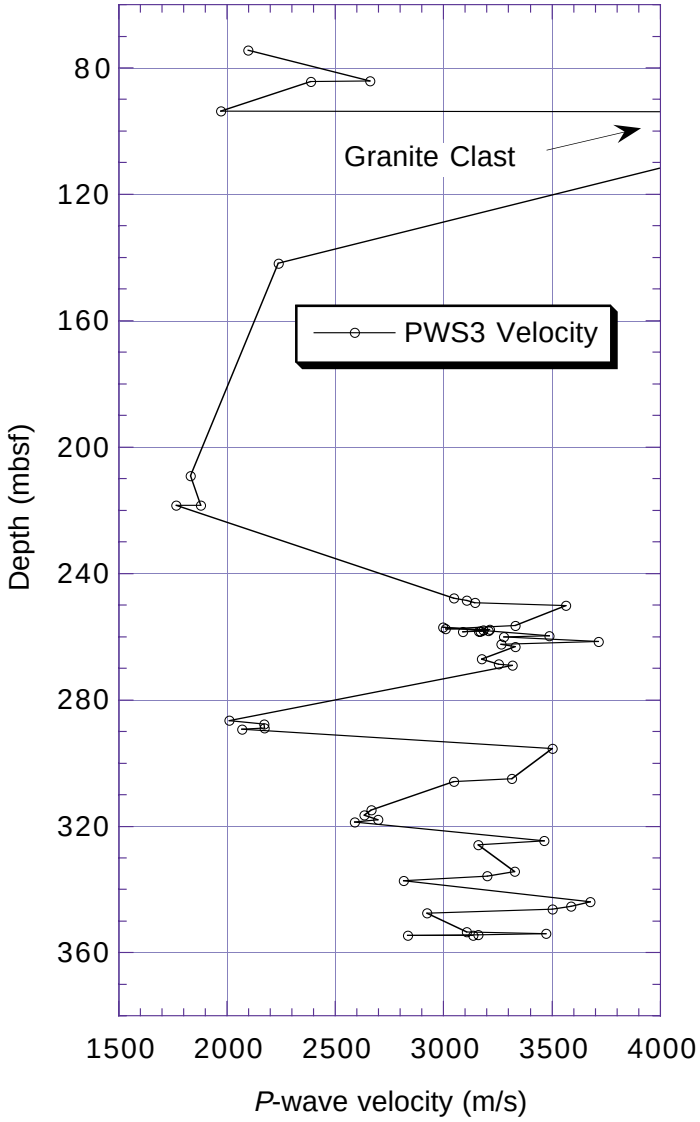

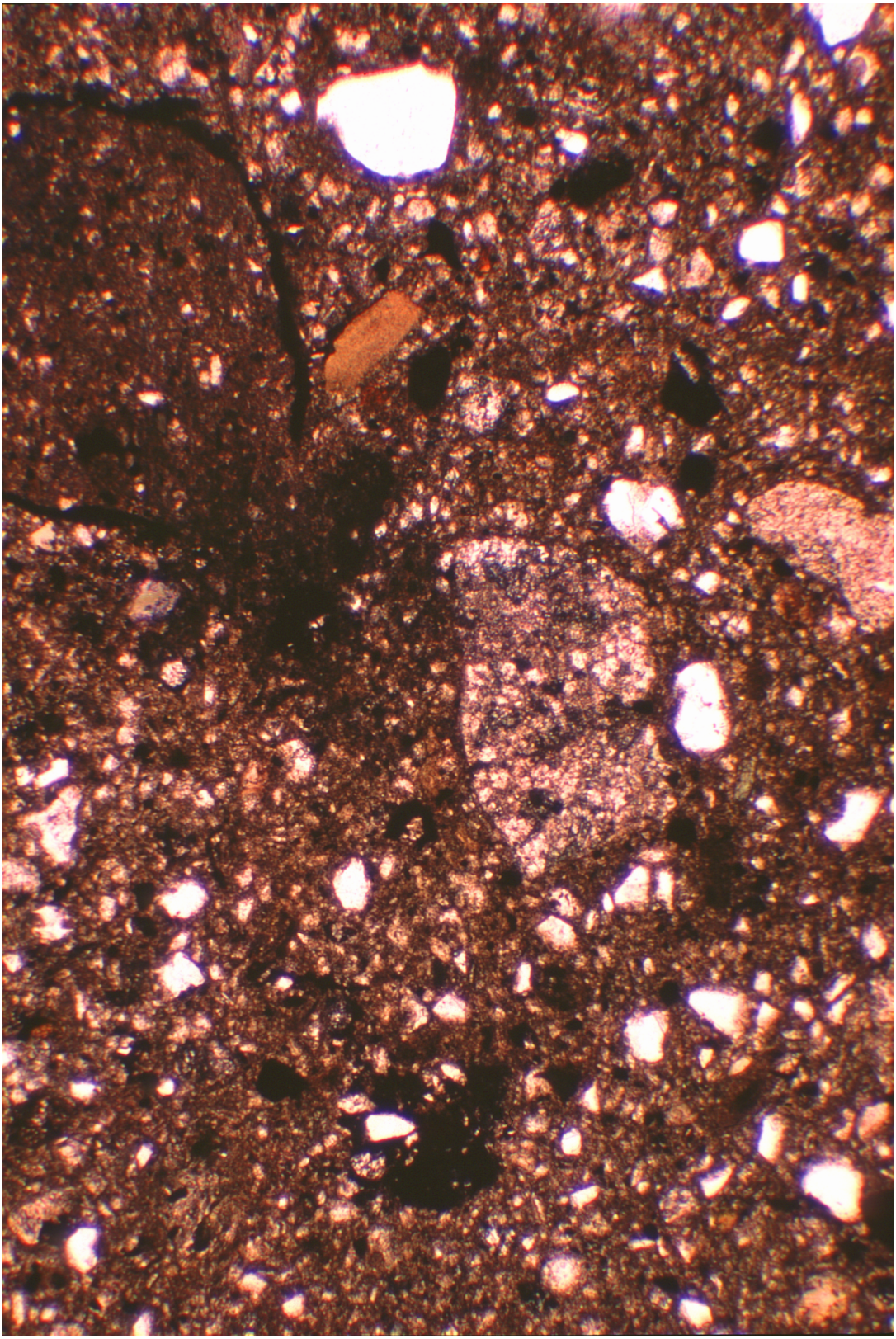

**Figure F25.** Photomicrograph of Sample 178-1103A-34R-1, 107 cm (plane-polarized light), taken across the boundary between a thick diamict and a thin (<3 cm thick) clay-rich bed, at 10:1 magnification. See "Micromorphology," p. 18, for details.

**Figure F26.** Graphic summary of downhole logging operations at Hole 1103A. Seafloor was picked on the basis of the step in natural gamma activity at the sediment/water boundary.

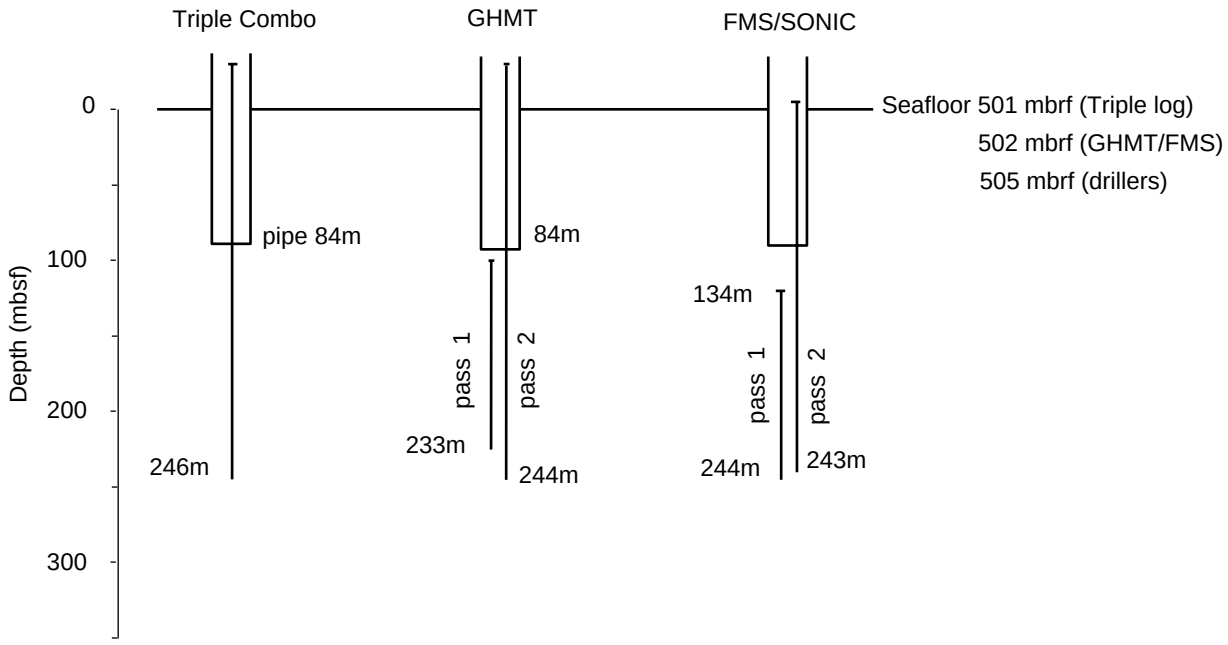

**Figure F27.** Downhole logs of hole diameter, total natural gamma (HSGR), bulk density (RHOM), porosity (IPLC), total natural gamma from GHMT (SGR), sonic velocity (see **"Log Quality,"** p. 19), and magnetic susceptibility (RMGS) from Hole 1103A, with core measurements of natural gamma, bulk density, porosity, sonic velocity, and magnetic susceptibility. Depth adjustments have been applied to bring all logs to a common measurement position below the seafloor.

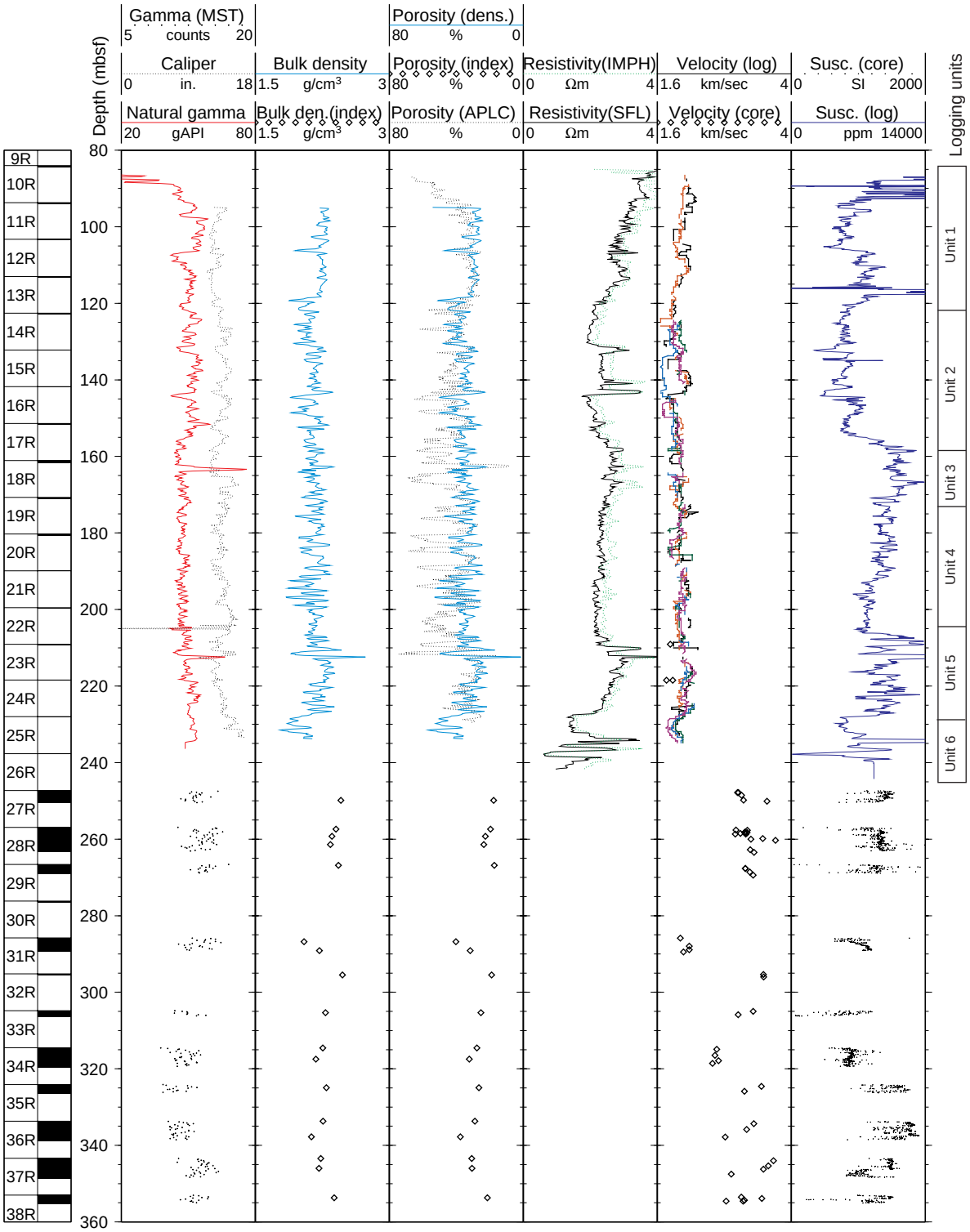

**Figure F28.** Downhole logs of natural gamma, uranium, thorium, thorium/potassium ratio from the natural gamma-ray tool (NGT) during the second FMS-sonic pass, photoelectric effect (PEF), and magnetic susceptibility in Hole 1103A. Depth adjustments have been applied to bring all logs to a common measurement position below the seafloor.

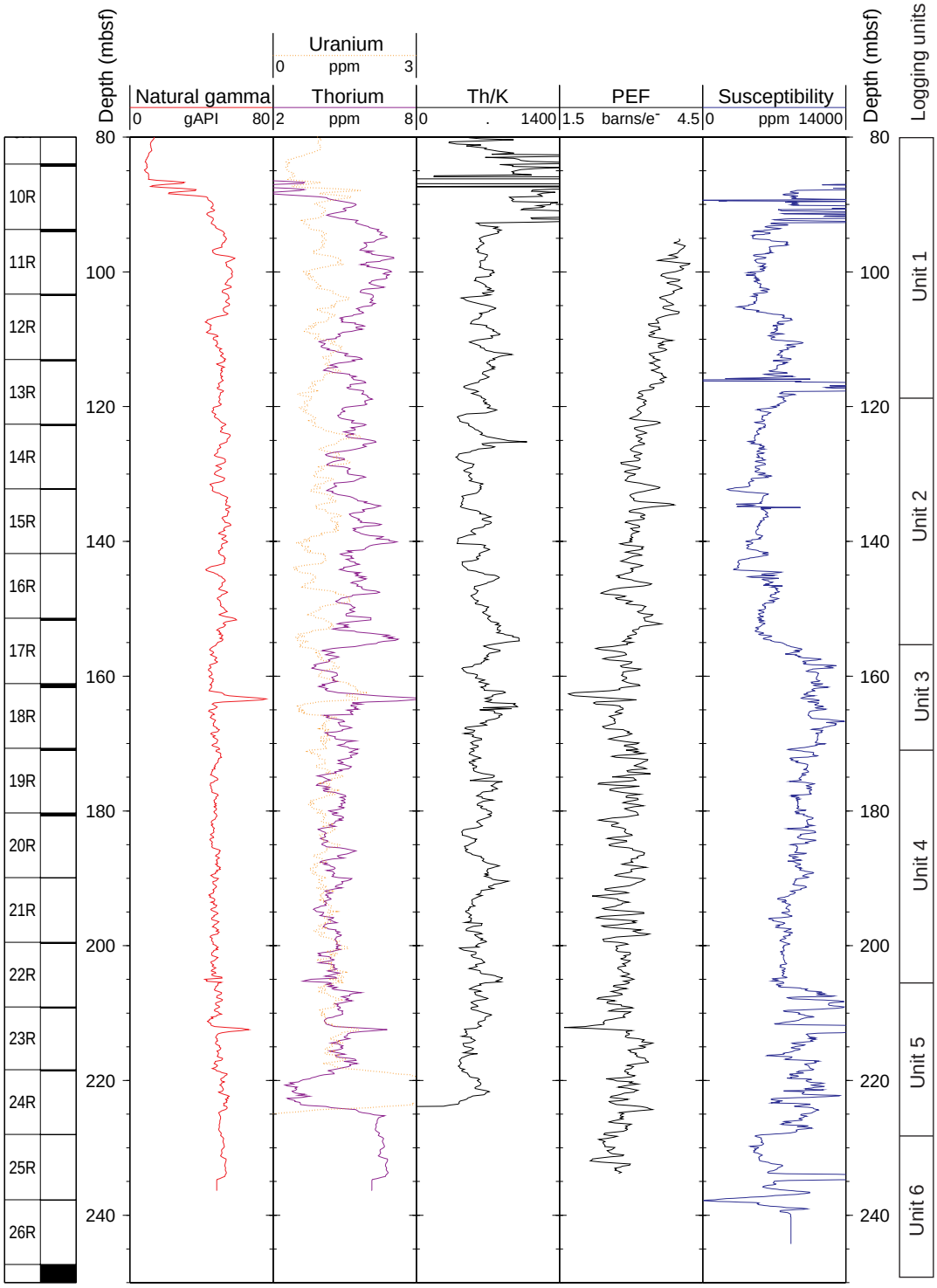

**Figure F29.** PEF vs. potassium in Hole 1103A. Both logs were corrected for sediment porosity. The points are divided according to their logging units. The mineral fields are from the Schlumberger chart and represent the positions if that mineral composed 100% of the sediment.

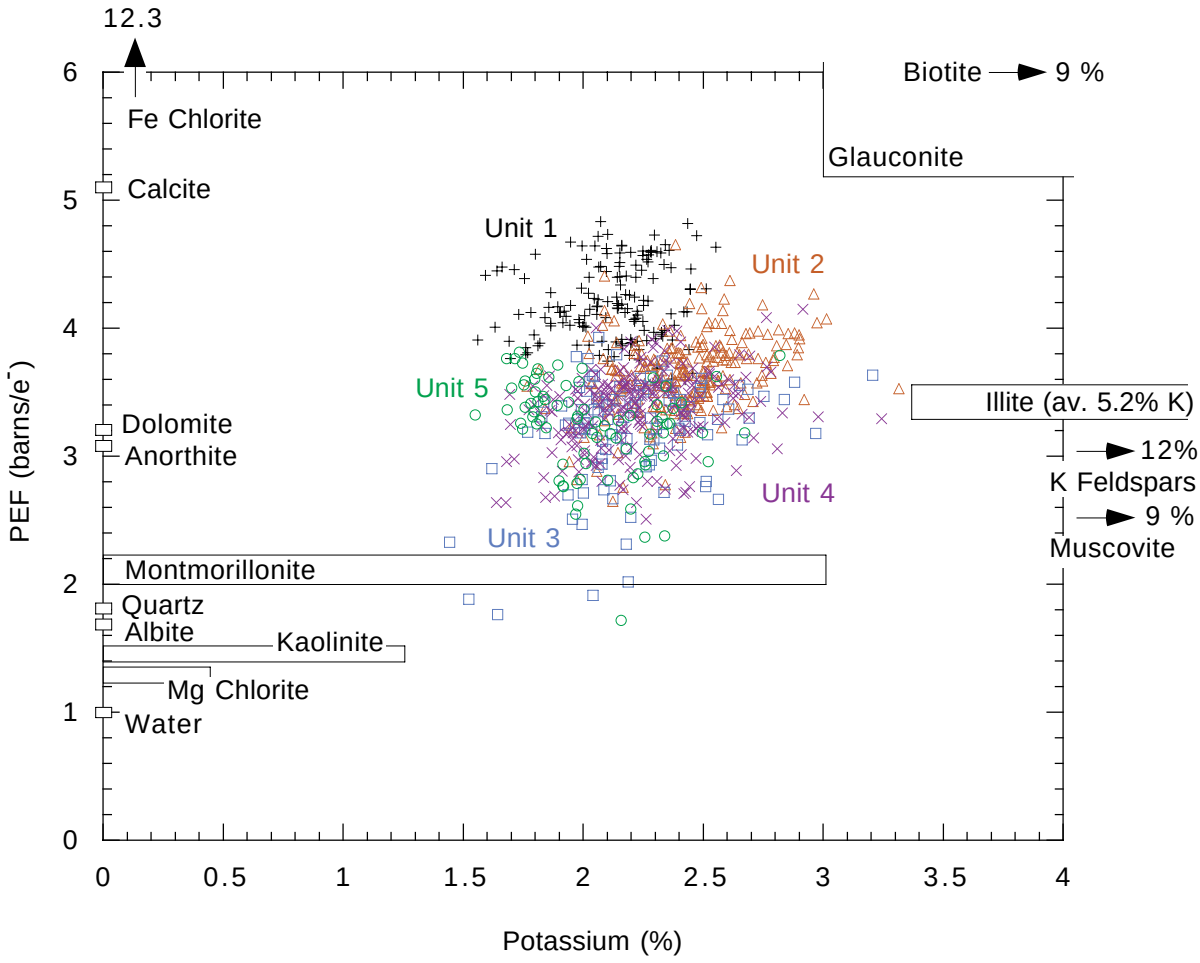

**Figure F30.** FMS resistivity images from Hole 1103A. **A.** Layered sediment containing a highly resistive, 25-cm-thick bed and individual pebbles, 208–213 mbsf. **B.** An example of a large clast (~20 cm × 40 cm), 157–158 mbsf.

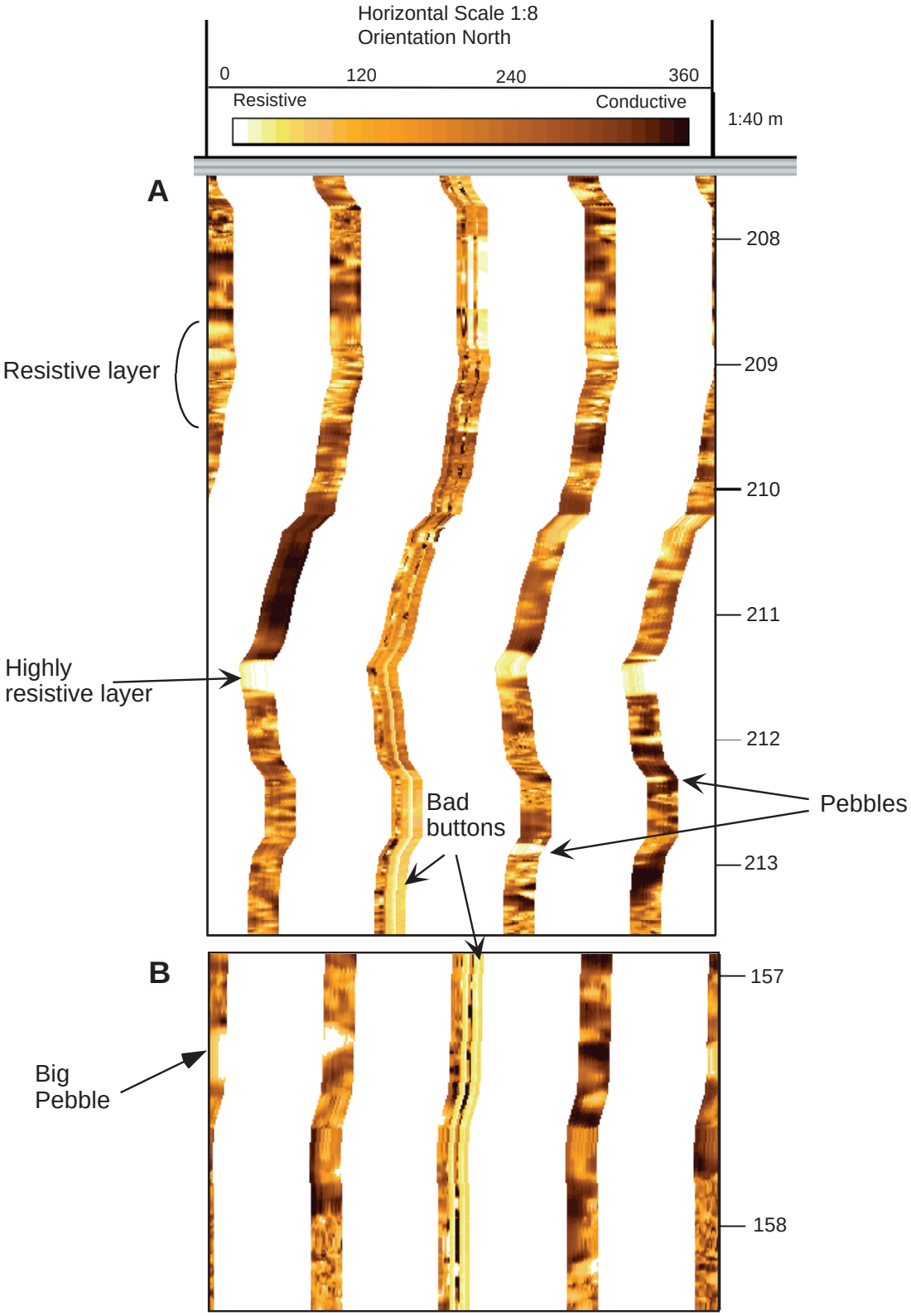

**Figure F31.** Magnetic field logs from Hole 1103A. All units are in nT. **A.** Total magnetic field (MAGB) (dotted), MAGB with spikes removed (solid), and the modeled pipe effect (dashed). **B.** Field anomaly minus the spikes and the pipe effect. **C.** Field anomaly produced by the induced magnetization of the sediment. **D.** The field anomaly produced by the remanent magnetization, calculated by subtracting the induction anomaly from the pipe-corrected total field anomaly.

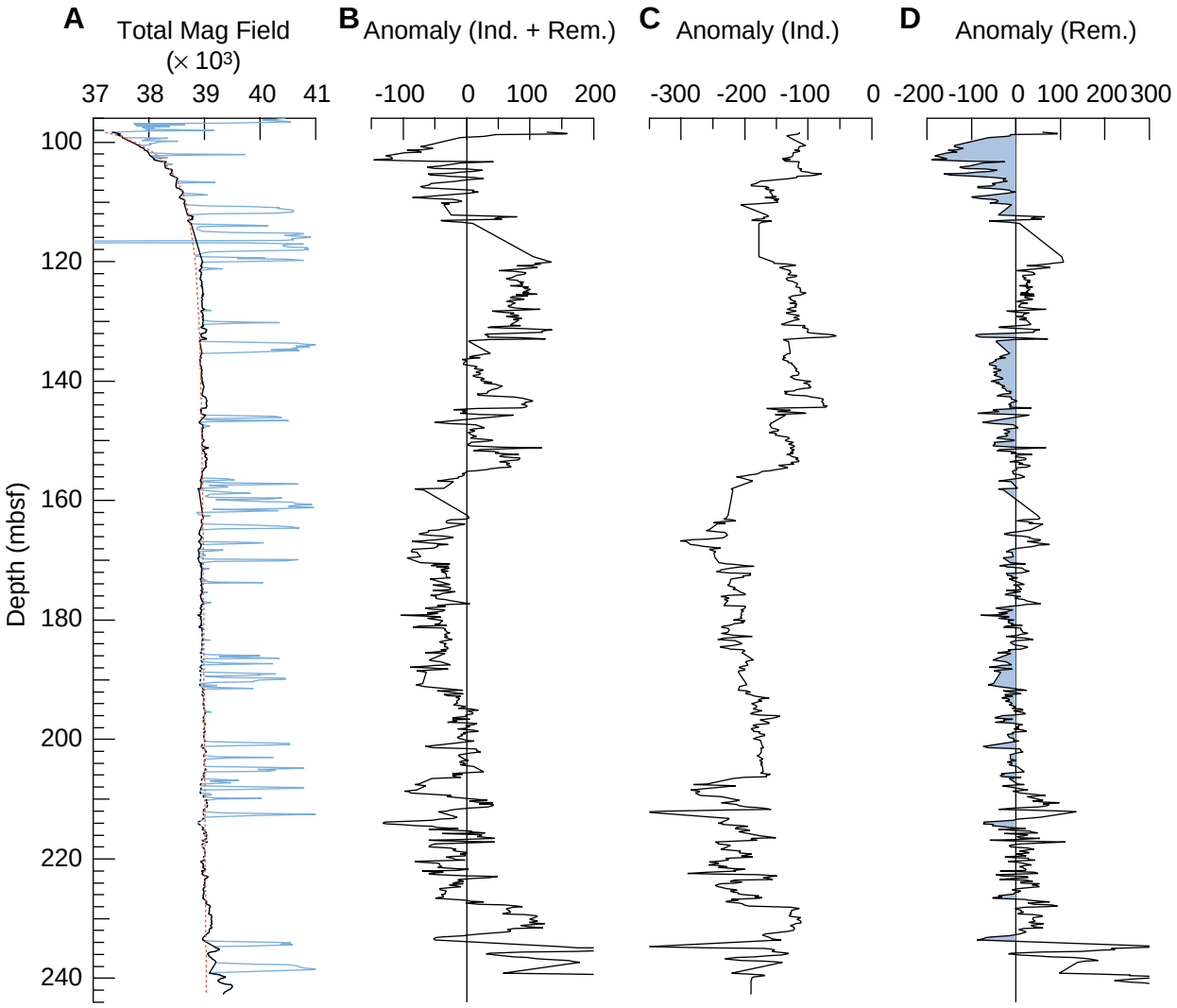

**Figure F32.** Temperature log from Hole 1103A, taken during the TC run. See "Temperature Log," p. 22, for explanation.

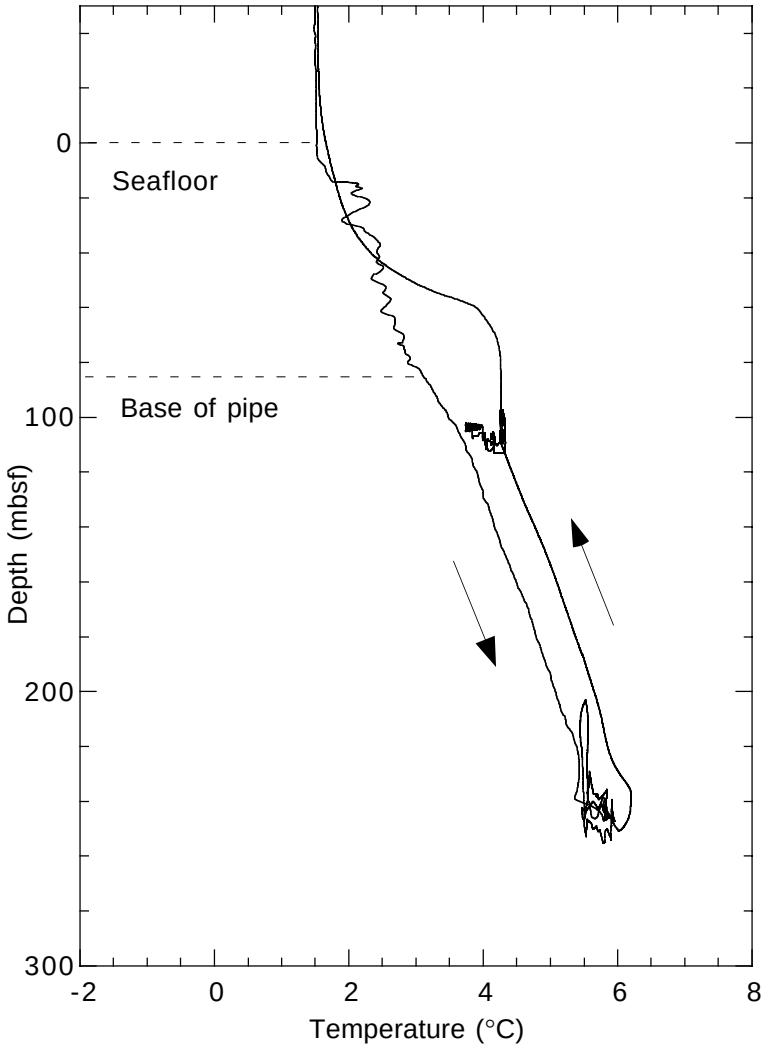

**Figure F33.** Comparison of different density data sets available for Site 1103.

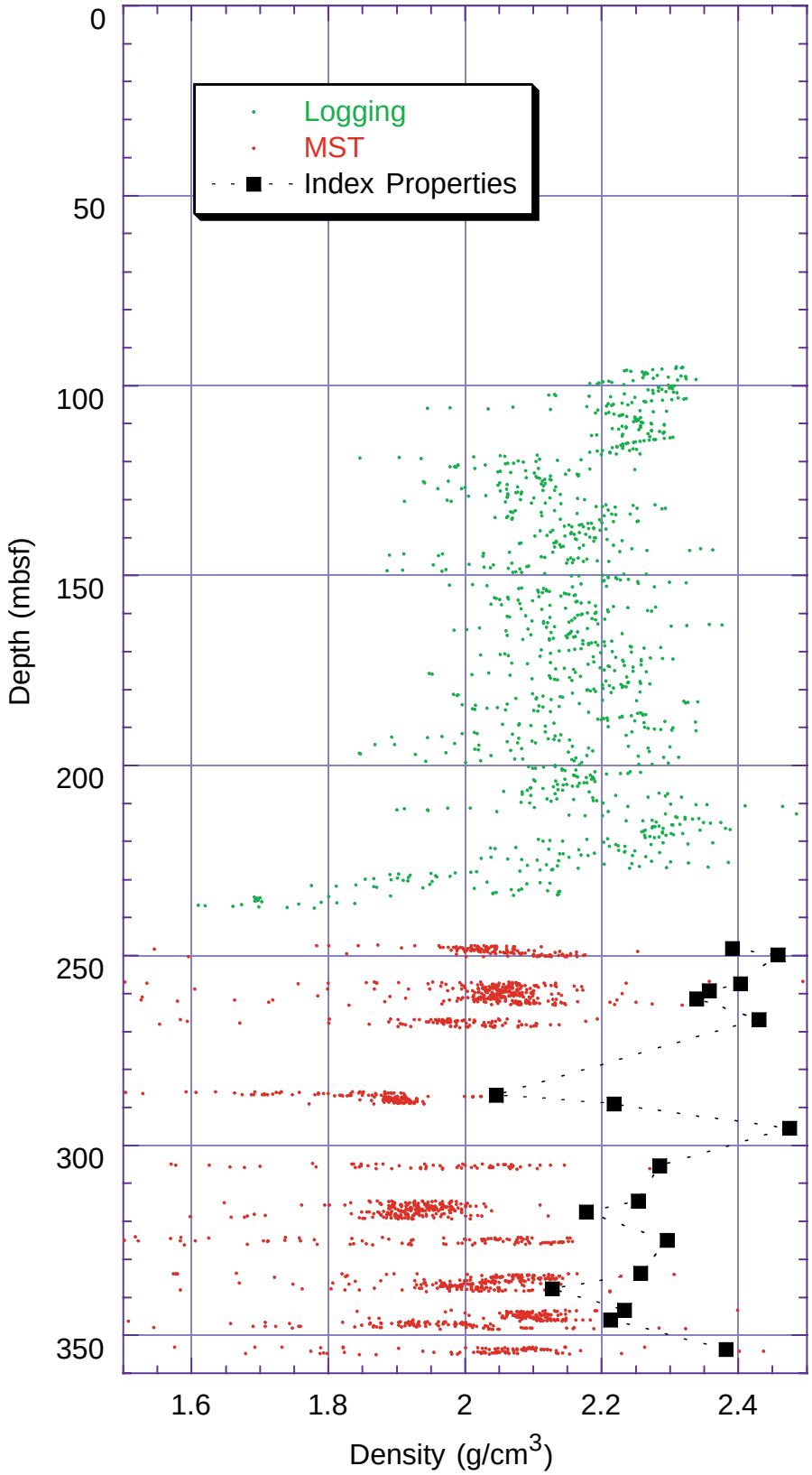

**Figure F34.** Downhole logging and Hamilton Frame velocities for Site 1103.

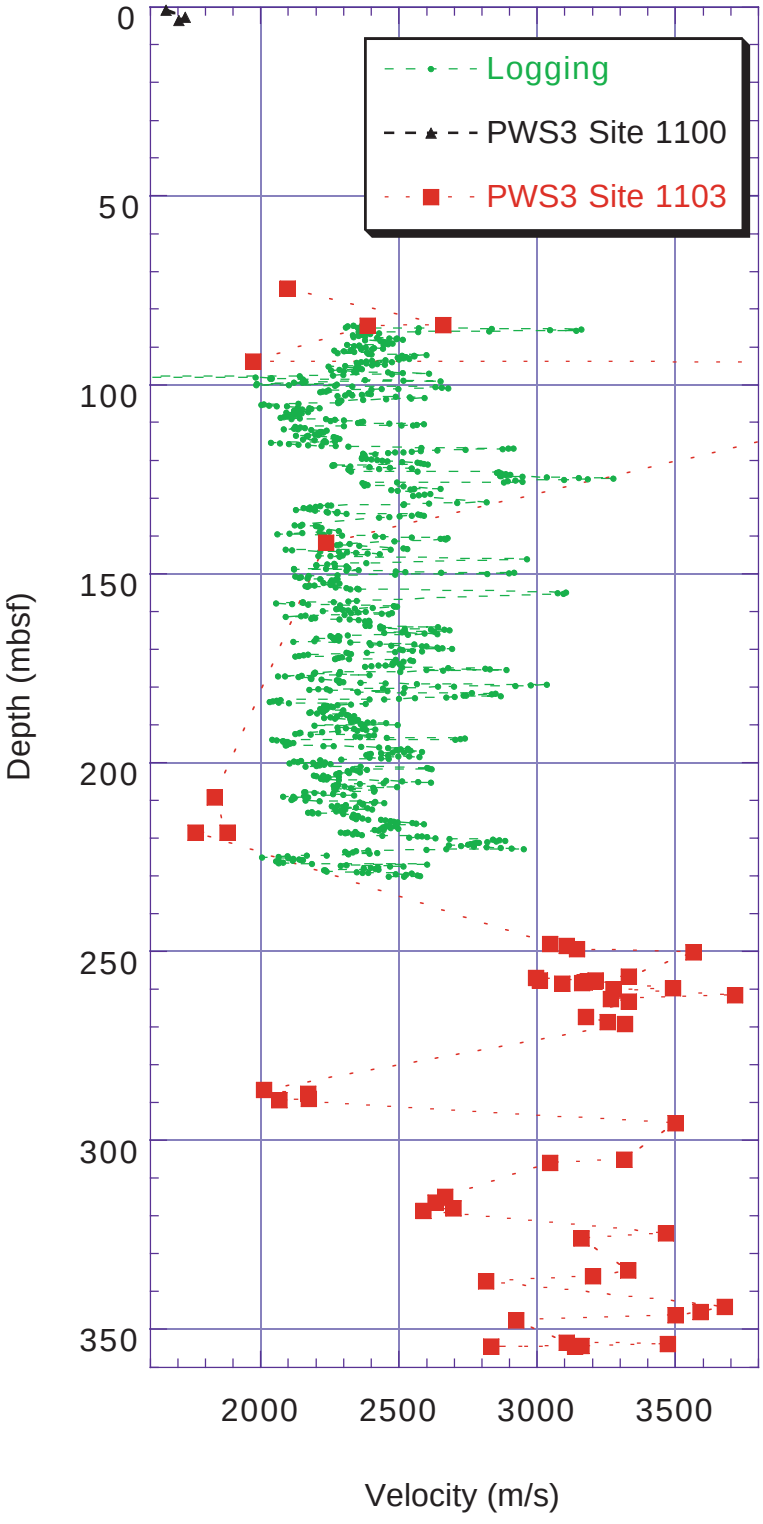

**Figure F35.** Traveltime/depth function for Site 1103.

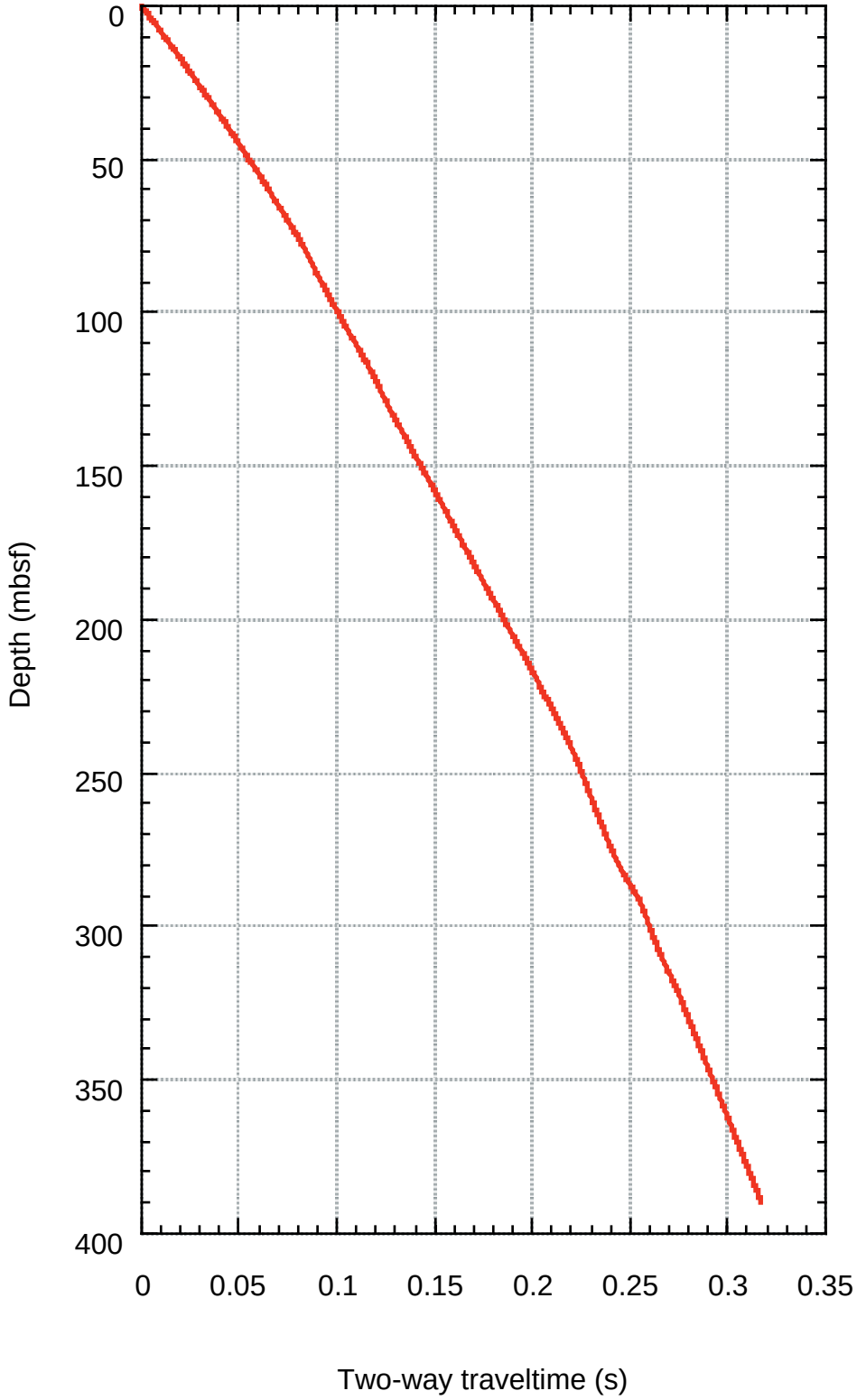

**Figure F36.** Seismic profile I95-152 over Site 1103 with important reflectors marked in the column to the left.

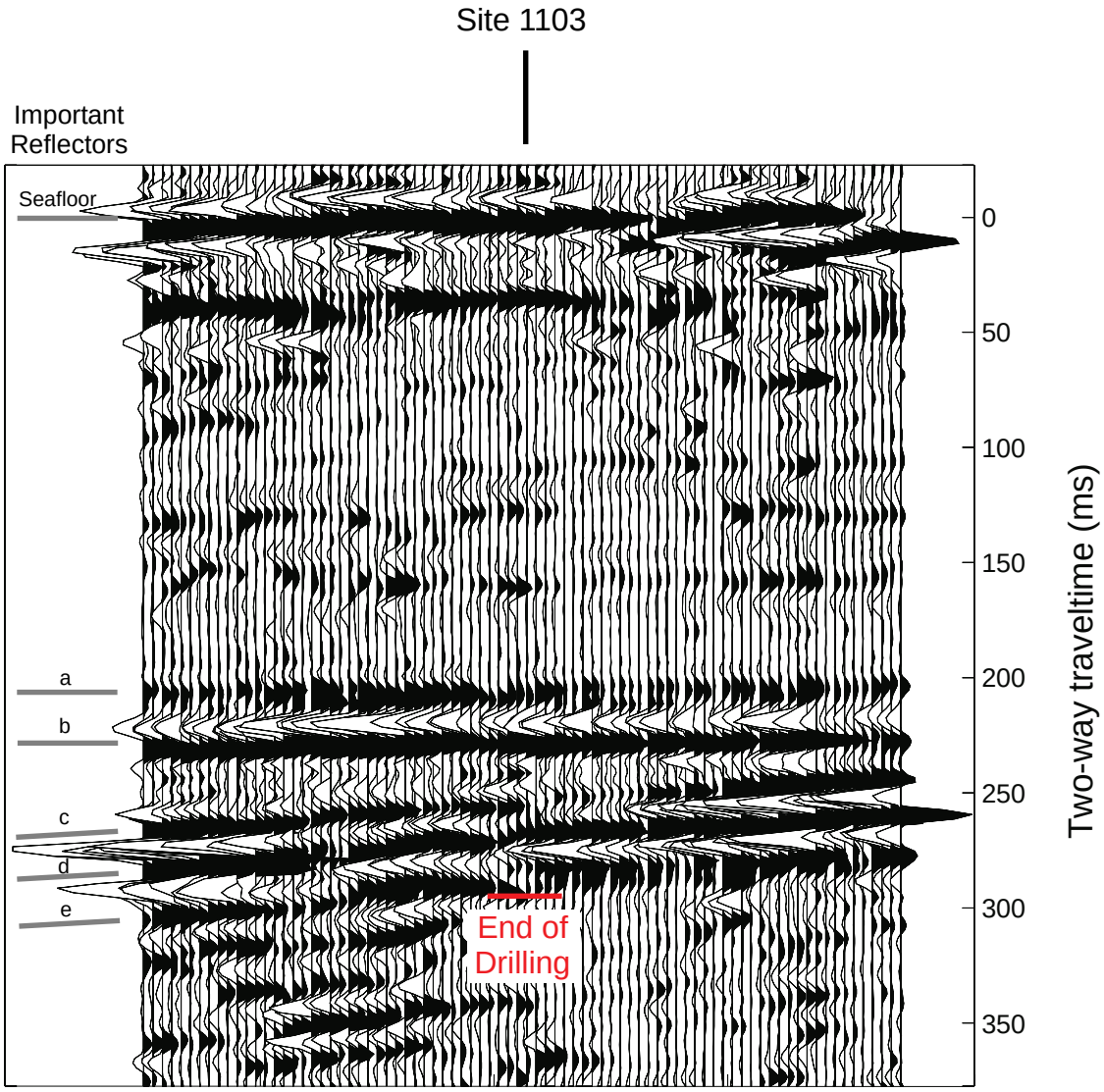

**Figure F37.** Multichannel seismic profile I95-152 across Site 1102. S.P. = shotpoint.

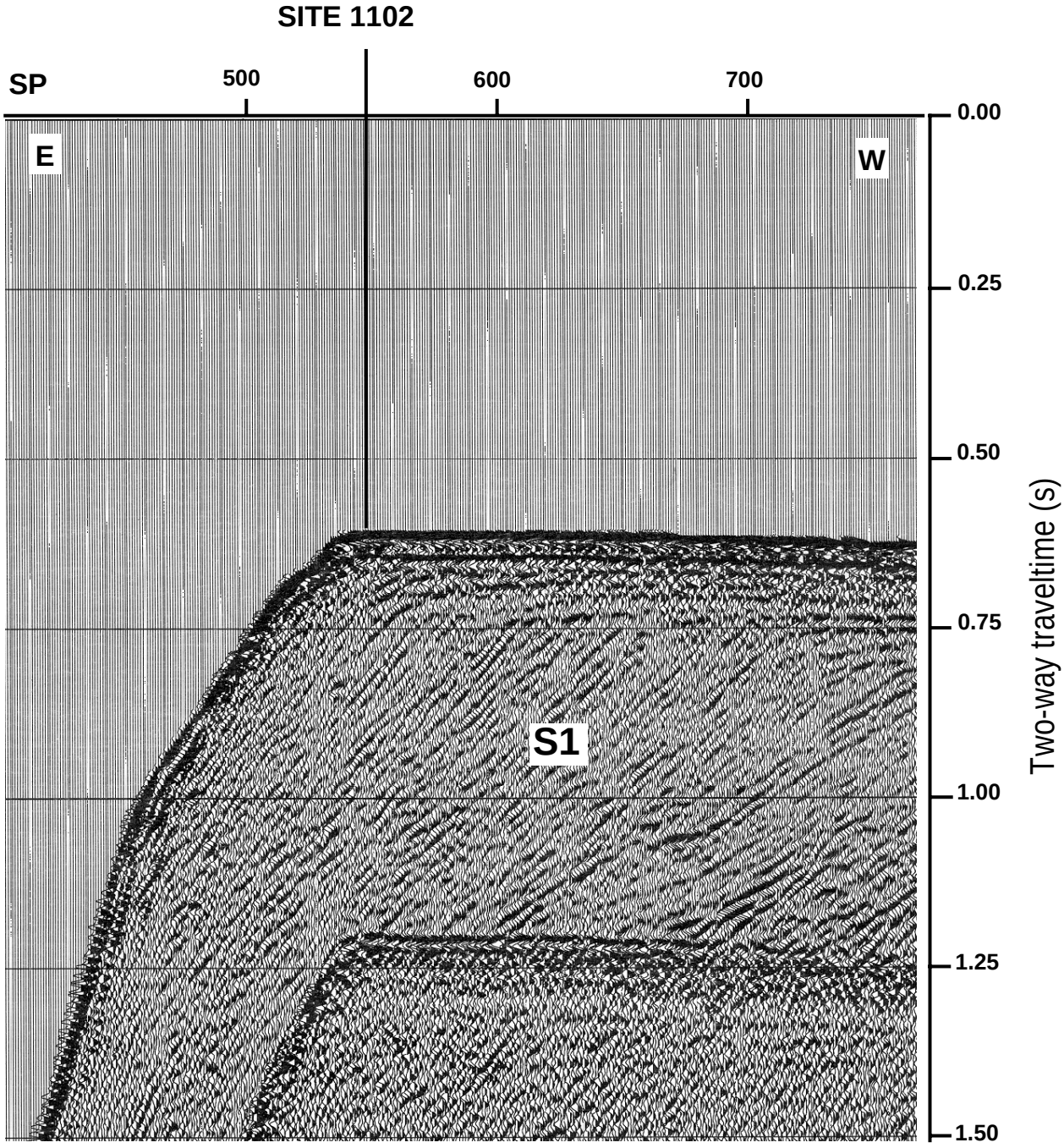

**Figure F38.** Multichannel seismic profile I95-152 across Site 1100. S.P. = shotpoint.

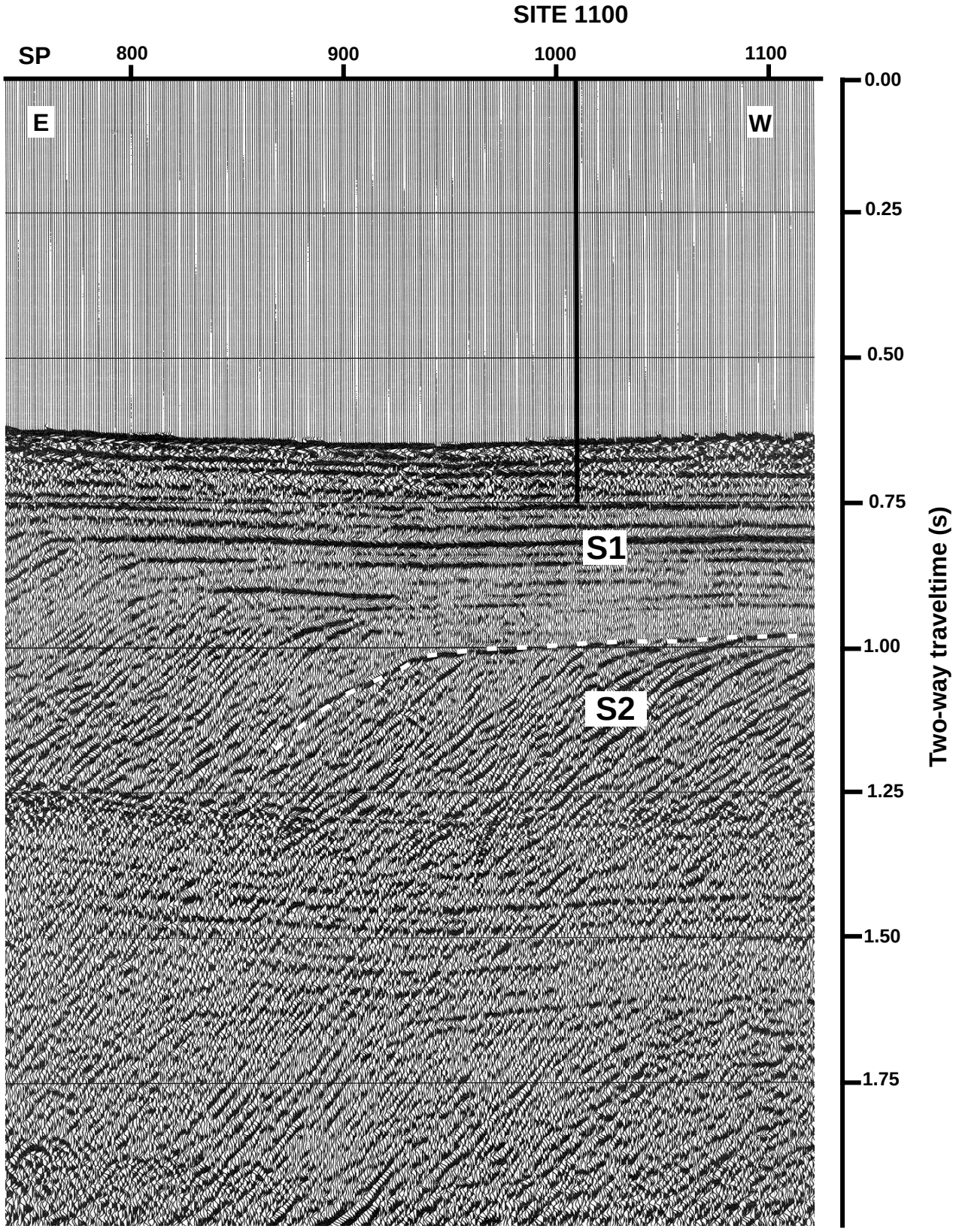

**Figure F39.** Multichannel seismic profile I95-152 across Site 1103. S.P. = shotpoint.

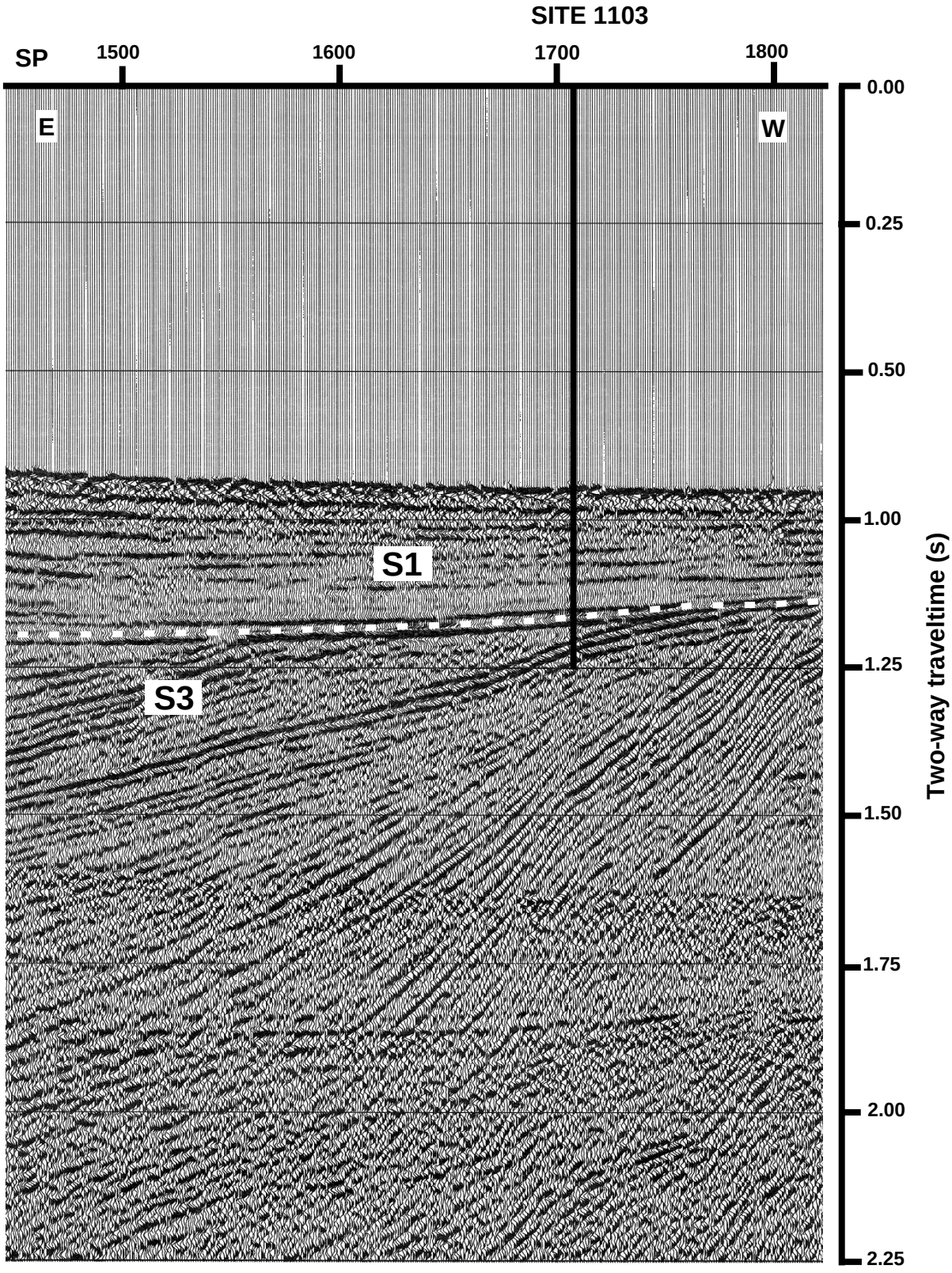

**Table T1.** Coring summary for Sites 1100, 1102, and 1103. (**See table note.** Continued on next page.)

| Core | Date (March 1998) | Time (UTC) | Depth (mbsf) | Length cored (m) | Length recovered (m) | Recovery (%) |
|---|---|---|---|---|---|---|
| 178-1100A- | | | | | | |
| 1R | 15 | 0000 | 0.0-5.0 | 5.0 | 0.00 | 0.0 |
| 2R | 15 | 0100 | 5.0-14.6 | 9.6 | 0.00 | 0.0 |
| 3R | 15 | 0150 | 14.6-24.2 | 9.6 | 0.00 | 0.0 |
| 4R | 15 | 0250 | 24.2-33.8 | 9.6 | 0.00 | 0.0 |
| Coring totals: | | | | 33.8 | 0.00 | 0.0 |
| 178-1100B- | | | | | | |
| | | ******Drilled from 0.0-33.9 mbsf****** | | | | |
| 1R | 15 | 1345 | 33.9-35.9 | 2.0 | 0.15 | 7.5 |
| Coring totals: | | | | 2.0 | 0.15 | 7.5 |
| Drilled: | | | | 33.9 | | |
| Total: | | | | 35.9 | | |
| 178-1100C- | | | | | | |
| 1R | 16 | 1000 | 0.0-5.0 | 5.0 | 4.05 | 81.0 |
| Coring totals: | | | | 5.0 | 4.05 | 81.0 |
| 178-1100D- | | | | | | |
| 1R | 16 | 1100 | 0.0-14.6 | 14.6 | 0.11 | 0.8 |
| 2R | 16 | 1145 | 14.6-24.2 | 9.6 | 0.08 | 0.8 |
| 3R | 16 | 1240 | 24.2-33.8 | 9.6 | 0.38 | 4.0 |
| 4R | 16 | 1400 | 33.8-43.4 | 9.6 | 0.14 | 1.5 |
| 5R | 16 | 1535 | 43.4-53.0 | 9.6 | 1.28 | 13.3 |
| 6R | 16 | 1720 | 53.0-62.5 | 9.5 | 1.63 | 17.2 |
| 7R | 16 | 2050 | 62.5-72.1 | 9.6 | 0.26 | 2.7 |
| 8R | 16 | 2200 | 72.1-76.8 | 4.7 | 0.12 | 2.6 |
| 9R | 17 | 0800 | 76.8-81.7 | 4.9 | 0.16 | 3.3 |
| 10R | 17 | 0850 | 81.7-91.3 | 9.6 | 0.33 | 3.4 |
| 11R | 17 | 0950 | 91.3-100.9 | 9.6 | 0.25 | 2.6 |
| Coring totals: | | | | 110.5 | 5.28 | 4.8 |
| 178-1102A- | | | | | | |
| 1R | 21 | 1930 | 0.0-7.9 | 7.9 | 0.42 | 5.3 |
| Coring totals: | | | | 7.9 | 0.42 | 5.3 |
| 178-1102B- | | | | | | |
| 1R | 21 | 1930 | 0.0-7.5 | 7.5 | 0.39 | 5.2 |
| Coring totals: | | | | 7.5 | 0.39 | 5.2 |
| 178-1102C- | | | | | | |
| 1R | 22 | 0500 | 0.0-4.0 | 4.0 | 0.00 | 0.0 |
| 2R | 22 | 0600 | 4.0-6.5 | 2.5 | 0.01 | 0.4 |
| Coring totals: | | | | 6.5 | 0.01 | 0.2 |
| 178-1102D- | | | | | | |
| 1R | 22 | 1850 | 0.0-14.9 | 14.9 | 0.85 | 5.7 |
| Coring totals: | | | | 14.9 | 0.85 | 5.7 |
| 178-1103A- | | | | | | |
| 1R | 22 | 2345 | 0.0-10.8 | 10.8 | 0.25 | 2.3 |
| 2R | 23 | 0130 | 10.8-16.8 | 6.0 | 0.18 | 3.0 |
| 3R | 23 | 0305 | 16.8-26.4 | 9.6 | 0.20 | 2.1 |
| 4R | 23 | 0435 | 26.4-36.0 | 9.6 | 0.09 | 0.9 |
| 5R | 23 | 0550 | 36.0-45.6 | 9.6 | 0.11 | 1.1 |
| 6R | 23 | 0635 | 45.6-55.2 | 9.6 | 0.03 | 0.3 |
| 7R | 23 | 0720 | 55.2-64.8 | 9.6 | 0.00 | 0.0 |
| 8R | 23 | 0840 | 64.8-74.4 | 9.6 | 0.52 | 5.4 |
| 9R | 23 | 1010 | 74.4-84.0 | 9.6 | 0.27 | 2.8 |
| 10R | 23 | 1110 | 84.0-93.7 | 9.7 | 0.41 | 4.2 |
| 11R | 23 | 1215 | 93.7-103.3 | 9.6 | 0.38 | 4.0 |
| 12R | 23 | 1300 | 103.3-113.0 | 9.7 | 0.22 | 2.3 |
| 13R | 23 | 1355 | 113.0-122.6 | 9.6 | 0.25 | 2.6 |
| 14R | 23 | 1435 | 122.6-132.2 | 9.6 | 0.25 | 2.6 |
| 15R | 23 | 1525 | 132.2-141.8 | 9.6 | 0.15 | 1.6 |
| 16R | 23 | 1610 | 141.8-151.4 | 9.6 | 0.02 | 0.2 |
| 17R | 23 | 1700 | 151.4-161.1 | 9.7 | 0.34 | 3.5 |

Table T1 (continued).

| | | | | | | |
|---|---|---|---|---|---|---|
| 18R | 23 | 1750 | 161.1-170.7 | 9.6 | 0.65 | 6.8 |
| 19R | 23 | 1845 | 170.7-180.3 | 9.6 | 0.36 | 3.8 |
| 20R | 23 | 2115 | 180.3-189.9 | 9.6 | 0.42 | 4.4 |
| 21R | 23 | 2200 | 189.9-199.5 | 9.6 | 0.07 | 0.7 |
| 22R | 23 | 2300 | 199.5-209.1 | 9.6 | 0.14 | 1.5 |
| 23R | 24 | 0030 | 209.1-218.4 | 9.3 | 0.20 | 2.2 |
| 24R | 24 | 0125 | 218.4-228.0 | 9.6 | 0.18 | 1.9 |
| 25R | 24 | 0220 | 228.0-237.7 | 9.7 | 0.03 | 0.3 |
| 26R | 24 | 0325 | 237.7-247.3 | 9.6 | 0.06 | 0.6 |
| 27R | 24 | 0530 | 247.3-256.9 | 9.6 | 3.31 | 34.5 |
| 28R | 24 | 0830 | 256.9-266.6 | 9.7 | 6.52 | 67.2 |
| 29R | 24 | 1125 | 266.6-276.2 | 9.6 | 2.50 | 26.0 |
| 30R | 24 | 1410 | 276.2-285.8 | 9.6 | 0.32 | 3.3 |
| 31R | 24 | 1520 | 285.8-295.2 | 9.4 | 3.57 | 38.0 |
| 32R | 24 | 1650 | 295.2-304.8 | 9.6 | 0.38 | 4.0 |
| 33R | 24 | 1920 | 304.8-314.5 | 9.7 | 1.71 | 17.6 |
| 34R | 24 | 2100 | 314.5-324.1 | 9.6 | 5.11 | 53.2 |
| 35R | 24 | 2355 | 324.1-333.7 | 9.6 | 2.44 | 25.4 |
| 36R | 25 | 0225 | 333.7-343.4 | 9.7 | 5.10 | 52.6 |
| 37R | 25 | 0445 | 343.4-353.0 | 9.6 | 5.41 | 56.4 |
| 38R | 25 | 0710 | 353.0-362.7 | 9.7 | 2.39 | 24.6 |
| Coring totals: | | | | 362.7 | 44.54 | 12.3 |

Notes: UTC = Universal Time Coordinated. An expanded version of this coring summary table that includes lengths and depths of sections and comments on sampling is included in ASCII format in the **TABLES** directory.

**Table T2.** Summary of gas concentrations for Hole 1103A.

| Core, section, interval (cm) | Depth (mbsf) | Sample method | Methane (ppm) | Ethane (ppm) |
|---|---|---|---|---|
| 178-1103A- | | | | |
| 28R-1, 99-100 | 257.89 | HS | 3,430 | 0 |
| 29R-1, 0-5 | 266.60 | HS | 2,260 | 0 |
| 31R-1, 142-143 | 287.22 | HS | 1,620 | 0 |
| 32R-1, 37-38 | 295.57 | HS | 545 | 0 |
| 33R-1, 0-5 | 304.80 | HS | 1,270 | 0 |
| 34R-4, 83-88 | 319.37 | HS | 2,770 | 0 |
| 35R-2, 93-94 | 326.32 | HS | 1,650 | 0 |
| 36R-3, 138-139 | 337.91 | HS | 11,600 | 0 |
| 37R-4, 132-133 | 348.45 | HS | 20,000 | 1 |

Note: HS = headspace.

**Table T3.** Profiles of interstitial water chemistry at Hole 1100C.

| Core, section, interval (cm) | Depth (mbsf) | pH | Salinity | $Cl^-$ (mM) | Alkalinity (mM) | $NH_4^+$ (mM) | $Si(OH)_4$ (mM) | $SO_4^{2-}$ (mM) | $Mn^{2+}$ (μM) | $PO_4^{3-}$ (μM) | $F^-$ (μM) | $Ca^{2+}$ (mM) | $Mg^{2+}$ (mM) | $K^+$ (mM) | $Sr^{2+}$ (μM) |
|---|---|---|---|---|---|---|---|---|---|---|---|---|---|---|---|
| 178-1100C- | | | | | | | | | | | | | | | |
| 1R-2, 145-150 | 2.95 | 7.6 | 35 | 557 | 3.56 | 0.08 | 0.57 | 29.3 | 29 | 9.5 | 62.3 | 12.0 | 56.5 | 13.5 | 85 |

**Table T4.** Summary of logging operations, Hole 1103A.

| Task | Start time |
|---|---|
| Hole preparation | 07:10, 25 March 1998 |
| IPLT | 15:15, 25 March 1998 |
| GHMT | 22:40, 25 March 1998 |
| FMS-sonic | 01:25, 26 March 1998 |
| End of logging operations | 07:00, 26 March 1998 |